

# Dimension-8 M-operators for Vector Boson Scattering: a UV complete model and its Effective Field Theory

Zur Erlangung des akademischen Grades eines  
DOKTORS DER NATURWISSENSCHAFTEN (Dr. rer. nat.)  
von der KIT-Fakultät für Physik des  
Karlsruher Instituts für Technologie (KIT)  
angenommene  
DISSERTATION

von

M.Sc Heiko Dietrich-Siebert

Tag der mündlichen Prüfung: 27.01.2023

Referent: Prof. Dr. D. Zeppenfeld

Korreferentin: Prof. Dr. M. Mühlleitner



This document is licensed under a Creative Commons Attribution-ShareAlike 4.0 International License (CC BY-SA 4.0): <https://creativecommons.org/licenses/by-sa/4.0/deed.en>

# Abstract

Vector boson scattering (VBS) processes provide an excellent probe of quartic gauge couplings at the LHC. A common way to parameterize anomalous quartic (aQGC) and triple (aTGC) gauge couplings is by using the framework of effective field theories (EFT). For purely transverse vector boson scattering it has been shown that there are models for which effects in the EFT are expected to appear first in the aQGC and therefore at dimension 8. For the scattering of two longitudinal and two transverse vector bosons such an analysis is still missing.

In this thesis a class of model containing multiple  $SU(2)_L$  fermion multiplets is proposed that are capable of enhancing the scattering of vector bosons of mixed helicities. The contributions of this class of models to vector boson and higgs boson propagators, three particle vertices and four particle vertices are calculated and an EFT is constructed as the low energy approximation of these models. The effects of the models are analyzed for dilepton production, vector boson production, anomalous higgs couplings, on-shell VBS and on-shell higgs boson pair production. The impacts of the model and its EFT are compared and the quality of the EFT as an approximation of the full model is assessed. Finally an outlook on where to look for these kind of models is made.



# Zusammenfassung

VBS-Prozesse (Vector Bosonen Streuung) bieten eine hervorragende Möglichkeit, quartische Eichkopplungen am LHC zu untersuchen. Eine gängige Methode zur Parametrisierung anomaler quartischer (aQGC) und dreifacher (aTGC) Eichkopplungen ist die Verwendung effektiver Feldtheorien (EFT). Für rein transversale Vektorbosonenstreuung wurde gezeigt, dass es Modelle gibt, bei denen Effekte in der EFT zuerst in den aQGC und damit in Dimension 8 auftreten sollten. Für die Streuung von zwei longitudinalen und zwei transversalen Vektorbosonen fehlt eine solche Analyse jedoch noch.

In dieser Arbeit wird eine Klasse von Modellen vorgestellt, die mehrere  $SU(2)_L$ -Fermionmultipletts enthalten, welche in der Lage sind, die Streuung von Vektorbosonen mit gemischten Helizitäten zu verstärken. Die Beiträge dieser Modelle zu den Propagatoren von Vektor-Bosonen und Higgs-Boson, zu den drei und vier Teilchen Vertices werden berechnet und eine EFT wird als Niedrigenergie-Näherung dieser Modelle konstruiert. Die Auswirkungen der Modelle werden für die Dileptonenproduktion, die Vektorbosonenproduktion, anomale Higgs-Kopplungen, On-Shell-VBS und On-Shell-Higgs-Bosonenpaarproduktion analysiert. Die Auswirkungen des Modells und seiner EFT werden verglichen und die Qualität der EFT als Annäherung des vollständigen Modells wird bewertet. Abschließend wird ein Ausblick gegeben, wo man nach dieser Art von Modellen suchen sollte.



# Contents

<b>1. Introduction</b>	<b>1</b>
<b>2. Theoretical Background and Notation</b>	<b>3</b>
2.1. The Standard Model . . . . .	3
2.1.1. Symmetries and Quantum Numbers . . . . .	3
2.1.2. Particle Content . . . . .	4
2.1.3. The SM Lagrangian . . . . .	6
2.2. Effective Field Theories . . . . .	8
2.2.1. The Standard Model Effective Field Theory . . . . .	9
2.2.1.1. Dimension-6 Basis . . . . .	9
2.2.1.2. Dimension-8 Basis . . . . .	11
2.3. 1-Loop Integrals . . . . .	12
2.4. Kinematics . . . . .	14
<b>3. Model</b>	<b>17</b>
3.1. Defining the Model . . . . .	17
3.1.1. Particle Content and Lagrangian . . . . .	17
3.1.2. Mass Eigenstates . . . . .	18
3.1.3. Mass Splitting at NLO . . . . .	20
3.1.4. Ignoring the Photon, $SU(2)$ -Limit . . . . .	22
3.2. 1-Loop Contributions for VBS . . . . .	23
3.2.1. Simplifying the 1-Loop Contributions . . . . .	23
3.2.2. Renormalization . . . . .	24
3.2.2.1. $\overline{\text{MS}}$ Scheme . . . . .	26
3.2.2.2. On-Shell Scheme . . . . .	26
3.3. Generalizations and related Models . . . . .	29
<b>4. EFT</b>	<b>31</b>
4.1. Constructing a Dedicated Basis . . . . .	31
4.1.1. Following the Contributions . . . . .	32
4.2. Building the Dedicated Basis . . . . .	33
4.2.1. Dimension-2 and Dimension-4 . . . . .	33
4.2.2. Dimension-6 . . . . .	34
4.2.2.1. $\phi^6$ . . . . .	34
4.2.2.2. $\phi^4 D^2$ . . . . .	34
4.2.2.3. $\phi^2 D^4$ . . . . .	35
4.2.2.4. $\phi^2 D^2 X$ . . . . .	35
4.2.2.5. $\phi^2 X^2$ . . . . .	35
4.2.2.6. $D^4 X$ . . . . .	36

4.2.2.7.	$D^2 X^2$	36
4.2.2.8.	$X^3$	36
4.2.3.	Dimension-8	37
4.2.3.1.	$\phi^8$	37
4.2.3.2.	$\phi^6 D^2$	37
4.2.3.3.	$\phi^4 D^4$	37
4.2.3.4.	$\phi^4 D^2 X$	39
4.2.3.5.	$\phi^4 X^2$	40
4.2.3.6.	$\phi^2 D^6$	40
4.2.3.7.	$\phi^2 D^4 X$	41
4.2.3.8.	$\phi^2 D^2 X^2$	41
4.2.3.9.	$\phi^2 X^3$	43
4.2.3.10.	$D^4 X^2$	44
4.2.3.11.	$D^2 X^3$	44
4.2.3.12.	$X^4$	46
4.2.4.	Renormalization	47
4.3.	Matching	48
<b>5.</b>	<b>Results</b>	<b>55</b>
5.1.	Production of opposite sign SM fermions	56
5.2.	Production of same sign SM fermions	59
5.3.	Vector Boson Pair Production	63
5.4.	Anomalous Higgs Boson Couplings	66
5.5.	On-Shell Four Particle Scattering	67
5.5.1.	VBS	69
5.5.1.1.	Full Model	69
5.5.1.2.	EFT	74
5.5.1.3.	Model vs EFT	79
5.5.1.4.	Polarized Cross Sections	81
5.6.	Higgs Pair Production From Two Vector Bosons	85
5.6.1.	Implications for LHC Searches	85
<b>6.</b>	<b>Conclusions</b>	<b>87</b>
<b>Appendix</b>		<b>91</b>
A.	Coefficient Functions for Passarino-Veltman-Reduction	91
B.	Counterterms for the Renormalization of the EFT	92
C.	VBS Plots for $W^+W^- \rightarrow ZZ$ , $W^+Z \rightarrow W^+Z$ and $ZZ \rightarrow ZZ$	92
<b>Bibliography</b>		<b>103</b>

# List of Figures

2.1. Example of a one-loop diagram, created using [1] . . . . .	14
3.1. Mass splitting between the lightest and second lightest particle in each multiplet at NLO . . . . .	22
3.2. Loop induced correction to the Z-Boson propagator . . . . .	23
3.3. Loop induced correction to the ZZhh vertex . . . . .	24
5.1. Drell-Yan: $q\bar{q} \rightarrow \mu^+\mu^-$ . . . . .	56
5.2. Propagator corrections to Drell-Yan for $J = 3$ . . . . .	57
5.3. Propagator corrections to Drell-Yan for $J = 4$ . . . . .	58
5.4. Propagator corrections to Drell-Yan for $J = 4$ and $m = 1100$ GeV . . . . .	59
5.5. Drell-Yan production of a same sign lepton pair . . . . .	60
5.6. Drell-Yan production of a same sign W pair . . . . .	60
5.7. Vector boson production ( $f\bar{f} \rightarrow W^+W^-$ ) with anomalous triple gauge coupling . . . . .	63
5.8. Cross section of the full model with $m = 700$ GeV for $W^+W^+ \rightarrow W^+W^+$	70
5.9. Cross section of the full model with $m = 700$ GeV for $W^+W^- \rightarrow W^+W^-$	71
5.10. Cross section of the full model with $m = 700$ GeV for $W^+W^- \rightarrow ZZ$	71
5.11. Cross section of the full model with $m = 700$ GeV for $W^+Z \rightarrow W^+Z$	72
5.12. Cross section of the full model with $m = 700$ GeV for $ZZ \rightarrow ZZ$ . . . . .	72
5.13. Cross section of the full model with $m = 1100$ GeV for $W^+W^+ \rightarrow W^+W^+$ . . . . .	73
5.14. Cross section of the full model with $m = 1100$ GeV for $W^+W^- \rightarrow W^+W^-$ . . . . .	73
5.15. Cross section of the EFT for $m = 700$ GeV, $J = 3$ and $\lambda = 1$ for $W^+W^+ \rightarrow W^+W^+$ . . . . .	75
5.16. Cross section of the EFT for $m = 700$ GeV, $J = 3$ and $\lambda = 1$ for $W^+W^- \rightarrow W^+W^-$ . . . . .	76
5.17. Cross section of the EFT for $m = 1100$ GeV, $J = 4$ and $\lambda = 3$ for $W^+W^+ \rightarrow W^+W^+$ . . . . .	77
5.18. Cross section of the EFT for $m = 1100$ GeV, $J = 4$ and $\lambda = 3$ for $W^+W^- \rightarrow W^+W^-$ . . . . .	78
5.19. Comparison of the full model and EFT cross section for $W^+W^+ \rightarrow W^+W^+$ . . . . .	80
5.20. Comparison of the full model and EFT cross section for $W^+W^- \rightarrow W^+W^-$ . . . . .	80
5.21. Polarized cross sections for the full model and for the EFT for $W^+W^+ \rightarrow W^+W^+$ . . . . .	82

5.22. Polarized cross sections for the full model and for the EFT for $W^+W^- \rightarrow W^+W^-$ . . . . .	83
5.23. Cross sections and polarized cross sections for $m = 1100$ GeV and $J = 3$ for $W^+W^- \rightarrow W^+W^-$ . . . . .	84
5.24. Cross sections for the full model for $W^+W^- \rightarrow hh$ . . . . .	86
C.1. Cross section of the full model with $m = 1100$ GeV for $W^+W^- \rightarrow ZZ$	93
C.2. Cross section of the full model with $m = 1100$ GeV for $W^+Z \rightarrow W^+Z$	93
C.3. Cross section of the full model with $m = 1100$ GeV for $ZZ \rightarrow ZZ$ . .	94
C.4. Cross section of the EFT for $m = 700$ GeV, $J = 3$ and $\lambda = 1$ for $W^+W^- \rightarrow ZZ$ . . . . .	94
C.5. Cross section of the EFT for $m = 700$ GeV, $J = 3$ and $\lambda = 1$ for $W^+Z \rightarrow W^+Z$ . . . . .	95
C.6. Cross section of the EFT for $m = 700$ GeV, $J = 3$ and $\lambda = 1$ for $ZZ \rightarrow ZZ$ . . . . .	96
C.7. Cross section of the EFT for $m = 1100$ GeV, $J = 4$ and $\lambda = 3$ for $W^+W^- \rightarrow ZZ$ . . . . .	97
C.8. Cross section of the EFT for $m = 1100$ GeV, $J = 4$ and $\lambda = 3$ for $W^+Z \rightarrow W^+Z$ . . . . .	98
C.9. Cross section of the EFT for $m = 1100$ GeV, $J = 4$ and $\lambda = 3$ for $ZZ \rightarrow ZZ$ . . . . .	99
C.10. Comparison of the full model and EFT cross section for $W^+W^- \rightarrow ZZ$	100
C.11. Comparison of the full model and EFT cross section for $W^+Z \rightarrow W^+Z$	100
C.12. Comparison of the full model and EFT cross section for $ZZ \rightarrow ZZ$ .	101
C.13. Polarized cross sections for the full model and for the EFT for $W^+W^- \rightarrow ZZ$ . . . . .	101
C.14. Polarized cross sections for the full model and for the EFT for $W^+Z \rightarrow W^+Z$ . . . . .	102
C.15. Polarized cross sections for the full model and for the EFT for $ZZ \rightarrow ZZ$	102

# List of Tables

3.1.	Mass splitting of minimal dark matter models for different hypercharges and heavy masses . . . . .	20
3.2.	Mass splitting of the mass eigenstate multiplets for $m_\psi = 700$ GeV, $\lambda = 1$ and $J = 3$ . . . . .	22
4.1.	Wilson coefficients for dimensions $d=2$ and $d=4$ showing the $m^0$ and $m^2$ terms. . . . .	48
4.2.	Wilson coefficients for dimensions $d=2$ , $d=4$ and $d=6$ for $J = 3$ and $J = 4$ . Only the $\frac{1}{m^2}$ and $\frac{1}{m^4}$ are shown. . . . .	51
4.3.	Wilson coefficients for dimensions $d=8$ , for operators with four, six or eight higgs fields for $J = 3$ and $J = 4$ . . . . .	52
4.4.	Wilson coefficients for dimensions $d=8$ , for operators with two higgs fields for $J = 3$ and $J = 4$ . . . . .	53
4.5.	Wilson coefficients for dimensions $d=8$ , for operators with no higgs fields for $J = 3$ and $J = 4$ . . . . .	54
4.6.	Limits on Wilson coefficients from anomalous higgs couplings [2] (one sigma), aTGC [3] (95% CL) and aQGC [4] (95% CL) compared with the coefficients for the model for two sets of parameters. Setup 1: $m = 700$ GeV, $J = 3$ , $\lambda = 1$ ; setup 2: $m = 1100$ GeV, $J = 4$ , $\lambda = 3$ . . . . .	54
5.1.	Values for the $pp \rightarrow \gamma^*/Z \rightarrow \mu^+\mu^-$ cross section for different virtualities	62
5.2.	Comparison of aTGC limits with expected values . . . . .	65
5.3.	Comparison of limits on anomalous higgs couplings with expected values	66



# 1. Introduction

The discovery of a Standard Model-like Higgs boson at the Large Hadron Collider (LHC) in 2012 [5, 6] marked the end of a decades-long search and is one of the most important confirmations of the Standard Model of particles physics. Ten years later with LHC run 3 on the way the LHC is closing in on  $300 \text{ fb}^{-1}$  of data [7] with ten times more expected for the High-Luminosity LHC [8]. This amount of data allows studying the structure of the SM to an unprecedented precision in channels that were inaccessible before. With early data confirming the presence of electroweak  $pp \rightarrow VVjj$  signals [9, 10] vector boson scattering processes (VBS) have become more and more important in probing the dynamics of electroweak symmetry breaking. While anomalous triple gauge boson couplings (aTGC) could already be probed at LEP [11, 12, 13, 14], VBS opens up the possibility of studying deviations from the SM in the form of anomalous quartic gauge couplings (aQGC). These aTGC and aQGC can be parameterized in a model independent way using the framework of effective field theories and operators of dimension  $d = 6$  and  $d = 8$  [15, 16, 17, 18], which are suppressed by the energy scale of the new physics they describe. As dimension 8 operators are suppressed by  $\frac{1}{\Lambda_{NP}^4}$ , compared to the suppression of  $\frac{1}{\Lambda_{NP}^2}$  for dimension 6 operators, one would naively expect effects of new physics to arise first in dimension 6 operators and only afterwards in dimension 8.

In a previous study [19] a model has been proposed that is capable of producing an EFT that is dominated by the so called T-operators, which parameterize aQGC for transverse scattering at dimension 8. However, for the M-operators, which parameterize aQGC for the scattering of two transverse and two longitudinal vector bosons at dimension 8, no such model has been proposed. Within this theses a very general class of models, that is theoretically able to produce M-operators in their corresponding EFT, is studied.

The first part of this thesis (chapter 2) lays the theoretical foundations for this thesis and introduces the relevant notations. A short overview over the SM is given (section 2.1) followed by an introduction to effective field theories (section 2.2). In section 2.3 the basic idea of the Passarino-Veltman-Reduction is introduced, as contributions by the proposed model firstly appear at one loop level. The chapter is finished by a brief description of the kinematics for two to two processes in section 2.4

In chapter 3 the proposed class of models is introduced starting with the model itself in section 3.1 followed by the discussion of the resulting one loop contributions (3.2.1) and the required renormalization (3.2.2). This chapter is concluded by a brief discussion on related models (3.3). Chapter 4 is dedicated to the EFT and contains a comparison between general and dedicated EFT bases (4.1). Afterward a dedicated basis of dimension 6 and dimension 8 operators is constructed (4.2) and the matching procedure to the proposed model is explained (4.3).

With the model and its EFT having been described the effects of them on dilepton production (5.1 and 5.2), on anomalous triple gauge couplings and on anomalous higgs couplings (5.3 and 5.4), and on VBS and higgs pair production (5.5) are presented and compared. This is followed by a summary and conclusion in chapter 6.

## 2. Theoretical Background and Notation

The model proposed in this thesis is an extension of the standard model (SM) of particle physics. In order to introduce the definitions and notations used throughout this thesis a short introduction to the SM, its symmetries, particles and its Lagrangian is given followed by a brief summary about effective field theories, one-loop integrals and the kinematics of two to two processes.

### 2.1. The Standard Model

The Standard Model of Particle Physics is a Lorentz invariant gauge theory that describes the elementary particles and their interactions under the strong, the weak and the electromagnetic interaction. These interactions are mediated by different gauge bosons with the eight gluons mediating the strong, the three massive vector bosons ( $Z$ ,  $W^\pm$ ) mediating the weak, and the massless vector boson ( $\gamma$ ) mediating the electromagnetic interaction. Its particle content is further made up of three families of leptons and quarks and the scalar Higgs boson. The masses of the SM particles are generated via the breaking of the electroweak symmetry due to a non-zero vacuum expectation value  $\hat{v}$  of the scalar Higgs field ( $h$ ).

#### 2.1.1. Symmetries and Quantum Numbers

As a gauge theory, the SM is a field theory with a Lagrangian that is invariant under local gauge transformations. The gauge group of the SM is a product of three gauge groups

$$SU(3)_C \times SU(2)_L \times U(1)_Y. \quad (2.1)$$

The gauge group of the strong interaction,  $SU(3)_C$ , is a special unitary group of degree three with the associated charge: "color". Its corresponding Lie-Algebra is made up of eight generators ( $T^a$ ). Therefore, there are eight mediators of the strong interactions, namely the gluons with the corresponding gauge fields  $G_\mu^a$ ,  $a = 1, \dots, 8$ . The field strength tensor is given as

$$G_{\mu\nu}^a = \partial_\mu G_\nu^a - \partial_\nu G_\mu^a - g_s f^{abc} G_\mu^b G_\nu^c \quad (2.2)$$

using the strong gauge coupling parameter  $g_s$  and the structure constants of the group  $f^{abc}$  which satisfy the commutator relation

$$[T^a, T^b] = i f^{abc} T^c. \quad (2.3)$$

The covariant derivative acting on a quark field  $q$  is given as

$$D_\mu q = \left( \partial_\mu + ig_s G_\mu^a T^a \right) q \quad (2.4)$$

The electromagnetic interaction and the weak interaction are unified into the electroweak interaction. Its gauge group,  $SU(2)_L \times U(1)_Y$  is a product of  $U(1)_Y$ , which is a unitary group with the associated charge  $Y$  (weak hypercharge), and the  $SU(2)_L$ , which is a special unitary group with degree two. Here, the index  $L$  stands for the property of the weak interaction only to couple to left-handed particles (or right-handed antiparticles). The mediated charge of the gauge group  $SU(2)_L$  is the weak isospin  $J$ . The gauge fields of the  $SU(2)_L$  are  $W_\mu^i$ ,  $i = 1, 2, 3$  and the gauge field of the gauge group  $U(1)_Y$  is  $B_\mu$ . The corresponding field strength tensors are defined as

$$W_{\mu\nu}^I = \partial_\mu W_\nu^I - \partial_\nu W_\mu^I - g\epsilon^{IJK} W_\mu^J W_\nu^K \quad (2.5)$$

$$B_{\mu\nu} = \partial_\mu B_\nu - \partial_\nu B_\mu \quad (2.6)$$

and the covariant derivatives acting on a field that doesn't trivially transform under the groups are given as

$$D_\mu \Psi = \left( \partial_\mu + ig W_\mu^I T^I \right) \Psi \quad (2.7)$$

$$D_\mu \Psi = \left( \partial_\mu + ig' Y B_\mu \right) \Psi. \quad (2.8)$$

Here  $\epsilon^{IJK}$  is the completely anti-symmetric tensor and  $T^I$  are the generators of the  $SU(2)_L$ . For the fundamental representation of  $SU(2)_L$  the generators are connected to the Pauli matrices  $\tau^I$  via

$$T^I = \frac{\tau^I}{2}. \quad (2.9)$$

The covariant derivatives of the field strength tensors are

$$(D_\rho W_{\mu\nu})^I = \partial_\rho W_{\mu\nu}^I - g\epsilon^{IJK} W_\rho^J W_{\mu\nu}^K, \quad (2.10)$$

$$D_\rho B_{\mu\nu} = \partial_\rho B_{\mu\nu}. \quad (2.11)$$

After electroweak symmetry breaking these fields mix and some of them receive a non vanishing mass. The mass eigenstates after electroweak symmetry breaking are identified as  $A_\mu$ ,  $Z_\mu$ , and  $W_\mu^\pm$ .

### 2.1.2. Particle Content

The transformation properties of the particle fields are determined by their quantum numbers and the representation of the group to which they belong. Denoting the quantum numbers in terms of  $(\mathbf{r}_{SU(3)_C}, \mathbf{r}_{SU(2)_L})_Y$  the quantum numbers of the leptons are given by

$$L^f = (\mathbf{1}, \mathbf{2})_{-1/2} = \begin{pmatrix} \nu_L^f \\ l_L^f \end{pmatrix} \quad (2.12)$$

$$l_R^f = (\mathbf{1}, \mathbf{1})_{-1} \quad (2.13)$$

$$f = e, \mu, \tau, \quad (2.14)$$

with  $L$  and  $R$  being the index for the left- and right-handed particles. The quantum numbers of the quarks are given by

$$Q_L^f = (\mathbf{3}, \mathbf{2})_{1/6} = \begin{pmatrix} u_L^f \\ d_L^f \end{pmatrix} \quad (2.15)$$

$$u_R^f = (\mathbf{3}, \mathbf{1})_{2/3} \quad d_R^f = (\mathbf{3}, \mathbf{1})_{-1/3} \quad (2.16)$$

$$f = \begin{pmatrix} u & c & t \\ d & s & b \end{pmatrix}. \quad (2.17)$$

Due to the chiral nature of the weak interaction, it is impossible to construct mass terms of the form

$$m\bar{\psi}\psi = m(\bar{\psi}_L\psi_R + \bar{\psi}_R\psi_L), \quad (2.18)$$

since these would not be invariant under gauge transformations. Similarly mass terms for the gauge bosons can not be constructed since they would break the  $SU(2)_L \times U(1)_Y$  gauge symmetry of the Lagrangian.

A way to generate masses is the introduction of the scalar Higgs field  $h$  within a  $SU(2)$  doublet  $\Phi$  with a non vanishing expectation value  $\hat{v}$  [20, 21]. The corresponding Lagrangian reads

$$\mathcal{L}_H = (D_\mu\Phi)^\dagger D^\mu\Phi - V(\Phi), \quad (2.19)$$

$$V(h) = \mu^2\Phi^\dagger\Phi + \lambda_h(\Phi^\dagger\Phi)^2 \quad (2.20)$$

Choosing  $\mu^2 < 0$  and  $\lambda > 0$  yields a non vanishing expectation value  $\hat{v}$  of the field  $\Phi$

$$\hat{v}^2 = \frac{-\mu^2}{\lambda_h} \quad (2.21)$$

and the physical field can be expanded around its vacuum as

$$\Phi = \begin{pmatrix} \varphi^+ \\ \frac{\hat{v}+h+i\varphi_Z}{\sqrt{2}} \end{pmatrix}. \quad (2.22)$$

This leads to a spontaneous breaking of the electroweak symmetry group

$$SU(2)_L \times U(1)_Y \rightarrow U(1)_{em} \quad (2.23)$$

at the scale of the energy  $\hat{v}$ . The charge of this group is the electric charge

$$Q = T_3 + Y \quad (2.24)$$

which is the sum of the third component of the isospin and the hypercharge. According to the Goldstone Theorem, breaking  $SU(2)_L \times U(1)_Y$  to a  $U(1)_{em}$  leads to three Goldstone bosons. These Goldstone bosons become the longitudinal degree of freedom of their corresponding weak gauge fields. These three gauge fields now acquire a mass. The corresponding mass term in the Lagrangian stems from the kinetic term for the Higgs field when inserting the non-zero vacuum expectation value

$$\mathcal{L}_{mass} = \frac{\hat{v}^2}{2} \left( (gW_\mu^1)^2 + (gW_\mu^2)^2 + (gW_\mu^3 - g'B_\mu)^2 \right). \quad (2.25)$$

The charge and mass eigenstates of the electroweak gauge bosons after symmetry breaking are given by

$$W_\mu^\pm = \frac{1}{\sqrt{2}}(W_\mu^1 \mp iW_\mu^2) \quad (2.26)$$

$$Z_\mu = \cos(\theta_w)W_\mu^3 - \sin(\theta_w)B_\mu \quad (2.27)$$

$$A_\mu = \sin(\theta_w)W_\mu^3 + \cos(\theta_w)B_\mu \quad (2.28)$$

$$\tan(\theta_w) = \frac{g'}{g}, \quad (2.29)$$

where  $\theta_w$  is the weak mixing angle (Weinberg angle). The masses of the four gauge bosons and the Higgs boson are

$$m_h^2 = -2\mu^2, \quad (2.30)$$

$$m_W = \frac{g\hat{v}}{2}, \quad (2.31)$$

$$m_Z = \frac{m_W}{\cos(\theta_w)}. \quad (2.32)$$

Finally the masses of the fermions are generated as interaction terms between right-handed and left-handed fields as terms of the form

$$\overline{L^f} Y_f \phi l_R^f + \text{h.c.} . \quad (2.33)$$

Here the  $SU(2)_L$  singlet  $l_R^f$  couples via the Higgs field, which is a  $SU(2)_L$  doublet, to the  $SU(2)_L$  doublet  $\overline{L^f}$ . As a whole this generates a  $SU(2)_L$  singlet which is therefore invariant under gauge transformations.  $Y_f$  is the Yukawa coupling which is in general a  $3 \times 3$  matrix in flavor space.

The linear realization is however not the only way to describe the Higgs/electroweak breaking sector that generates masses. In a non linear realization of the Higgs sector [22, 23] a similar Lagrangian can be constructed which contains additional degrees of freedom for the Higgs boson interactions and therefore introduces additional free parameters. However, measurement of Higgs couplings do not show any deviation from the prediction of the linear representation.

### 2.1.3. The SM Lagrangian

With all fields, field strength tensors and covariant derivative defined the Lagrangian of the standard model is given as

$$\mathcal{L}_{\text{Gauge}} = -\frac{1}{4}G_{\mu\nu}^a G^{a\mu\nu} - \frac{1}{4}W_{\mu\nu}^I W^{I\mu\nu} - \frac{1}{4}B_{\mu\nu} B^{\mu\nu}, \quad (2.34)$$

$$\mathcal{L}_{\text{Fermion}} = i\overline{Q}\not{D}Q + i\overline{u}\not{D}u + i\overline{d}\not{D}d + i\overline{L}\not{D}L + i\overline{l}\not{D}l, \quad (2.35)$$

$$\mathcal{L}_{\text{Higgs}} = (D_\mu\phi)^\dagger D^\mu\phi - \mu^2\phi^\dagger\phi - \lambda_h(\phi^\dagger\phi)^2, \quad (2.36)$$

$$\mathcal{L}_{\text{Yukawa}} = -\overline{L}Y_f\phi l - \overline{Q}Y_u\tilde{\phi}u - \overline{Q}Y_d\phi d + \text{h.c.} . \quad (2.37)$$

The last definition needed based on the SM Lagrangian are the equations of motion for the gauge bosons and the Higgs boson

$$(D^\mu D_\mu \phi)^j = -\mu^2 \phi^j - 2\lambda_h (\phi^\dagger \phi) \phi^j - \bar{l} Y_f^\dagger L^j - i\sigma_2^{j,k} \bar{Q}^k Y_u u - \bar{d} Y_d^\dagger Q^j \quad (2.38)$$

$$(D^\nu W_{\nu\mu})^I = \phi^\dagger \frac{ig\tau^I}{2} D_\mu \phi - (D_\mu \phi)^\dagger \frac{ig\tau^I}{2} \phi + \bar{Q} \gamma_\mu \frac{g\tau^I}{2} Q + \bar{L} \gamma_\mu \frac{g\tau^I}{2} L \quad (2.39)$$

$$\partial^\nu B_{\nu\mu} = \phi^\dagger ig' Y_\phi D_\mu \phi - (D_\mu \phi)^\dagger ig' Y_\phi \phi + g' \bar{\Psi} \gamma_\mu Y_\Psi \Psi \quad (2.40)$$

$$(D^\nu G_{\nu\mu})^a = \bar{Q} \gamma_\mu g_s T^a Q + \bar{u} \gamma_\mu g_s T^a u + \bar{d} \gamma_\mu g_s T^a d \quad (2.41)$$

## 2.2. Effective Field Theories

An effective field theory is an approximation of an underlying field theory at a given scale. It describes the effects of the underlying theory at this scale but breaks down once its finite range of validity is reached. There are two main approaches to build up such an effective theory, the "top-down" approach and the "bottom-up" approach.

- "top-down": For the top-down approach the underlying theory needs to be known. It is used when a solution for a given problem is only needed at a certain scale and the computation of the solution with the whole theory is impractical. A non field theory example of an effective theory would be the multipole expansion for multibody dynamics in electromagnetism. The precision of top-down theories is impacted by the order up to which the expansion is made.
- "bottom-up": For the bottom-up approach the theory is only known at a certain scale but unknown beyond it. The effective theory is built using the elements of the known theory (e.g. particles, symmetries etc.) and tries to parametrize the physics beyond this scale. An important historical example of a bottom-up theory is the Fermi-theory [24]. This theory postulates a four fermion vertex (which is a dimension six operator) in order to explain the beta decay. This description breaks down at the scale of  $4\pi\hat{v}$  and therefore predicted new physics in the form of  $W$  bosons below that scale.

There are many open questions that are not explained by the SM like the existence of dark matter or baryogenesis. Additionally, the theory of gravitation is also not described by the SM. Therefore, the SM itself can be seen as an EFT and we expect new physics at higher scales. Therefore, it is necessary to explore the beyond the SM (BSM) sector. To do so there are mainly two paths one may chose from. The first one is by proposing an underlying theory which includes new particles. This theory has to produce similar results as the SM in the low energy limit and explain deviation from the SM at higher energies.

Instead of proposing such an UV complete underlying theory, where the SM is embedded, a bottom-up effective field theory can be used. This kind of theory is made up by the SM particles and obeys its symmetries and properties. The following statements need to be true [25] in order for the theory to be useful to describe physics beyond the Standard Model:

- The S-matrix in the extended model respects unitarity and is analytical.
- The extended model obeys the gauge group  $SU(3)_C \times SU(2)_L \times U(1)_Y$  and is Lorentz invariant.
- The extended model is general enough to capture any BSM physics while giving guidance on where to look for and find new physics.
- Radiative corrections are possible to be calculated at any order in any interactions (SM and new) in the extended model.

Lastly one point should be added to the list of requirements for any EFT to be actually useful

- There exists a UV complete model which, up to a certain scale, is well described by the EFT

### 2.2.1. The Standard Model Effective Field Theory

The standard model effective field theory (SMEFT) is an EFT that is based on the SM. Its content is the SM and additional higher dimensional operators that are invariant under  $SU(3)_C \times SU(2)_L \times U(1)_Y$ . The building blocks for these operators are the (dual) field-strength tensors of the SM, the fermion fields of the standard model, the Higgs field, the covariant derivative as well as generators of the gauge groups and  $\gamma$ -matrices in order to fulfill lorentz and gauge invariance. The BSM effects are expected to come from massive particles that are heavier than the measured value of  $\hat{v}$ . These higher dimensional operators  $\mathcal{O}_i^{(d)}$  ( $d > 4$ ) are suppressed by a scale  $\Lambda$  to the power of  $d - 4$  and come with a Wilson coefficient  $c_i^{(d)}$ . The operators are often named according to the objects they contain, resulting in names like  $\mathcal{O}_{WWW}$  with the coefficient being written as  $c_{WWW}$  accordingly. The SMEFT Lagrangian then reads

$$\mathcal{L}_{\text{SMEFT}} = \mathcal{L}_{\text{SM}} + \sum_{d=5} \sum_i^{n(d)} \frac{c_i^{(d)}}{\Lambda^{d-4}} \mathcal{O}_i^{(d)}. \quad (2.42)$$

Since the suppression factor is a constant scale operators are only sufficiently suppressed up to that scale. Going beyond this scale the effects of the operators can continue to grow with energy and at some point break unitarity. SMEFT therefore comes with a finite range of validity.

#### 2.2.1.1. Dimension-6 Basis

The Warsaw basis [17] is a minimal set of operators that form a basis for all operators that can appear at dimension-6 using the fields and gauge symmetries of the SM. This set contains a total of 63 operators (2499 when accounting for flavor). They achieve this minimal set by grouping the operators into different classes depending on the number of field strength tensors ( $X_{\mu\nu} = \{G_{\mu\nu}^a, W_{\mu\nu}^I, B_{\mu\nu}\}$ ), derivatives, higgs fields and fermionic fields. These classes are then ordered from highest to lowest so that all transformations that are used only generate operators of the same or of a lower class. The methods used are:

- Total derivatives of gauge invariant objects give no contribution to physical effects and are therefore ignored.
- The commutator of covariant derivatives is proportional to field strength tensors  $[D_\mu, D_\nu] \sim X_{\mu\nu}$  and lead to operator classes with less derivatives.
- The EOMs can be used to reduce the number of field strength tensors at the cost of more fermionic fields or higgs fields. The number of covariant derivatives is reduced or stays the same.
- Integration by parts (IBP) can be used to move derivatives around.
- Fierz identities, the Bianchi identity, identities for products of generators as well as identities of the Dirac-algebra are used to reorder contractions of particles.
- Symmetry arguments can be used in order to discard or transform operators.

None of these methods can increase the number of covariant derivatives or reduce the number of fermionic fields, meaning an operator with more derivatives is in a higher class, while an operator with more fermionic fields is in a lower class. For operators

with the same number of derivatives and fermionic fields the EOM for the field strength tensors can allow transformations from operators with more field strength tensors to ones with more higgs fields. By applying these methods rigorously one arrives at the minimal set known as the Warsaw Basis.

Using the aforementioned methods and the ordering of classes can be more easily understood looking at two examples from [17] explicitly. For the first example one starts with the operator

$$(D_\mu D_\nu \phi)^\dagger D^\nu D^\mu \phi, \quad (2.43)$$

from the operator class  $\phi^2 D^4$  (two higgs fields and four derivatives). Firstly one can observe that changing the order of derivatives produces an operator of the same class plus an operator of a class with two derivatives less (so a lower class) and one more field strength tensor

$$(D_\mu D_\nu \phi)^\dagger D^\nu D^\mu \phi = (D_\mu D_\nu \phi)^\dagger D^\mu D^\nu \phi + \mathcal{O}(\phi^2 X D^2). \quad (2.44)$$

As this operator would be addressed later on when dealing with that class of operators it can be ignored for the moment. Next up one is free to move derivatives from one field to the other by IBP since the remaining part is a total derivative, which gives no physical effect

$$(D_\mu D_\nu \phi)^\dagger D^\nu D^\mu \phi \sim (D_\mu D_\mu \phi)^\dagger D^\nu D^\nu \phi + \mathcal{O}(\phi^2 X D^2). \quad (2.45)$$

Therefore all operators of this class are identical up to operators of a lower class. Finally one can use the EOMs (2.38) in order to get rid of this operator and therefore its whole class.

As a second example one can look at the operator class  $\phi^4 D^2$ . In general there are two possible structures for the higgs fields

$$(\phi^\dagger \phi) (\phi^\dagger \phi) \quad (2.46)$$

$$(\phi^\dagger \tau^I \phi) (\phi^\dagger \tau^I \phi) \quad (2.47)$$

and four possible places for each derivative. As many of these operators are identical to each other one can reduce the problem to the following cases

- Both derivatives act on the same field.
- Both derivatives act on unconjugated (conjugated) fields
- One derivative acts on an unconjugated and one on a conjugated field.

The first case can be ignored as EOMs can be used and one is left with operators of lower classes. For the second case one can use IBP in order to get the first or the third case. Finally one can use an identity for the generators

$$\tau_{jk}^I \tau_{lm}^I = 2\delta_{jm} \delta_{lk} - \delta_{jk} \delta_{lm}, \quad (2.48)$$

in order to get rid of all operators that originate from the structure in equation (2.47). One finally arrives at the operators

$$(\phi^\dagger D_\mu \phi) ((D^\mu \phi^\dagger) \phi) \quad (2.49)$$

$$((D^\mu \phi^\dagger) D_\mu \phi) (\phi^\dagger \phi), \quad (2.50)$$

which can then be rewritten in terms of the two operators that are used in the Warsaw Basis.

### 2.2.1.2. Dimension-8 Basis

At dimension-8 in theory the same procedure as for the Warsaw Basis at dimension-6 can be applied. The operator classes that contain no fermions are still small enough to do so by hand since they contain a total of 89 operators [26]. As there are 1030 operators (44807 when accounting for flavor) in total one can easily see that the operator classes with fermions are a lot larger than at dimension-6. In [26] a procedure to produce all of these operators is shown. A slightly different and more formal approach is presented in [27], in which operators in terms of the irreducible representation of the Lorentz group are used.

Looking at vector boson scattering the Éboli basis [18] is usually used for modeling anomalous quartic gauge couplings. The operators are grouped into three classes: operators that contain four derivatives and four higgs fields (S operators), operators that contain two derivatives, two higgs fields and two field strength tensors (M operators) and operators that contain four field strength tensors (T operators). As operators including  $B_{\mu\nu}$  will not appear later on in this thesis one can focus on the following operators

$$\mathcal{O}_{S0} = ((D_\mu\phi)^\dagger D^\nu\phi)((D_\mu\phi)^\dagger D^\nu\phi), \quad (2.51)$$

$$\mathcal{O}_{S1} = ((D_\mu\phi)^\dagger D^\mu\phi)((D_\nu\phi)^\dagger D^\nu\phi), \quad (2.52)$$

$$\mathcal{O}_{S2^*} = ((D_\mu\phi)^\dagger D^\nu\phi)((D_\nu\phi)^\dagger D^\mu\phi), \quad (2.53)$$

$$\mathcal{O}_{M0} = \frac{1}{2}(D_\alpha\phi)^\dagger D^\alpha\phi W_{\mu\nu}^I W^{I\mu\nu}, \quad (2.54)$$

$$\mathcal{O}_{M1} = \frac{1}{2}(D_\mu\phi)^\dagger D^\nu\phi W_{\nu\alpha}^I W^{I\alpha\mu}, \quad (2.55)$$

$$\mathcal{O}_{M7^{**}} = \frac{1}{2}i\epsilon_{IJK}((D_\mu\phi)^\dagger \tau^I D^\nu\phi) W_{\nu\alpha}^J W^{K\alpha\mu}, \quad (2.56)$$

$$\mathcal{O}_{T0} = \frac{1}{4}W_{\mu\nu}^I W^{I\mu\nu} W_{\alpha\beta}^J W^{J\alpha\beta}, \quad (2.57)$$

$$\mathcal{O}_{T1} = \frac{1}{4}W_{\mu\nu}^I W^{I\alpha\beta} W_{\alpha\beta}^J W^{J\mu\nu}, \quad (2.58)$$

$$\mathcal{O}_{T2} = \frac{1}{4}W_\mu^{I\nu} W_\nu^{I\alpha} W_\alpha^{J\beta} W_\beta^{J\mu}, \quad (2.59)$$

$$\mathcal{O}_{T3^*} = \frac{1}{4}W_{\mu\nu}^I W_{\alpha\beta}^I W^{J\nu\alpha} W^{J\beta\mu}. \quad (2.60)$$

The operators labeled with one star ( $\mathcal{O}_{S2^*}$  and  $\mathcal{O}_{T3^*}$ ) were missing in the original set and were added later on while redundant operators were dropped [28, 29, 30, 31, 19]. The operator  $\mathcal{O}_{M7^{**}}$  is identical to the original one but rewritten using

$$2i\epsilon_{IJK}\tau_K = [\tau_I, \tau_I]. \quad (2.61)$$

The factors of  $\frac{1}{4}$  and  $\frac{1}{2}$  stem from the trace in the original definition and the denominator of  $\frac{\tau_I}{2}$ . These operators also appear in [26] as  $\mathcal{Q}_{H^4}^{(1)}$ ,  $\mathcal{Q}_{H^4}^{(2)}$ ,  $\mathcal{Q}_{H^4}^{(3)}$  (S),  $\mathcal{Q}_{W^2H^2D^2}^{(1)}$ ,  $\mathcal{Q}_{W^2H^2D^2}^{(2)}$ ,  $\mathcal{Q}_{W^2H^2D^2}^{(4)}$  (M) and  $\mathcal{Q}_{W^4}^{(1)}$ ,  $\mathcal{Q}_{W^4}^{(2)}$ ,  $\mathcal{Q}_{W^4}^{(3)}$ ,  $\mathcal{Q}_{W^4}^{(4)}$  (T). As these are the operators that are used to constrain aQGC, they should be part of any basis describing vector boson scattering at dimension-8 level.

### 2.3. 1-Loop Integrals

When doing next-to-leading order (NLO) calculations one has to deal with one-loop diagrams. These one-loop diagrams can give contributions to existing n-point functions of the given model. When naively integrating over all possible loop momenta in four dimensions one can get into the trouble of getting UV divergences. One common way of dealing with these divergences is dimensional regularization. In dimensional regularization the integration is not performed in four space-time dimensions but in  $d = 4 - 2\epsilon$  using analytical continuation. Using this method the UV divergences appear as  $\frac{1}{\epsilon}$  poles which can be separated and renormalized.

Taking the two-point function as an example, one can write the possible one loop contributions in dimensional regularization in terms of the different tensor structures of the integral as

$$\begin{aligned}
\Pi^{\mu_1\mu_2}(p, m_0, m_1) = & c_1(p, m_0, m_1)g^{\mu_1\mu_2}\frac{\mu^{2\epsilon}}{(2\pi)^d}\int d^dk\frac{1}{(k^2+m_0^2)((k+p)^2+m_1^2)} \\
& + c_2(p, m_0, m_1)g^{\mu_1\mu_2}\frac{\mu^{2\epsilon}}{(2\pi)^d}\int d^dk\frac{k^2}{(k^2+m_0^2)((k+p)^2+m_1^2)} \\
& + c_3(p, m_0, m_1)g^{\mu_1\mu_2}p_\rho\frac{\mu^{2\epsilon}}{(2\pi)^d}\int d^dk\frac{k^\rho}{(k^2+m_0^2)((k+p)^2+m_1^2)} \\
& + c_4(p, m_0, m_1)p^{\mu_1}\frac{\mu^{2\epsilon}}{(2\pi)^d}\int d^dk\frac{k^{\mu_2}}{(k^2+m_0^2)((k+p)^2+m_1^2)} \\
& + c_5(p, m_0, m_1)p^{\mu_2}\frac{\mu^{2\epsilon}}{(2\pi)^d}\int d^dk\frac{k^{\mu_1}}{(k^2+m_0^2)((k+p)^2+m_1^2)} \\
& + c_6(p, m_0, m_1)p^{\mu_1}p^{\mu_2}\frac{\mu^{2\epsilon}}{(2\pi)^d}\int d^dk\frac{1}{(k^2+m_0^2)((k+p)^2+m_1^2)} \\
& + c_7(p, m_0, m_1)\frac{\mu^{2\epsilon}}{(2\pi)^d}\int d^dk\frac{k^{\mu_1}k^{\mu_2}}{(k^2+m_0^2)((k+p)^2+m_1^2)}. \quad (2.62)
\end{aligned}$$

Here  $\mu$  is the renormalization scale that is introduced so that the energy dimension stays unchanged

$$[d^4k] = [d^dk \cdot \mu^{2\epsilon}]. \quad (2.63)$$

In order to calculate the two point function one can use the fact that the tensor integrals can be written as

$$\int d^dk\frac{k^{\mu_1}k^{\mu_2}}{(k^2+m_0^2)((k+p)^2+m_1^2)} = C_{2,00}g^{\mu_1\mu_2} + C_{2,11}p^{\mu_1}p^{\mu_2} \quad (2.64)$$

$$\int d^dk\frac{k^{\mu_1}}{(k^2+m_0^2)((k+p)^2+m_1^2)} = C_{2,1}p^{\mu_1} \quad (2.65)$$

as these are the only possible lorentz structures.

Starting with equation (2.65) one can multiply both sides with  $p_{\mu_1}$  and get

$$\begin{aligned}
C_{2,1} &= \frac{1}{p^2} \int d^d k \frac{p \cdot k}{(k^2 + m_0^2)((k+p)^2 + m_1^2)} \\
&= \frac{1}{p^2} \int d^d k \frac{\frac{1}{2}((k+p)^2 + m_1^2 - k^2 - m_0^2 + m_0^2 - p^2 - m_1^2)}{(k^2 + m_0^2)((k+p)^2 + m_1^2)} \\
&= \frac{1}{p^2} \int d^d k \frac{1}{2(k^2 + m_0^2)} \\
&\quad - \frac{1}{p^2} \int d^d k \frac{1}{2((k+p)^2 + m_1^2)} \\
&\quad + \frac{m_0^2 - p^2 - m_1^2}{p^2} \int d^d k \frac{1}{2(k^2 + m_0^2)((k+p)^2 + m_1^2)} \tag{2.66}
\end{aligned}$$

$$\tag{2.67}$$

where all integrals are scalar and have no numerator left. In a similar vein one can multiply equation (2.64) with  $g_{\mu_1 \mu_2}$  and  $p_{\mu_1}$  and generate a set of two equations with only scalar integrals.

This implies that only two scalar master integrals need to be calculated

$$\int d^d k \frac{1}{(k^2 + m_0^2)} \tag{2.68}$$

$$\int d^d k \frac{1}{(k^2 + m_0^2)((k+p)^2 + m_1^2)}. \tag{2.69}$$

This reduction of tensor integrals down to scalar integrals is known as Passarino-Veltman-Reduction [32][33] and can be generalized to tensor integrals

$$T^{\mu_1 \mu_2 \dots \mu_n} = \int \frac{k^{\mu_1} k^{\mu_2} \dots k^{\mu_n}}{(k^2 - m_0^2)(k + q_1)^2 - m_1^2 \dots (k + q_{n-1})^2 - m_{n-1}^2}. \tag{2.70}$$

that can arise from loops with  $n$  external legs like figure 2.1. By multiplying with an external momentum, which is the difference of the momenta in the adjacent propagators

$$p_j^{\mu_k} = q_j^{\mu_k} - q_{j-1}^{\mu_k} \tag{2.71}$$

one can use

$$k \cdot p_j = \frac{1}{2} \left( ((k + q_j)^2 - m_j^2) - ((k + q_{j-1})^2 - m_{j-1}^2) + m_j^2 - m_{j-1}^2 - q_j^2 + q_{j-1}^2 \right) \tag{2.72}$$

to produce either tensor integrals with one less loop momentum in the numerator or tensor integrals with one less momentum in the numerator and one less propagator in the denominator. Doing this for all external momenta and metric tensors one gets a linear set of equations that one can solve for the coefficients of the decomposition. Within this thesis  $n$ -point functions up to  $n = 4$  are studied, which requires the decomposition of tensor functions with rank of up to four. The decomposition can be found in the appendix (section A). The remaining scalar coefficients can be expressed in terms of four scalar functions in total. Following the conventions used for the analytical (Package-X[34]) and numerical (LoopTools [35]) calculations these scalar

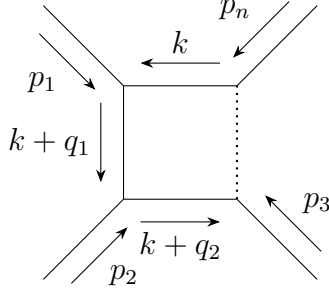


**Figure 2.1.:** Example of a one-loop diagram, created using [1]

functions are

$$A_0(m) = \frac{(2\pi\mu)^{4-d}}{i\pi^2} \int \frac{d^d k}{(k^2 - m^2)} \quad (2.73)$$

$$B_0(p, m_0, m_1) = \frac{(2\pi\mu)^{4-d}}{i\pi^2} \int \frac{d^d k}{(k^2 - m_0^2)((k+p)^2 - m_1^2)} \quad (2.74)$$

$$C_0(p_i, m_i) = \frac{(2\pi\mu)^{4-d}}{i\pi^2} \int \frac{d^d k}{(k^2 - m_0^2)((k+q_1)^2 - m_1^2)(k+q_2)^2 - m_2^2)} \quad (2.75)$$

$$D_0(p_i, m_i) = \frac{(2\pi\mu)^{4-d}}{i\pi^2} \int \frac{d^d k}{(k^2 - m_0^2)(k+q_1)^2 - m_1^2)(k+q_2)^2 - m_2^2)(k+q_3)^2 - m_3^2)} \quad (2.76)$$

$$q_j = \sum_{i=1}^j p_i \quad (2.77)$$

These scalar functions can explicitly be calculated using Feynman parametrization, Wick rotation and d-dimensional spherical coordinates, which can be found in many quantum field theory textbooks (e.g. [36]).

## 2.4. Kinematics

Within this thesis at multiple points cross sections need to be calculated, for which it is necessary to understand the underlying kinematics. The notations and later the implementations for this follow the ones used for the particle data group review [37]. In general the cross section for a two to n process can be written as

$$d\sigma = \frac{(2\pi)^4}{4\sqrt{(p_1 p_2)^2 - m_1^2 m_2^2}} |\mathcal{M}|^2 d\Phi_n \quad (2.78)$$

where  $\mathcal{M}$  is the matrix element for the process and  $\Phi_n$  the final particles phase space. As all cross sections within this thesis are for  $2 \rightarrow 2$  processes, the integration over the final state phase space can be simplified to

$$d\sigma = \frac{1}{64\pi s |p_{1,\text{cm}}|^2} |\mathcal{M}|^2 dt, \quad (2.79)$$

using the Mandelstam variables

$$s = (p_1 + p_2)^2 \quad (2.80)$$

$$t = (p_1 - p_3)^2 \quad (2.81)$$

$$u = (p_1 - p_4)^2 \quad (2.82)$$

$$(2.83)$$

The Mandelstam variables are connected to the masses of the four particles  $m_i$  via

$$s + t + u = \sum_i m_i^2 \quad (2.84)$$



## 3. Model

### 3.1. Defining the Model

The purpose of this thesis is studying models that can produce an EFT with significantly large M-operators at dimension-8 (e.g.  $\mathcal{O}_{M0}$ ). Historically EFT operators that include field strength tensors could be achieved by integrating out heavy charged particles that introduced correction at the loop level [38]. Dominant dimension-8 operators containing field strength tensors have been shown to be achievable [19] by introducing heavy  $SU(2)_L$  multiplets of fermions (or scalars) with large isospin  $J$  which lays the foundation for this work. From this previous work one can also get the first restriction for the isospin,  $J \leq 4$ , as larger values can break partial wave unitarity. These models coincide with a class of minimal dark matter models presented in [39].

#### 3.1.1. Particle Content and Lagrangian

Starting with one multiplet of  $2J + 1$  non-chiral Dirac fermions  $\Psi$ , that transforms under a  $SU(2)_L$  representation defined by the multiplet's isospin  $J$  with a mass of  $m_\Psi$ , one can generate the additional Lagrangian as

$$\mathcal{L}_\Psi = \bar{\Psi}_J^{Y=0} \not{D} \Psi_J^{Y=0} - m_\Psi \bar{\Psi}_J^{Y=0} \Psi_J^{Y=0}. \quad (3.1)$$

In order to generate M-operators this multiplet needs to couple to the higgs field. The higgs boson appears in a  $J = \frac{1}{2}$  multiplet with  $m_J = -\frac{1}{2}$  and hypercharge  $Y = \frac{1}{2}$ . When looking for states that can couple to  $\Psi_{j,m}^{Y=0}$  via the higgs boson the following particles are possible

$$\Psi_{j \pm \frac{1}{2}, m \pm \frac{1}{2}}^{Y = \frac{1}{2}}. \quad (3.2)$$

The coupling term in the Lagrangian would then be

$$\lambda \bar{\Psi}_j^{Y=0} \Phi \Psi_{j \pm 1/2}^{Y=-1/2} + h.c. \quad (3.3)$$

where  $\lambda$  is the Yukawa-like coupling coefficient, that is chosen as real since a complex phase can be absorbed in the fields. In a similar vein one can also couple to a second multiplet via the complex conjugate of the higgs field ( $m_J = \frac{1}{2}$ ,  $Y = \frac{1}{2}$ )

$$\tilde{\phi} = i\sigma_2 \Phi^* \quad (3.4)$$

resulting in a second possible term in the Lagrangian

$$\lambda \bar{\Psi}_j^{Y=0} \tilde{\Phi} \Psi_{j \pm 1/2}^{Y=1/2} + h.c. \quad (3.5)$$

In terms of isospin one is looking at tensor products

$$\langle J, m_j | J \pm 1/2, m_j + 1/2; 1/2, -1/2 \rangle, \quad (3.6)$$

$$\langle J, m_j | J \pm 1/2, m_j - 1/2; 1/2, +1/2 \rangle, \quad (3.7)$$

due to the  $J \pm 1/2$  multiplet coupling via the higgs field ( $J = 1/2$ ) to the  $J$  multiplet. These resulting coefficients are the Clebsch-Gordon coefficients.

When only one additional multiplet is present either the particle with the highest or lowest electrical charge has no partner from the other multiplet to couple to. The problems that this can cause will be presented in section 3.3. By adding two multiplets with the same isospin and opposite hypercharge the model is again symmetric under  $Q \rightarrow -Q$  and these possible problems can be avoided. The remaining decision is therefore whether to add the  $J + 1/2$ -,  $J - 1/2$ - or all multiplets. The simplest model is just adding one of these sets and throughout this thesis the  $J - 1/2$  multiplets are chosen.

With this decision done the coupling term of the multiplets for the particles with an electric charge  $Q = m_j + 0$  can explicitly be written out as

$$\begin{pmatrix} \bar{\Psi}_{m_j+1/2}^{Y=-1/2} \\ \bar{\Psi}_{m_j}^{Y=0} \\ \bar{\Psi}_{m_j-1/2}^{Y=1/2} \end{pmatrix}^T \begin{pmatrix} 0 & \lambda_1 \frac{\hat{v}+h}{\sqrt{2}} c_-(J, m_j) & 0 \\ \lambda_1 \frac{\hat{v}+h}{\sqrt{2}} c_-(J, m_j) & 0 & \lambda_2 \frac{\hat{v}+h}{\sqrt{2}} c_+(J, m_j) \\ 0 & \lambda_2 \frac{\hat{v}+h}{\sqrt{2}} c_+(J, m_j) & 0 \end{pmatrix} \begin{pmatrix} \Psi_{m_j+1/2}^{Y=-1/2} \\ \Psi_{m_j}^{Y=0} \\ \Psi_{m_j-1/2}^{Y=1/2} \end{pmatrix} \quad (3.8)$$

$$c_-(J, m_j) = \langle J, m_j | J - 1/2, m_j + 1/2; 1/2, -1/2 \rangle = \sqrt{\frac{J - m_j}{2J}}, \quad (3.9)$$

$$c_+(J, m_j) = \langle J, m_j | J - 1/2, m_j - 1/2; 1/2, +1/2 \rangle = \sqrt{\frac{J + m_j}{2J}}, \quad (3.10)$$

where  $c_{\pm}$  are the Clebsch-Gordon coefficients. Starting with equal masses for all multiplets and identical couplings  $\lambda_1 = \lambda_2 = \lambda$ , the additional Lagrangian reads

$$\begin{aligned} \mathcal{L}_{\Psi} = & \bar{\Psi}_j^{Y=0} \not{D} \Psi_j^{Y=0} - m_{\Psi} \bar{\Psi}_j^{Y=0} \Psi_j^{Y=0} \\ & + \bar{\Psi}_{j-1/2}^{Y=-1/2} \not{D} \Psi_{j-1/2}^{Y=-1/2} - m_{\Psi} \bar{\Psi}_{j-1/2}^{Y=-1/2} \Psi_{j-1/2}^{Y=-1/2} \\ & + \bar{\Psi}_{j-1/2}^{Y=1/2} \not{D} \Psi_{j-1/2}^{Y=1/2} - m_{\Psi} \bar{\Psi}_{j-1/2}^{Y=1/2} \Psi_{j-1/2}^{Y=1/2} \\ & + \lambda \bar{\Psi}_j^{Y=0} \Phi \Psi_{j-1/2}^{Y=-1/2} + \lambda \bar{\Psi}_j^{Y=0} \tilde{\Phi} \Psi_{j-1/2}^{Y=1/2} + h.c. \end{aligned} \quad (3.11)$$

Using the same logic as before, one is also free to add multiplets with  $j - 1$  and  $Y \in \{-1, 0, 1\}$  or multiplets with isospin  $j$  and  $Y = \pm 1$  that couple to the  $j - \frac{1}{2}$  multiplets. As none of these additional multiplets change the fundamental phenomenology of the model one can restrict oneself to the three multiplets in equation (3.11). One is also free to add a constant offset  $\Delta Y$  to the hypercharge of all three multiplets which can be used to enhance the U(1) coupling, which however is not the goal of this thesis. A brief discussion of the influence of choosing different masses for each multiplet, choosing different couplings for the two additional multiplets or adding an axial coupling to the higgs field can be found in section 3.3.

### 3.1.2. Mass Eigenstates

Due to the mixing of the different multiplets via the higgs field, one can observe shifts in the masses after spontaneous symmetry breaking. The mass matrix for the

fermions for a given isospin  $J$  and its third component  $m_j$  then read

$$\begin{aligned} \begin{pmatrix} \bar{\Psi}_{m_j+1/2}^{Y=-1/2} \\ \bar{\Psi}_{m_j}^{Y=0} \\ \bar{\Psi}_{m_j-1/2}^{Y=1/2} \end{pmatrix}^T & \begin{pmatrix} m_\Psi & \lambda \frac{\hat{v}}{\sqrt{2}} c_-(J, m_j) & 0 \\ \lambda \frac{\hat{v}}{\sqrt{2}} c_-(J, m_j) & m_\Psi & \lambda \frac{\hat{v}}{\sqrt{2}} c_+(J, m_j) \\ 0 & \lambda \frac{\hat{v}}{\sqrt{2}} c_+(J, m_j) & m_\Psi \end{pmatrix} \begin{pmatrix} \Psi_{m_j+1/2}^{Y=0-1/2} \\ \Psi_{m_j}^{Y=0} \\ \Psi_{m_j-1/2}^{Y=0+1/2} \end{pmatrix} \\ & = \begin{pmatrix} \bar{\chi}_1 \\ \bar{\chi}_2 \\ \bar{\chi}_3 \end{pmatrix}^T U^{-1} U \begin{pmatrix} m_{\chi_1} & 0 & 0 \\ 0 & m_{\chi_2} & 0 \\ 0 & 0 & m_{\chi_3} \end{pmatrix} U^{-1} U \begin{pmatrix} \chi_1 \\ \chi_2 \\ \chi_3 \end{pmatrix}, \end{aligned} \quad (3.12)$$

with the Clebsch-Gordon coefficients from eq. (3.9) and (3.10). The mass matrices for  $m_j = J$  and  $m_j = -J$  are only 2x2 matrices as either the first or the last state doesn't exist due to  $m_j + \frac{1}{2} > J$  or  $m_j - \frac{1}{2} < -J$ . Otherwise they have a similar form. From this one can now read off the masses of the new eigenstates

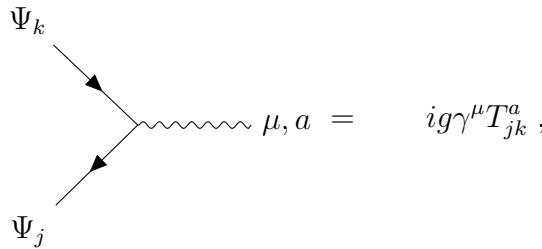
$$m_{\chi_1} = m_\Psi, \quad (3.13)$$

$$m_{\chi_2} = m_\Psi - \frac{1}{\sqrt{2}} \lambda \hat{v}, \quad (3.14)$$

$$m_{\chi_3} = m_\Psi + \frac{1}{\sqrt{2}} \lambda \hat{v}, \quad (3.15)$$

$$\chi_1^{m=j} = \chi_1^{m=-j} = 0, \quad (3.16)$$

and order them in two multiplets with  $2J + 1$  ( $\chi_2$  and  $\chi_3$ ) particles and one with  $2J - 1$  particles ( $\chi_1$ ). As expected in this basis the coupling to the higgs boson is now diagonal. The coupling to the vector bosons however is not. Starting with a vector boson  $W_\mu^a$  coupling to two fermions  $\Psi_j, \Psi_k$



$$\begin{array}{c} \Psi_k \\ \searrow \\ \text{---} \mu, a = ig\gamma^\mu T_{jk}^a \\ \nearrow \\ \Psi_j \end{array} \quad (3.17)$$

one can calculate the corresponding feynman rule after mixing as

$$\chi_j = j_1 \Psi_{1,j} + j_2 \Psi_{2,j} + j_3 \Psi_{3,j}, \quad (3.18)$$

$$\chi_k = k_1 \Psi_{1,k} + k_2 \Psi_{2,k} + k_3 \Psi_{3,k}, \quad (3.19)$$

$$\begin{aligned} \Gamma_{jka}^\mu &= ig\gamma^\mu (j_1 k_1 T_{1,jk}^a + j_2 k_2 T_{2,jk}^a + j_3 k_3 T_{3,jk}^a) \\ &= ig\gamma^\mu \mathcal{T}_{jk}^a. \end{aligned} \quad (3.20)$$

This preserves the SM structure but uses a different operator that replaces the SU(2) generator. In a similar vein one can write the feynman rule for higgs coupling to the new fermions as

$$\begin{aligned} \Gamma_{jk} &= \lambda \frac{\hat{v}}{\sqrt{2}} ((j_1 k_2 + j_2 k_1) c_-(J, T_3) + (j_1 k_3 + j_3 k_1) c_+(J, T_3)) \\ &= \lambda \frac{\hat{v}}{\sqrt{2}} \mathcal{T}_{jk}. \end{aligned} \quad (3.21)$$

Within this thesis coupling matrices will usually appear with only two particles indices in which the information about its isospin ( $J, T_3$ ) and which multiplet the particle belongs to is stored. Sometimes however the full dependence is written out to show explicitly over which index a sum is taken

$$\mathcal{T}_{mn}^{(c)} = \mathcal{T}_{J;(\chi_{a(m)} T_3(m)),(\chi_{b(n)} T_3(n))}^{(c)}. \quad (3.22)$$

The free parameters for this model are the masses (in the simplest case only one mass), the coupling parameter  $\lambda$  and the isospin  $J$  of the first multiplet.

### 3.1.3. Mass Splitting at NLO

Similarly to the model with only one multiplet, one can calculate the masses of the multiplets at SM-NLO, in order to study the mass splitting within each multiplet and whether this model can generate a dark matter candidate. The first restriction coming from this is the existence of a neutral particle within the multiplets. This can be achieved by

$$J + Y \in \mathbb{N}_0, \quad (3.23)$$

$$Y \leq J. \quad (3.24)$$

According to the review of minimal dark matter models in [39] the mass splitting for one multiplet with hypercharge  $Y$  and mass  $M$  between two particles with charge  $Q$  and  $Q'$  can be approximated as

$$M_Q - M_{Q'} = \frac{g^2}{16\pi^2} 2\pi((Q^2 - Q'^2) \sin^2(\theta_W) M_Z + (Q - Q')(Q + Q' - 2Y)(M_W - M_Z)) + \mathcal{O}\left(\frac{M_W}{M}\right). \quad (3.25)$$

The resulting mass splittings between the neutral particle and its neighbors in isospin are shown in table 3.1. From these values it can already be seen that the lightest particle for  $Y = \pm\frac{1}{2}$  is charged which directly rules out these models as they would produce charged tracks in a detector. In the same paper ([39]) the authors show, that the dominant decay channel of the charged states, given large enough mass splitting  $\Delta M > m_\pi = 139.57$  MeV, is the emission of charged pions. Finally the life-time of the single charged states for  $J = 3$  is given as

$$\tau_c \simeq 44/((2J + 1)^2 - 1) \text{ cm} \approx 1 \text{ cm}. \quad (3.26)$$

For the viability of model in this theses this poses the following limitations:

**Table 3.1.:** Mass splitting of minimal dark matter models for different hypercharges and heavy masses

Y	$M_1 - M_0$	$M_{-1} - M_0$
0	0.166 GeV	0.166 GeV
$\frac{1}{2}$	0.354 GeV	-0.022 GeV
$-\frac{1}{2}$	-0.022 GeV	0.354 GeV

- Small values for the isospin might rule out the model, as the single charged states can become longer lived and too many charged particles could reach a detector
- The central hypercharge should be  $Y = 0$  as having large hypercharges for all three multiplets can cause charged states to be the lightest ones
- The mass splitting of the lightest multiplet needs to be larger than the pion mass

The first two limitations motivate fixing the isospin and hypercharge of the three original multiplets as

$$(J, Y) = \left\{ \left( \frac{5}{2}, -\frac{1}{2} \right); (3, 0); \left( \frac{5}{2}, \frac{1}{2} \right) \right\}, \quad (3.27)$$

or

$$(J, Y) = \left\{ \left( \frac{7}{2}, -\frac{1}{2} \right); (4, 0); \left( \frac{7}{2}, \frac{1}{2} \right) \right\}, \quad (3.28)$$

while the third one calls for the explicit calculation of the mass splitting.

In general the inverse fermion propagator at NLO can be written as

$$S_{ij}^{-1} = (\not{p} - m_i)\delta_{ij} - \Sigma_{ij}(p) \quad (3.29)$$

where  $\Sigma_{ij}(p)$  contains all loop contributions to the two point function. For the case of non interacting multiplets the inverse propagator becomes diagonal and the mass splitting can, in good approximation, be calculated without further renormalization as

$$\Delta M(Q, Q') = (\Sigma_{ii, Q}(p) - \Sigma_{ii, Q'}(p))|_{\not{p}=m_i} \quad (3.30)$$

When including the coupling of the multiplets one can further analyze the elements of  $\Sigma_{ij}(p)$ . A general way to write them is

$$\Sigma_{ij}(p) = \sum_X \sum_k \mathcal{T}_{ik}^{(x)} \mathcal{T}_{kj}^{(x)} \mathcal{I}(X, p, m_k, m_X) \quad (3.31)$$

where  $\mathcal{I}(X, p, m_k, m_X)$  is the loop integral, containing a particle  $X$  coupling to a fermion with mass  $m_k$ , The  $SU(2)$  structure of the vertices is split into  $\mathcal{T}_{ik}^a$ , which are the matrices from equation (3.20) or their analog for the higgs/goldstone boson coupling to the new model from equation (3.21). These coupling coefficients are what differentiates the diagonal and the off-diagonal elements. For all particles  $X \in W^\pm, Z, \gamma, h, \phi^0, \phi^\pm$  and all values of isospin  $J$  and its third component  $m_J$  (except  $m_J = 0$  for  $Z$ ) the relation

$$\mathcal{T}_{ii} \gg \mathcal{T}_{ij}, \quad j \neq i \quad (3.32)$$

holds true. Therefore the additional mass splitting introduced by the off-diagonal elements is expected to be small compared to the mass splitting introduced by the diagonal elements. Therefore ignoring the off-diagonal elements one can use (3.30) to calculate the mass splitting. Values for  $m_\psi = 700$  GeV,  $\lambda = 1$  and  $J = 3$  can be found in table 3.2. From these values one can see that the splitting between the lightest and the second lightest particle  $M_{\pm 1, \chi_2} - M_{0, \chi_2}$  is larger than the mass of

**Table 3.2.:** Mass splitting of the mass eigenstate multiplets for  $m_\psi = 700$  GeV,  $\lambda = 1$  and  $J = 3$ .

	$M_0$	$M_{\pm 1} - M_0$	$M_{\pm 2} - M_0$	$M_{\pm 3} - M_0$
$\chi_1$	700 GeV	0.110 GeV	0.442 GeV	—
$\chi_2$	525.9 GeV	0.192 GeV	0.768 GeV	1.728 GeV
$\chi_3$	874.1 GeV	0.179 GeV	0.715 GeV	1.608 GeV

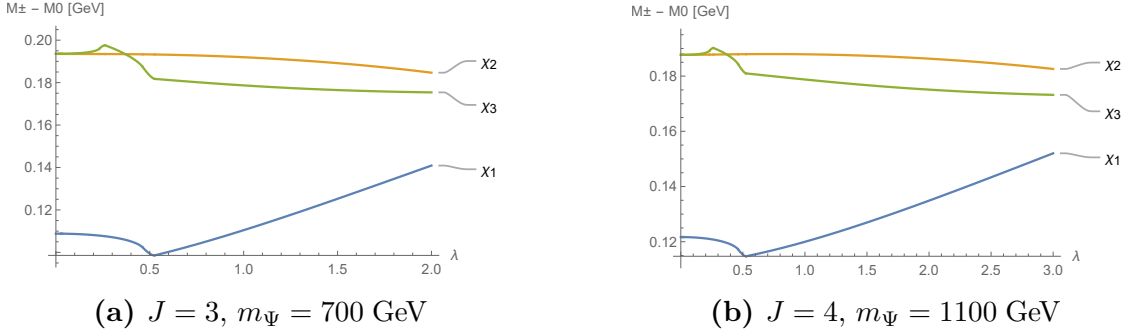


**Figure 3.1.:** Mass splitting between the lightest and second lightest particle in each multiplet at NLO

the charged Pion. For the multiplet with the medium mass ( $\chi_1$ ) however this is not the case and they therefore need a different decay channel in order to decay before reaching a detector. Since they can decay into the lightest multiplet by emitting a W- or Z-boson this is not an issue.

Lastly one can further look at the influence of  $J$ ,  $\lambda$  and  $m_\Psi$ . In figure 3.1 one can see that the general behavior for the two cases  $J = 3, m_\Psi = 700$  GeV and  $J = 4, m_\Psi = 1100$  GeV is similar. Furthermore one can see, that the most critical value  $M_{\pm 1, \chi_2} - M_{0, \chi_2}$  stays above the charged pion mass for all reasonable values of lambda, which keeps the lifetime of the second lightest state small enough so that it decays before reaching a detector.

### 3.1.4. Ignoring the Photon, $SU(2)$ -Limit

The model of this thesis couples via the hypercharge  $Y$ , the isospin  $J$  and the Yukawa coupling  $\lambda$  to the standard model. When comparing the size of the contributions one can expect the effects, that stem from the  $SU(2)$  coupling, to dominate the ones coming from the  $U(1)$  coupling for  $J \gg Y$ . This holds true for all cases in which the isospin dependence is not completely negated due to interference or renormalization (e.g. see section 3.1.3). However in these cases the whole contribution of the model compared to the SM is expected to be small as the main method of enhancement of this model (namely the large isospin) is gone. When comparing the effects caused by the coupling  $\lambda$  and the hypercharge the hierarchy becomes less clear. Depending on the choice of  $\lambda$  the effects due to the hypercharge can be larger or of the same size, or smaller than the effects caused by lambda. If they are larger or of the same size, then both of them are small compared to the isospin and one can simply study the model without coupling. If the effects due to the hypercharge are smaller they can be neglected anyways. Therefore, unless doing precision calculations, neglecting the hypercharge of the multiplets is a reasonable approximation that doesn't interfere with the dominant effects of this model. This approximation can be formalized by

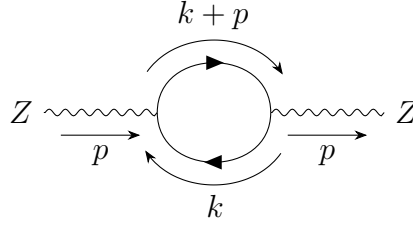


**Figure 3.2.:** Loop induced correction to the Z-Boson propagator

setting  $g' = 0$  which gives the  $SU(2)_L$  limit of the electroweak sector. In this limit the covariant derivative is given as

$$D_\mu = \partial_\mu + igt_R^a W_\mu^a \quad (3.33)$$

where  $t_R^a$  are the generators for a given representation R. At the same time the vector boson masses and couplings are further simplified, as the weak mixing angle vanishes and the masses become equal  $m_Z = m_W$ . All in all the limit  $g' = 0$  roughly halves the number of n-point functions and EFT-operators (as photons and  $B_{\mu\nu}$  can be ignored) while simplifying the remaining ones.

## 3.2. 1-Loop Contributions for VBS

In order to study this model for  $VV \rightarrow VV$  and  $VV \rightarrow hh$  processes at next to leading order the corrections to all relevant n-point functions need to be known

$$\Gamma^{\mu_1 \mu_2 \dots}(p_2, p_2, \dots, m_1, m_2, \dots) = \Gamma_{SM}^{LO} + \Gamma_{SM}^{NLO} + \Gamma_{BSM}^{LO} + \Gamma_{BSM}^{NLO} + \Gamma_{mixed}^{LO} + \Gamma_{mixed}^{NLO}. \quad (3.34)$$

At leading order the new model only gives contributions to processes with external BSM fermions which eliminates  $\Gamma_{BSM}^{LO}$  and  $\Gamma_{mixed}^{LO}$ . Furthermore the new fermions don't couple to the fermions in the standard model which eliminates  $\Gamma_{mixed}^{NLO}$ . Lastly the contributions from new fermions at large energies (similar or larger than their mass) are required to be larger than the next to leading order corrections in the SM in order to have a detectable signal, which leaves  $\Gamma_{BSM}^{NLO}$  as the relevant contribution that has to be calculated. For  $VV \rightarrow VV$  and  $VV \rightarrow hh$  this leaves corrections to the vector boson and higgs propagators (see e.g. figure 3.2), three boson vertices, four boson vertices (see e.g. figure 3.3) as well as a higgs tadpole to be computed (sec 3.2.1). Since all of these contributions are potentially UV divergent the theory needs to be renormalized (see sec. 3.2.2).

### 3.2.1. Simplifying the 1-Loop Contributions

When looking at loop induced diagrams like e.g. Z propagator corrections (fig. 3.2) and the correlated equation

$$\Pi^{\mu\nu}(p, m_i, m_j) = (-1) \frac{\mu^{(4-d)}}{(2\pi)^d} \int d^d k \frac{i(\not{k} + m_i)ig\gamma^\nu \mathcal{T}_{ij}^3 i(\not{k} + \not{p} + m_j)ig\gamma^\mu \mathcal{T}_{ji}^3}{(k^2 - m_i^2)((k+p)^2 - m_j^2)} \quad (3.35)$$

$$= \mathcal{T}_{ij}^3 \mathcal{T}_{ji}^3 \mathcal{I}^{\mu\nu}(p, m_i, m_j), \quad (3.36)$$

one can find an isospin dependent part  $\mathcal{T}_{ij}^3 \mathcal{T}_{ji}^3$  and a remaining integral, which only depends on the masses and the external momentum. As the masses from equation

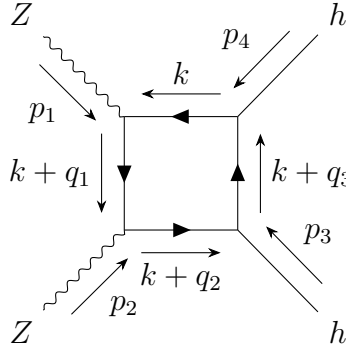


**Figure 3.3.:** Loop induced correction to the ZZhh vertex

(3.13)-(3.15) don't depend on the isospin or its third component, the remaining integral is both explicitly and implicitly independent of the isospin. The full propagator correction in the model which is the sum over all possible particles  $i$  and  $j$  then reads

$$\Pi^{\mu\nu}(p, m, \lambda, J) = \sum_{i,j} \mathcal{T}_{ij}^3 \mathcal{T}_{ji}^3 \mathcal{I}^{\mu\nu}(p, m_i, m_j) \quad (3.37)$$

$$= \sum_{a=1}^3 \sum_{b=1}^3 \left( \sum_{T_3(a)} \sum_{T_3(b)} \mathcal{T}_{J;(a T_3(a)),(b T_3(b))}^3 \mathcal{T}_{J;(b T_3(b)),(a T_3(a))}^3 \right) \mathcal{I}^{\mu\nu}(p, m_{\chi_a}, m_{\chi_a}) \quad (3.38)$$

$$= \sum_{a=1}^3 \sum_{b=1}^3 ZZ(a, b, J) \mathcal{I}^{\mu\nu}(p, m_{\chi_a}, m_{\chi_b}). \quad (3.39)$$

This decomposition now contains a coupling factor that depends on which particles are in the loop and the isospin (but not their masses or  $\lambda$ ) and an integral that depends on the momenta and the masses of the internal particles but not their isospin. Taking this same approach the four particle  $ZZhh$  vertex in figure 3.3 can be expressed as

$$\Gamma^{\mu\nu}(p_1, p_2, p_3, m, \lambda, J) = \sum_{a,b,c,d=1}^3 \text{HHZZ}(a, b, c, d, J) \mathcal{I}^{\mu\nu}(p_1, p_2, p_3, m_{\chi_a}, m_{\chi_b}, m_{\chi_c}, m_{\chi_d}). \quad (3.40)$$

Going to the limit of only one multiplet and therefore no coupling between multiplets these coupling coefficients become traces of  $SU(2)$  generators

$$\sum_{i,j} \mathcal{T}_{ij}^a \mathcal{T}_{ji}^b \rightarrow \text{Tr}(t^a t^b) = T_R \delta_{ab} = \frac{J(J+1)(2J+1)}{3} \quad (3.41)$$

The integrals  $\mathcal{I}^{\mu_1 \mu_2 \dots}$  that are needed for this theses can be calculated analytically within Mathematica in terms of Passarino-Veltman-Function using PackageX [34]

### 3.2.2. Renormalization

After calculating the 1-loop contributions one is still left with UV-divergent parts in all n-point functions which need to be renormalized [40, 41, 42]. For the two-point functions one needs to renormalize the  $p^0$  part (mass part) as well as the  $p^2$  part. The required counter terms to the masses in the  $SU_2$ -limit are  $\delta_{M_W^2}$  and  $\delta_{M_h^2}$ , the  $p^2$

part is addressed by the wave function renormalizations  $\delta_{Z_W}$  and  $\delta_{Z_h}$ . These wave function renormalizations also affect the divergences in the three- and four-point functions and are supplemented by renormalizing the couplings  $\delta_g$  and  $\delta_{\lambda_h}$ . Finally in order to handle the divergence in the higgs tadpole a counterterm  $\delta_{t_h}$  is introduced. This set

$$M_{W,0}^2 = M_W^2 + \delta_{M_W^2} \quad (3.42)$$

$$M_{h,0}^2 = M_h^2 + \delta_{M_h^2} \quad (3.43)$$

$$g_0 = g + \delta_g \quad (3.44)$$

$$\lambda_{h,0} = \lambda_h + \delta_{\lambda_h} \quad (3.45)$$

$$T_{h,0} = T_h + \delta_{t_h} \quad (3.46)$$

$$W_0^{I,\mu} = \sqrt{Z_W} W^{I,\mu} = W^{I,\mu} + \frac{1}{2} \delta_{Z_W} W^{I,\mu} \quad (3.47)$$

$$\phi_0 = \sqrt{Z_h} \phi = \phi + \frac{1}{2} \delta_{Z_h} \phi, \quad (3.48)$$

however is not linearly independent of each other and can be reduced to four counterterms for the four operators of the SM that can be used as counterterms

$$W_{\mu\nu}^I W^{I\mu\nu}, (D_\mu \phi)^\dagger D^\mu \phi, \mu^2 \phi^\dagger \phi, \lambda_h (\phi^\dagger \phi)^2 \quad (3.49)$$

$$\mu_0^2 = \mu^2 + \delta_{\mu^2}. \quad (3.50)$$

In order to avoid unnecessary confusion between the renormalization scale  $\mu$ , the coupling to the new fermions  $\lambda$  and the coefficients in the higgs potential  $\mu^2$  and  $\lambda_h$  the latter ones are avoided whenever possible.

Starting with  $W_{\mu\nu}^I W^{I\mu\nu}$  and looking at the resulting two-point function one can directly read off the coefficient to be  $\delta_{Z_W}$ . By construction the same coefficient has to appear for the three- and four-point gauge boson function resulting in

$$\frac{3}{2} \delta_{Z_W} + \frac{\delta_g}{g} = \delta_{Z_W} \quad (3.51)$$

$$2\delta_{Z_W} + 2\frac{\delta_g}{g} = \delta_{Z_W}, \quad (3.52)$$

and therefore

$$\frac{\delta_g}{g} = -\frac{1}{2} \delta_{Z_W}. \quad (3.53)$$

The covariant derivative stays therefore unchanged making it again easy to read off the coefficient of  $(D_\mu \phi)^\dagger D^\mu \phi$  as  $\delta_{Z_h}$ . As  $\delta_{M_W^2}$  is now also accounted for one is left with the higgs potential. By comparing the one- and two-point higgs function one can read off the remaining relations:

$$\delta_{t_h} = -\delta_{\lambda_h} v^3 - \delta_{\mu^2} v - \delta_{Z_h} \frac{m_h^2 v}{2} \quad (3.54)$$

$$\delta_{M_h^2} = 3\delta_{\lambda_h} v^2 + \delta_{\mu^2} + \frac{3}{2} \delta_{Z_h} m_h^2 \quad (3.55)$$

$$\delta_{\lambda_h} = \frac{\delta_{t_h} + \delta_{M_h^2} v - \delta_{Z_h} m_h^2 v}{2v^3} \quad (3.56)$$

$$\delta_{\mu^2} = \frac{-3\delta_{t_h} - \delta_{M_h^2} v}{2v} \quad (3.57)$$

### 3.2.2.1. $\overline{\text{MS}}$ Scheme

In the minimal subtraction  $\overline{\text{MS}}$  scheme not only the UV-divergent part is absorbed but also a finite part that appears together with the  $\frac{1}{\epsilon}$  pole. Using the Mathematica package package-X this finite part is already implicitly included in the  $\frac{1}{\epsilon}$  term as

$$\left(\frac{1}{\epsilon}\right)_{\overline{\text{MS}}} = \frac{1}{\epsilon} + \gamma_E + \log(4\pi), \quad (3.58)$$

so one can directly expand in  $\frac{1}{\epsilon}$  and read off the contributions. From the vector boson propagator one finds

$$D_W^{\mu\nu}(p^2)_\epsilon = \left(\frac{1}{\epsilon}\right)_{\overline{\text{MS}}} \frac{g^2}{12\pi^2} \left( (T_j + 2T_{j-1/2})(p^\mu p^\nu - p^2 g^{\mu\nu}) + \lambda^2 v^2 \frac{3(2j+1)}{8} g^{\mu\nu} \right) \quad (3.59)$$

$$\delta_{Z_W, \epsilon} = - \left(\frac{1}{\epsilon}\right)_{\overline{\text{MS}}} \frac{g^2}{12\pi^2} (T_j + 2T_{j-1/2}) \quad (3.60)$$

$$\delta_{Z_h, \epsilon} = - \left(\frac{1}{\epsilon}\right)_{\overline{\text{MS}}} \lambda^2 \frac{(2j+1)}{8\pi^2}. \quad (3.61)$$

The remaining counter terms can be calculated using the higgs propagator and the higgs tadpole

$$\Pi_h(p^2)_\epsilon = \left(\frac{1}{\epsilon}\right)_{\overline{\text{MS}}} \frac{-\lambda^2}{8\pi^2} (3\lambda^2 v^2 + 6m_\Psi^2 - p^2)(2j+1) \quad (3.62)$$

$$T_{h, \epsilon} = \left(\frac{1}{\epsilon}\right)_{\overline{\text{MS}}} \frac{-\lambda^2}{8\pi^2} (\lambda^2 v^3 + 6m_\Psi^2 v)(2j+1) \quad (3.63)$$

$$\delta_{\mu^2, \epsilon} = \left(\frac{1}{\epsilon}\right)_{\overline{\text{MS}}} \frac{-(2j+1)}{16\pi^2} (\lambda^2 m_h^2 + 12\lambda^2 m_\Psi^2) \quad (3.64)$$

$$\delta_{\lambda_h, \epsilon} = \left(\frac{1}{\epsilon}\right)_{\overline{\text{MS}}} \frac{-(2j+1)}{8\pi^2 v^2} (\lambda^4 v^2 - \lambda^2 m_h^2). \quad (3.65)$$

By construction, these counterterms also cancel all divergences that appear in higher n-point functions. At this point it should be mentioned that  $\delta_{Z_h, \epsilon}$  also affects the Yukawa couplings of the SM and new fermions. As these should stay unchanged a counterterm for the Yukawa coupling that exactly cancels the higgs wavefunction renormalization can be introduced. In the end this procedure gives the same result as ignoring  $\delta_{Z_h, \epsilon}$  for the Yukawa sector.

### 3.2.2.2. On-Shell Scheme

In order to use the physical W- and H-masses one wants to go one step further and use the on-shell renormalization scheme [43]. For this the finite part of the tadpole has to vanish as well as the real part of the propagator corrections at  $p^2 = m^2$

$$T_h + \delta_{t_h} = 0 \quad (3.66)$$

$$\text{Re}[p^2 - m_W^2 - \delta_{M_W^2} + \Pi_W(p^2)] \Big|_{p^2=m_W^2} = 0 \quad (3.67)$$

$$\text{Re}[p^2 - m_h^2 - \delta_{M_h^2} + \Pi_h(p^2)] \Big|_{p^2=m_h^2} = 0. \quad (3.68)$$

Finally one can require the real part of residue of the propagator at its pole to be equal to one. In total these are five requirements with only four free parameters

to account for them. Explicitly  $\delta_{Z_h}$  and  $\delta_{Z_W}$  are overconstrained as they have to account for the W-mass as well as the W- and H-residues. In order to fulfill all five restrictions a background field  $\hat{\Phi}$  is introduced following [44]

$$\Phi \rightarrow \Phi + \hat{\Phi} = \begin{pmatrix} \varphi^+ \\ \frac{h+i\varphi_Z}{\sqrt{2}} \end{pmatrix} + \begin{pmatrix} \hat{\varphi}^+ \\ \frac{\hat{v}+\hat{h}+i\hat{\varphi}_Z}{\sqrt{2}} \end{pmatrix}. \quad (3.69)$$

This background field now allows for two independent renormalization constants for the two fields. They will be named  $(\delta_{Z_h})$  and  $\delta_{Z_v}$  since they renormalize the higgs field and the vev. This new renormalization constant changes the relations from equations (3.54)-(3.57). Including the vev renormalization they read

$$\delta_{t_h} = -\delta_{\lambda_h} v^3 - \delta_{\mu^2} v - \delta_{Z_v} \frac{m_h^2 v}{2} \quad (3.70)$$

$$\delta_{M_h^2} = 3\delta_{\lambda_h} v^2 + \delta_{\mu^2} + \frac{3}{2}\delta_{Z_v} m_h^2 \quad (3.71)$$

$$\delta_{\lambda_h} = \frac{\delta_{t_h} + \delta_{M_h^2} v - \delta_{Z_v} m_h^2 v}{2v^3} \quad (3.72)$$

$$\delta_{\mu^2} = \frac{-3\delta_{t_h} - \delta_{M_h^2} v}{2v} \quad (3.73)$$

By expanding the W-two-point function around  $p^2 = m_W^2$

$$\Pi_W(p^2) = \Pi_W(m_W^2) + (p^2 - m_W^2) \frac{d\Pi_W}{dp^2}(m_W^2) + \dots \quad (3.74)$$

one can read off

$$\delta_{m_W^2} = \text{Re}[\Pi_W(m_W^2)]. \quad (3.75)$$

With the pole fixed a residue of one can be achieved using the wave function renormalization for the W-field. The relevant part of the propagator now reads

$$\frac{1}{Z_W} \frac{1}{(p^2 - m_W^2 - \delta_{m_W^2} + \Pi_W(m_W^2)) + (p^2 - m_W^2) \frac{d\Pi_W}{dp^2}(m_W^2) + \dots} \quad (3.76)$$

$$= \frac{1}{Z_W} \frac{1}{(p^2 - m_W^2)(1 + \frac{d\Pi_W}{dp^2}(m_W^2) + \dots)}. \quad (3.77)$$

The wave function renormalizations are therefore given as

$$\delta_{Z_W} = Z_W - 1 = -\text{Re} \left[ \frac{d\Pi_W}{dp^2}(m_W^2) \right] \quad (3.78)$$

$$\begin{aligned} \delta_{Z_v} &= \frac{\delta_{m_W^2}}{m_W^2} - \frac{2\delta_g}{g} \\ &= \frac{\delta_{m_W^2}}{m_W^2} + \delta_{Z_W} \\ &= \frac{\text{Re}[\Pi_W(m_W^2)]}{m_W^2} - \text{Re} \left[ \frac{d\Pi_W}{dp^2}(m_W^2) \right]. \end{aligned} \quad (3.79)$$

Similarly to the W-propagator the higgs-mass counterterm and the higgs wave function renormalization can also be read off as

$$\delta_{M_h^2} = \text{Re}[\Pi_h(m_h^2)] \quad (3.80)$$

$$\delta_{Z_h} = Z_h - 1 = -\text{Re} \left[ \frac{d\Pi_H}{dp^2}(m_h^2) \right] \quad (3.81)$$

The remaining renormalization of  $\delta_{\mu^2}$  and  $\delta_{\lambda_h}$  follows from the equations (3.72) and (3.73) by plugging in  $\delta_{M_h^2}$ ,  $\delta_{Z_v}$  and  $\delta_{t_h}$  from their respective equations (3.80), (3.79) and (3.66).

### 3.3. Generalizations and related Models

There are many parameters and choices within this model where changes can lead to a slightly or largely different phenomenology. The following changes can be investigated

- A different number of multiplets (explicitly only 2 multiplets)
- Different masses of the multiplets
- Different Yukawa-couplings between the multiplets
- A different coupling structure to the higgs

Starting with only two multiplets, e.g.  $\Psi_{J=3}^{Y=0}$  and  $\Psi_{J=2.5}^{Y=-0.5}$ , one can see that  $\Psi_{J=3, m_J=J}^{Y=0}$  has no partner to couple to. Therefore the mass of  $\Psi_{J=3, m_J=J}^{Y=0}$  stays unchanged after the rotation into the mass eigenstates. On the other side of the spectrum  $\Psi_{J=3, m_J=-3}^{Y=0}$  and  $\Psi_{J=2.5, m_J=-2.5}^{Y=-0.5}$  produce two mass eigenstates with masses of  $m_\Psi \pm \frac{\sqrt{2}}{2}\lambda\hat{v}$ . The remaining states within each mass eigenstate multiplet then lie between  $m_\Psi \pm \frac{\sqrt{2}}{2}\lambda\hat{v}$  and  $m_\Psi$ . The lightest state in the new multiplets therefore has a charge of  $Q = -3$  and is stable. This would result in charged tracks from a stable particle in a detector making this type of model easily observable.

A similar behavior can be observed when adding two additional multiplets with different masses e.g.  $m_{\Psi_2} = m_{\Psi_1}$  and  $m_{\Psi_3} = m_{\Psi_1} + \Delta m$ . The mass of the  $Q = J$  and  $Q = -J$  mass eigenstates are

$$m_{-J} = m_{\Psi_1} \pm \frac{\sqrt{2}}{2}\lambda\hat{v}, \quad (3.82)$$

$$m_J = m_{\Psi_1} + \frac{1}{2}\Delta m \pm \frac{\sqrt{2\lambda^2\hat{v}^2 + \Delta m^2}}{2}, \quad (3.83)$$

and all other masses lie between them. This setup therefore again results in a charged particle being the lightest one, which then again results in charged tracks in a detector.

Another way of changing the masses is having both additional multiplets be heavier (or lighter) than the first multiplet  $m_{\Psi_2} = m_{\Psi_1} + \Delta m$  and  $m_{\Psi_3} = m_{\Psi_1} + \Delta m$ . For this setup the symmetry between  $Q = -J$  and  $Q = J$  is preserved and the three masses, after rotation into mass eigenstates, are

$$m_{\chi_1} = m_{\Psi_1} + \Delta m, \quad (3.84)$$

$$m_{\chi_{2,3}} = m_{\Psi_1} + \frac{1}{2}\Delta m \pm \frac{\sqrt{2\lambda^2\hat{v}^2 + \Delta m^2}}{2}. \quad (3.85)$$

The difference between this setup and the setup with three identical masses is mostly the mass  $m_{\chi_1}$ , which is no longer right in the middle of the other two masses but shifted to one of them depending on the sign of  $\Delta m$ . As this is not expected to add any new phenomenology one can stick with the easier case of three identical masses. Different Yukawa couplings  $\lambda_1, \lambda_2$  and identical masses produces the masses

$$m_{-J} = m_{\Psi_1} \pm \frac{\sqrt{2}}{2}\lambda_1\hat{v}, \quad (3.86)$$

$$m_J = m_{\Psi_1} \pm \frac{\sqrt{2}}{2}\lambda_2\hat{v}, \quad (3.87)$$

which leads to the same issue as before.

Within this thesis the coupling between the different multiplets and the higgs field is explicitly built to be CP-even. When building the Lagrangian one is however free to add terms like

$$\lambda_{CP} \bar{\Psi}_j^{Y=0} \gamma_5 \Phi \Psi_{j\pm 1/2}^{Y=-1/2} + h.c. , \quad (3.88)$$

which can generate graphs with an even or an odd number of  $\gamma_5$  matrices at the one loop level. In [45] it is explicitly shown how CP-odd EFT operators (dimension 6) can arise from these loops with an odd number of  $\gamma_5$  matrices and how much of an impact they can have.

## 4. EFT

The goal of searches for new physics using EFT operators is setting limits on BSM contributions (in the form of EFT coefficients) while being as model independent as possible. The most model independent starting point would be a complete basis, like the Warsaw basis, for each dimension necessary. As this implies thousands of operators one might want to step away from these general bases and find a dedicated basis suitable for the EFT search one has in mind.

### 4.1. Constructing a Dedicated Basis

A dedicated basis can be constructed in the following ways

- Starting with a complete basis, operators (or groups of operators) are eliminated using assumptions made for the underlying theory.
- A set of operators is specifically generated for a certain problem.
- Starting with a subset of operators of a general basis (or a dedicated basis), operators are added till a set of operators is generated, that can accommodate for the expected effects of underlying theories.

The first step for most of these approaches is restricting the number of higher dimensions that are included. By reducing the number of higher dimensions looked at (e.g. only dimension-6) one already starts neglecting certain models in which the dominant EFT contribution firstly appears at higher dimension (e.g. [19])

Starting with a complete basis one can assume symmetries for the underlying theory in order to reduce the number of operators. Some of these possible assumptions include the  $U(3)^5$ -limit or minimal flavor violation (MFV) [46, 47, 48], which are implemented in the SMEFTsim package [49] which uses FeynRules [50]. One can also make assumptions on where new physics should appear first (e.g. certain processes and therefore vertices) and how it behaves (e.g. CP-even/-odd) in order to reduce the number of relevant operators. Another way of reducing the number of operators that need to be accounted for, is by throwing out groups of operators using the argument, that the BSM scenarios one wants to study only couple to certain sectors of the SM. An example of this are searches for new physics that couples to the higgs and vector boson sector, for which one can therefore ignore the fermionic and strong interaction sector.

When doing this, one has to be careful that these sectors are connected, due to the use of equations of motion for the derivation of the complete basis. Depending on the processes one wants to use such an EFT for, some operators might need to be reintroduced to the set. An example of this can be found in section 4.1.1.

When building a basis for a specific problem from the ground up (or starting from an existing set), one also needs to be careful that the operators actually form a basis for the given problem. An example from the field of vector boson scattering is the Éboli basis that has the purpose of parameterizing anomalous quartic gauge couplings (aQGC). This basis featured both redundant (e.g.  $\mathcal{O}_{M6}$ ) as well as missing operators (e.g.  $\mathcal{O}_{T3}$ , see section 2.2.1.2). As this basis is still used for setting limits on aQGC it is a good starting point for a dedicated basis for the model used in this thesis.

The more assumptions are made the smaller one can make the dedicated basis used. This can be done till one arrives at single operator searches. With all the assumptions gone into such a basis, one shouldn't forget that they are also assumptions made for an underlying theory and that there should be theories left that can fulfill these assumptions.

### 4.1.1. Following the Contributions

As mentioned in section 4.1, using equations of motion for generating a basis of EFT operators links different classes of operators together, which therefore shouldn't be looked at separately. This can best be demonstrated with an example. Starting with an operator that is generated from an underlying theory, one can then follow the contributions of this operator for different processes in order to understand, in which cases a reduced operator set is acceptable and which it is not.

Starting with an underlying theory that only introduces new interactions for the vector boson and higgs sector, one can generate the operator

$$(D_\mu D^\mu \phi)^\dagger D_\nu D^\nu \phi, \quad (4.1)$$

which is not part of the Warsaw basis. Using the EOM from equation (2.38) one can rewrite this operators in terms of classes of operators that appear

$$(D_\mu D^\mu \phi)^\dagger D_\nu D^\nu \phi \sim \mathcal{O}(\phi^2) + \mathcal{O}(\phi^4) + \mathcal{O}(\phi^6) + \mathcal{O}(\psi^2 \phi) + \mathcal{O}(\psi^2 \phi^3) + \mathcal{O}(\psi^4). \quad (4.2)$$

The classes  $\mathcal{O}(\phi^{n2})$  are classes that one would also expect from the underlying theory, the fermionic ones however are only introduced through the EOM.

When looking at a process only involving vector bosons, like  $VV \rightarrow VV$ , one can see, that the fermionic operators have no influence on the process and can rightfully be ignored. However in most cases vector boson scattering is not studied in a vacuum, but vector bosons are produced and decay and for these processes one needs to make sure that the fermionic operators have little to no effect (including new diagrams that might arise due to  $\mathcal{O}(\psi^4)$  operators). For the original operators this task is significantly easier, as it only requires studying the effect on vector boson propagators. Going one dimension further an operator like

$$\epsilon_{IJK} (D^\alpha W_{\mu\nu})^I (D^\beta W^{\mu\nu})^J W_{\alpha\beta}^K, \quad (4.3)$$

generates quite a few operators after using EOM (equation (2.39)), with some of them being in the  $\mathcal{O}(\psi^4 X)$  class. With these operators two vector bosons don't need to scatter and then decay ( $VV \rightarrow VV \rightarrow 4\psi$ ), but can directly scatter into four fermions through a four-fermion-two-vector-boson vertex. Arguing that such operators can be ignored is then quite a task.

## 4.2. Building the Dedicated Basis

In order to build an EFT basis for a model like the one presented in section 3.1, one first needs to define the building blocks used for the operators. In the  $SU(2)_L$ -limit the model only couples to weak bosons and  $\phi$  and not to photons. Furthermore the model is CP-even. The building blocks one can use, are therefore the field strength tensor  $W_{\mu\nu}^I$ , the higgs field  $\phi$  and the covariant derivative  $D_\mu$ . The following rules can be made for these objects:

- Due to  $SU(2)_L$  the number of higgs fields has to be even.
- Higgs fields are contracted as either a singlet ( $\phi^\dagger\phi$ ) or a triplet ( $\phi^\dagger\tau^I\phi$ ). Additional derivatives can be applied.
- As there shouldn't be any tadpoles introduced by higher dimensional operators, singlet products of higgs fields should be written as  $(\phi^\dagger\phi - \frac{\hat{v}^2}{2})$ .
- As all lorentz indices need to be contracted, the total number of lorentz indices also needs to be even, resulting in an even number of covariant derivatives.
- Covariant derivatives shouldn't act on products of building blocks.
- Operators have to be hermitian.

Starting with an object  $\mathcal{O}$  one can produce a hermitian operator via

$$\mathcal{O}_1 = \mathcal{O} + \mathcal{O}^\dagger, \quad (4.4)$$

$$\mathcal{O}_2 = i(\mathcal{O} - \mathcal{O}^\dagger). \quad (4.5)$$

As all of the building block are P-even one finds that one of these combinations is C-even while the other is C-odd (or vanishing). Only the CP-even combination is considered.

With these guidelines one can construct the basis one dimension at a time and one operator class at a time.

### 4.2.1. Dimension-2 and Dimension-4

All operators of the SM can also appear as operators of the EFT. The cause for this is for one the usage of  $(\phi^\dagger\phi - \frac{\hat{v}^2}{2})$  over  $\phi^\dagger\phi$ , as this can generate lower dimensional operators

$$\frac{1}{\Lambda_{\text{EFT}}^2} \phi^\dagger\phi W_{\mu\nu}^I W^{I\mu\nu} = \frac{1}{\Lambda_{\text{EFT}}^2} \left( \phi^\dagger\phi - \frac{\hat{v}^2}{2} \right) W_{\mu\nu}^I W^{I\mu\nu} + \frac{\hat{v}^2}{2\Lambda_{\text{EFT}}^2} W_{\mu\nu}^I W^{I\mu\nu}. \quad (4.6)$$

Secondly the appearance of SM operators in the EFT depends on the renormalization used for the underlying model. When looking at an operator of the class  $D^2X^2$  it can easily be seen, that such an operator can produce an effect proportional to  $\frac{p^4}{\Lambda_{\text{EFT}}^2}$  to the vector boson propagator. When using an on-shell renormalization scheme this effect can be countered by terms proportional to  $\frac{m_W^2}{\Lambda_{\text{EFT}}^2} (D_\mu\phi)^\dagger D^\mu\phi$  or  $\frac{m_W^2}{\Lambda_{\text{EFT}}^2} W_{\mu\nu}^I W^{I\mu\nu}$ . The SM operators needed for a complete basis are therefore

$$\mathcal{O}_{H2} = -\phi^\dagger\phi, \quad (4.7)$$

$$\mathcal{O}_{H4} = -(\phi^\dagger\phi)^2, \quad (4.8)$$

$$\mathcal{O}_{\text{Gauge}} = \frac{-1}{4} W_{\mu\nu}^I W^{I\mu\nu}, \quad (4.9)$$

$$\mathcal{O}_{\text{kin}} = (D_\mu\phi)^\dagger D^\mu\phi. \quad (4.10)$$

These operators are intentionally kept identical to the ones in the SM in order to facilitate renormalization.

## 4.2.2. Dimension-6

At dimension-6 there are a total of eight operator classes that need to be filled. They are ordered firstly by the number of higgs fields (most to least) and secondly by the number of derivatives (most to least).

### 4.2.2.1. $\phi^6$

The operator class  $\phi^6$  contains three higgs fields and three conjugated higgs fields, which together can either form triplets or singlets under  $SU(2)_L$ . As all of the fields are identical the term from three triplets vanishes

$$\epsilon^{IJK} (\phi^\dagger \tau^I \phi) (\phi^\dagger \tau^J \phi) (\phi^\dagger \tau^K \phi) = 0. \quad (4.11)$$

Two triplets and a singlet is identical to three singlets and lower dimensional operators due to equation (2.48)

$$\left( \phi^\dagger \phi - \frac{\hat{v}^2}{2} \right) (\phi^\dagger \tau^I \phi) (\phi^\dagger \tau^I \phi) = \left( \phi^\dagger \phi - \frac{\hat{v}^2}{2} \right)^3 + \mathcal{O}(\phi^4) + \mathcal{O}(\phi^2). \quad (4.12)$$

The only remaining operator is therefore

$$\mathcal{O}_{H6} = \left( \phi^\dagger \phi - \frac{\hat{v}^2}{2} \right)^3 \quad (4.13)$$

### 4.2.2.2. $\phi^4 D^2$

Following the discussion in section 2.2.1.1 we have the operators

$$\mathcal{O}_{HD1} = ((D_\mu \phi)^\dagger \phi) (\phi^\dagger D^\mu \phi), \quad (4.14)$$

$$\mathcal{O}_{HD2} = \left( \phi^\dagger \phi - \frac{\hat{v}^2}{2} \right) ((D_\mu \phi)^\dagger D^\mu \phi). \quad (4.15)$$

As we are not using EOMs, the operator with two derivatives acting on the same field is no longer proportional to operators of a lower class. Using IBP we get three operators where the derivatives are acting on different fields, two of them being already mentioned above. The third and missing operator is

$$\mathcal{O}_{HD3} = ((D_\mu \phi)^\dagger \phi) ((D_\mu \phi)^\dagger \phi) + (\phi^\dagger D^\mu \phi) (\phi^\dagger D^\mu \phi). \quad (4.16)$$

The operators with two triplets

$$\mathcal{O}_{HD1*} = ((D_\mu \phi)^\dagger \tau^I \phi) (\phi^\dagger \tau^I D^\mu \phi), \quad (4.17)$$

$$\mathcal{O}_{HD2*} = (\phi^\dagger \tau^I \phi) ((D_\mu \phi)^\dagger \tau^I D^\mu \phi), \quad (4.18)$$

$$\mathcal{O}_{HD3*} = ((D_\mu \phi)^\dagger \tau^I \phi) ((D_\mu \phi)^\dagger \tau^I \phi) + (\phi^\dagger \tau^I D^\mu \phi) (\phi^\dagger \tau^I D^\mu \phi), \quad (4.19)$$

are all proportional to linear combinations of the first three operators and lower dimensional ones after using equation (2.48).

Finally one can rearrange the operators in order to build two operators that conserve custodial  $SU(2)_C$  symmetry

$$2\mathcal{O}_{HD1} + \mathcal{O}_{HD3} \quad (4.20)$$

$$\mathcal{O}_{HD2} \quad (4.21)$$

and one that breaks  $SU(2)_c$

$$2\mathcal{O}_{HD1} - \mathcal{O}_{HD3} \quad (4.22)$$

operator.

#### 4.2.2.3. $\phi^2 D^4$

For this class we can observe, that the order and position of the derivatives can be chosen freely, as all of these are identical up to lower class operators, using the commutator of covariant derivatives and IBP. The only operator that needs to be considered is therefore

$$\mathcal{O}_{HDD} = (D_\mu D^\mu \phi)^\dagger (D_\nu D^\nu \phi). \quad (4.23)$$

#### 4.2.2.4. $\phi^2 D^2 X$

The only  $SU(2)_L$  structure that produces a singlet overall is the two higgs fields being contracted to a triplet. Afterwards one is left with four possibilities for distributing the derivatives

- Both derivatives act on the field strength tensor.
- Both derivatives act on the same higgs field.
- Both derivatives act on different higgs fields.
- One derivative acts on a higgs field and one on the field strength tensor.

The first two options can be ignored as we can rewrite

$$D_\mu D_\nu = \frac{1}{2}\{D_\mu, D_\nu\} + \frac{1}{2}[D_\mu, D_\nu] \quad (4.24)$$

where the second part only generates lower class operators. One is therefore left with a symmetric part from the derivatives and an antisymmetric part from the field strength tensor. The operator therefore vanishes. Using IBP one can then link the remaining two cases to each other, leaving only one operator

$$\mathcal{O}_{HDDW} = i((D^\mu \phi)^\dagger \tau^I D^\nu \phi) W_{\mu\nu}^I \quad (4.25)$$

#### 4.2.2.5. $\phi^2 X^2$

For this class one can either contract the two higgs fields to a singlet or a triplet

$$\phi^\dagger \phi W_{\mu\nu}^I W^{I\mu\nu}, \quad (4.26)$$

$$\epsilon^{IJK} \phi^\dagger \tau^I \phi W_{\mu\nu}^J W^{K\mu\nu}. \quad (4.27)$$

As the second term is symmetric under interchanging the two field strength tensors, and therefore under interchanging  $J$  and  $K$ , while at the same time containing  $\epsilon^{IJK}$ , it vanishes. The only relevant operator is therefore

$$\mathcal{O}_{HW} = \left( \phi^\dagger \phi - \frac{\hat{v}^2}{2} \right) W_{\mu\nu}^I W^{I\mu\nu}. \quad (4.28)$$

#### 4.2.2.6. $D^4X$

In the operator class  $D^4X$  all derivatives act on the field strength tensor. Therefore all operators are identical up to commutators of covariant derivatives. So one can chose a structure like

$$D_\alpha D^\alpha D^\mu D^\nu W_{\mu\nu}^I \quad (4.29)$$

and see that the derivatives are symmetric under swapping  $\mu$  and  $\nu$  (up to lower class operators) while the field strength tensor is asymmetric. At the same time the  $SU(2)$  index is not contracted which leaves no operator for this class. Further classes in which the  $SU(2)$  index can't be contracted will be omitted.

#### 4.2.2.7. $D^2X^2$

For the operator class  $D^2X^2$  there are two relevant lorentz structures.

- The two derivatives have the same lorentz index.
- The two derivatives are contracted with different field strength tensors.

The position of the derivatives can again be chosen arbitrarily as all of these possibilities are identical up to IBP and commutators of derivatives. Starting with the second option one can use the Bianchi identity

$$D_\rho X_{\mu\nu} + D_\mu X_{\nu\rho} + D_\nu X_{\rho\mu} = 0, \quad (4.30)$$

and relabeling the indices, to show that the two structures are linearly dependent:

$$\begin{aligned} (D^\mu W^{\nu\rho})^I (D_\rho W_{\mu\nu})^I &= - (D^\mu W^{\nu\rho})^I [(D_\mu W_{\nu\rho})^I + (D_\nu W_{\rho\mu})^I] \\ (D^\mu W^{\nu\rho})^I (D_\rho W_{\mu\nu})^I + (D^\mu W^{\nu\rho})^I (D_\nu W_{\rho\mu})^I &= - (D^\mu W^{\nu\rho})^I (D_\mu W_{\nu\rho})^I \\ (D^\mu W^{\nu\rho})^I (D_\rho W_{\mu\nu})^I + (D^\mu W^{\rho\nu})^I (D_\rho W_{\nu\mu})^I &= - (D^\mu W^{\nu\rho})^I (D_\mu W_{\nu\rho})^I \\ 2 (D^\mu W^{\nu\rho})^I (D_\rho W_{\mu\nu})^I &= - (D^\mu W^{\nu\rho})^I (D_\mu W_{\nu\rho})^I, \end{aligned} \quad (4.31)$$

Therefore only one operator appears for this class

$$\mathcal{O}_{DW} = (D_\alpha W_{\mu\nu})^I (D^\alpha W^{\mu\nu})^I. \quad (4.32)$$

#### 4.2.2.8. $X^3$

In order to generate an overall  $SU(2)_L$  singlet, while having field strength tensors with two nonidentical lorentz indices, one can come up with only one possible structure. The chosen operator reads

$$\mathcal{O}_W = \epsilon_{IJK} W_\mu^{I\nu} W_\nu^{J\rho} W_\rho^{K\mu}. \quad (4.33)$$

### 4.2.3. Dimension-8

The ordering for the classes of dimension-8 operators is the same as for dimension-6. More higgs fields imply a higher class and for the same number of higgs fields more derivatives mean a higher class. In total there are twelve relevant classes.

#### 4.2.3.1. $\phi^8$

Similarly to the operator class  $\phi^6$ , there are multiple possible ways to form an overall singlet using  $\phi^\dagger\phi$  and  $\phi^\dagger\tau^I\phi$  terms. As all of the fields are identical, operators containing  $\epsilon^{IJK}$  can be ignored. Using equation (2.48) the remaining possible operators can be shown to be related, leaving only one operator to consider

$$\mathcal{O}_{H8} = \left( \phi^\dagger\phi - \frac{\hat{v}^2}{2} \right)^4. \quad (4.34)$$

#### 4.2.3.2. $\phi^6 D^2$

In this class we can have three  $SU(2)_L$  structures, three triplets and a Levi-Civita tensor, two triplets and one singlet and three singlets. In the case of the three triplets, the derivatives have to act on different triplets and one on an unconjugated field and one on a conjugated one. Otherwise there would be two similar terms (up to the index of the Pauli matrices) and the whole operator would vanish due to the anti symmetric nature of the Levi-Civita tensor. Therefore one can write down only one operator for this configuration:

$$i\epsilon^{IJK}(\phi^\dagger\tau^I\phi)(D_\mu\phi^\dagger\tau^J\phi)(\phi^\dagger\tau^K D^\mu\phi) \quad (4.35)$$

Using equation (2.48) structures with two triplets can be reduced to only singlets. Furthermore using IBP one can assume that the two derivatives act on different fields, giving three possible operators for this structure. For the structure with  $\epsilon^{IJK}$  one can use

$$Tr(\tau^I\tau^J\tau^K) = 2i\epsilon^{IJK}. \quad (4.36)$$

and (2.48) in order to write it in terms of operators without the epsilon tensor. Hence in total there are three linearly independent operators:

$$\mathcal{O}_{H61} = \left( \phi^\dagger\phi - \frac{\hat{v}^2}{2} \right)^2 ((D_\mu\phi)^\dagger D^\mu\phi), \quad (4.37)$$

$$\mathcal{O}_{H62} = \left( \phi^\dagger\phi - \frac{\hat{v}^2}{2} \right) ((D_\mu\phi)^\dagger\phi)(\phi^\dagger D^\mu\phi), \quad (4.38)$$

$$\mathcal{O}_{H63} = \left( \phi^\dagger\phi - \frac{\hat{v}^2}{2} \right) ((D_\mu\phi)^\dagger\phi)(D^\mu\phi)^\dagger\phi + \phi^\dagger D_\mu\phi\phi^\dagger D^\mu\phi. \quad (4.39)$$

#### 4.2.3.3. $\phi^4 D^4$

The operator class  $\phi^4 D^4$  contains the S-operators from the Éboli basis. In order to make comparisons easier, these operators are set as the first three operators of this class:

$$\mathcal{O}_{S0} = ((D_\mu\phi)^\dagger D^\nu\phi)((D^\mu\phi)^\dagger D_\nu\phi), \quad (4.40)$$

$$\mathcal{O}_{S1} = ((D_\mu\phi)^\dagger D^\mu\phi)((D_\nu\phi)^\dagger D^\nu\phi), \quad (4.41)$$

$$\mathcal{O}_{S2} = ((D_\mu\phi)^\dagger D^\nu\phi)((D_\nu\phi)^\dagger D^\mu\phi). \quad (4.42)$$

Starting with the structure of the higgs fields one can either have two triplets or two singlets. Using equation (2.48) one can again ignore the triplets. For the placement of the derivatives one can group the resulting operators in the following way:

- All four derivatives act on the same field.
- Three derivatives act on the same field.
- Two derivatives, that are contracted, act on the same field, while the other two act on one different field.
- Two derivatives, that are contracted, act on the same field, while the other two act on two different fields.
- Two derivatives, that are not contracted, act on the same field.
- All derivatives act on different fields.

Four derivatives acting on the same field can be connected to three derivatives acting on the same field using IBP. Similarly one can move from this group to the group where two not contracted derivatives act on the same field using IBP. This again renders this group linearly dependent. For the third group one can use IBP for one derivative of each lorentz index once. This results in operators where at most two derivatives, that are not contracted, act on the same field. This group can therefore also be linked to the last two groups. Similarly for the fourth group one can use IBP for one of the derivatives that act on the same field, to move to the last two groups. If two not contracted derivatives act on the same field the other two can either act both on one other field

$$\mathcal{O}_{H4D41} = \frac{1}{2} \left( (D_\mu D^\nu \phi)^\dagger \phi (D^\mu D_\nu \phi)^\dagger \phi + \phi^\dagger D_\mu D^\nu \phi \phi^\dagger (D^\mu D_\nu \phi) \right), \quad (4.43)$$

$$\mathcal{O}_{H4D42} = \left( \phi^\dagger \phi - \frac{\hat{v}^2}{2} \right) ((D_\mu D^\nu \phi)^\dagger D^\mu D_\nu \phi), \quad (4.44)$$

$$\mathcal{O}_{H4D43} = \frac{1}{2} \left( (D_\mu D^\nu \phi)^\dagger \phi \phi^\dagger (D^\mu D_\nu \phi) \right), \quad (4.45)$$

or act on two other fields

$$\mathcal{O}_{H4D44} = \frac{1}{2} \left( (D_\mu D^\nu \phi)^\dagger D^\mu \phi \phi^\dagger D_\nu \phi + (D_\mu \phi)^\dagger D^\mu D^\nu \phi (D_\nu \phi)^\dagger \phi \right), \quad (4.46)$$

$$\mathcal{O}_{H4D45} = \frac{1}{2} \left( (D_\mu D^\nu \phi)^\dagger D^\mu \phi (D_\nu \phi)^\dagger \phi + (D_\mu \phi)^\dagger D^\mu D^\nu \phi \phi^\dagger D_\nu \phi \right), \quad (4.47)$$

$$\mathcal{O}_{H4D46} = \frac{1}{2} \left( (D_\mu \phi)^\dagger D_\nu \phi \right) \left( (D^\mu D^\nu \phi)^\dagger \phi + \phi^\dagger D^\mu D^\nu \phi \right). \quad (4.48)$$

The last group of operators contains the three S-operators.

A slightly different approach of constructing the operators is starting with the four higgs fields

$$(\phi^\dagger \phi)(\phi^\dagger \phi) \quad (4.49)$$

and adding the derivatives one by one. The first derivative can be fixed to one position as all resulting possibilities are identical up to hermitian conjugation

$$((D_\mu \phi)^\dagger \phi)(\phi^\dagger \phi) \quad (4.50)$$

Using IBP one can forbid one position for each further derivative thereby avoiding two contracted derivatives acting on the same field giving the following possibilities

$$((D_\mu\phi)^\dagger D^\mu\phi)(\phi^\dagger\phi), \quad (4.51)$$

$$((D_\mu\phi)^\dagger\phi)((D^\mu\phi)^\dagger\phi), \quad (4.52)$$

$$((D_\mu\phi)^\dagger\phi)(\phi^\dagger D_\mu\phi). \quad (4.53)$$

Once all derivatives are placed one arrives at 27 possible operators. After eliminating identical operators, operators that are identical after interchanging the two lorentz indices and operators that are the hermitian conjugate of each other, one arrives at the same nine operators mentioned beforehand.

#### 4.2.3.4. $\phi^4 D^2 X$

The operator class  $\phi^4 D^2 X$  can contain two structures that produce a  $SU(2)_L$  singlet

$$\phi^\dagger\phi[\phi^\dagger\tau^I\phi]W_{\mu\nu}^I, \quad (4.54)$$

$$\epsilon^{IJK}[\phi^\dagger\tau^I\phi][\phi^\dagger\tau^J\phi]W_{\mu\nu}^K. \quad (4.55)$$

Starting with the first structure one finds the following groups of operators

- Both derivatives act on the field strength tensor.
- One derivative acts on the field strength tensor.
- Both derivatives act on the same higgs field.
- The derivatives act on different higgs fields.

The first group only contains one operator that due to

$$D^\mu D^\nu W_{\mu\nu}^I = D^\nu D^\mu W_{\mu\nu}^I + \mathcal{O}(X^2), \quad (4.56)$$

$$2D^\mu D^\nu W_{\mu\nu}^I = \mathcal{O}(X^2), \quad (4.57)$$

is proportional to lower class operators. The operators that appear in the second group (up to hermitian conjugation) are

$$\phi^\dagger D^\nu\phi[\phi^\dagger\tau^I\phi](D^\mu W_{\mu\nu})^I, \quad (4.58)$$

$$\phi^\dagger\phi[\phi^\dagger\tau^I D^\nu\phi](D^\mu W_{\mu\nu})^I. \quad (4.59)$$

Using IBP on the first group, one generates the sum of these operators which, since the first group vanishes, makes them linearly dependent up to lower class operators. The third group is again symmetric under swapping the derivatives (up to lower class operators) and anti symmetric under exchanging the lorentz indices due to the field strength tensor. Consequently this group vanishes. The fourth group contains four operators

$$i\phi^\dagger\phi\left((D^\mu\phi)^\dagger\tau^I D^\nu\phi - (D^\nu\phi)^\dagger\tau^I D^\mu\phi\right)W_{\mu\nu}^I, \quad (4.60)$$

$$i\left([\phi^\dagger(D^\mu\phi)^\dagger\tau^I\phi][\phi^\dagger(D^\nu\phi)^\dagger\phi] - [\phi^\dagger\tau^I D^\mu\phi][\phi^\dagger D^\nu\phi]\right)W_{\mu\nu}^I, \quad (4.61)$$

$$i\left([\phi^\dagger(D^\mu\phi)^\dagger\tau^I\phi][\phi^\dagger D^\nu\phi] - [\phi^\dagger\tau^I D^\mu\phi][\phi^\dagger(D^\nu\phi)^\dagger\phi]\right)W_{\mu\nu}^I, \quad (4.62)$$

$$i\phi^\dagger\tau^I\phi\left((D^\mu\phi)^\dagger D^\nu\phi - (D^\nu\phi)^\dagger D^\mu\phi\right)W_{\mu\nu}^I. \quad (4.63)$$

These operators are connected to the second group by using IBP for the derivative, that acts on the field strength tensor in that group. In total one is left with six operators and three equations linking them to each other from using IBP. In terms of equations one can write these three equations

$$(4.58) + (4.59) \propto 0, \quad (4.64)$$

$$(4.58) \propto (4.61) + (4.62) + (4.63), \quad (4.65)$$

$$(4.59) \propto (4.61) + (4.62) + (4.60). \quad (4.66)$$

Equations (4.65) and (4.66) implies that (4.58) and (4.59) linearly depend on the fourth group. Using (4.64) one can subsequently find a linear relation between (4.63) and the other three operators. So only three of these operators are linearly independent leaving

$$\mathcal{O}_{HHDDW_1} = i \left( \phi^\dagger \phi - \frac{\hat{v}^2}{2} \right) \left( (D^\mu \phi)^\dagger \tau^I D^\nu \phi - (D^\nu \phi)^\dagger \tau^I D^\mu \phi \right) W_{\mu\nu}^I, \quad (4.67)$$

$$\mathcal{O}_{HHDDW_2} = i \left( [(D^\mu \phi)^\dagger \tau^I \phi] [(D^\nu \phi)^\dagger \phi] - [\phi^\dagger \tau^I D^\mu \phi] [\phi^\dagger D^\nu \phi] \right) W_{\mu\nu}^I, \quad (4.68)$$

$$\mathcal{O}_{HHDDW_3} = i \left( [(D^\mu \phi)^\dagger \tau^I \phi] [\phi^\dagger D^\nu \phi] - [\phi^\dagger \tau^I D^\mu \phi] [(D^\nu \phi)^\dagger \phi] \right) W_{\mu\nu}^I. \quad (4.69)$$

For the second structure one can rewrite the epsilon tensor as

$$Tr(\tau^I \tau^J \tau^K) = 2i \epsilon^{IJK}. \quad (4.70)$$

Using equation (2.48) one can now rewrite all operators of the second structure in a similar structure as 4.54. Therefore all of the operators in the second structure can be written in terms of the first structure making them redundant.

#### 4.2.3.5. $\phi^4 X^2$

In the operator class  $\phi^4 X^2$  one can construct the following  $SU(2)_L$  structures

$$[\phi^\dagger \phi] [\phi^\dagger \phi] W_{\mu\nu}^I W^{I\mu\nu}, \quad (4.71)$$

$$[\phi^\dagger \tau^J \phi] [\phi^\dagger \tau^J \phi] W_{\mu\nu}^I W^{I\mu\nu}, \quad (4.72)$$

$$[\phi^\dagger \tau^I \phi] [\phi^\dagger \tau^J \phi] W_{\mu\nu}^I W^{J\mu\nu}, \quad (4.73)$$

$$\epsilon^{IJK} [\phi^\dagger \phi] [\phi^\dagger \tau^I \phi] W_{\mu\nu}^J W^{K\mu\nu}. \quad (4.74)$$

The first two structures are identical after using equation (2.48) while the last structure vanishes as it is symmetric under swapping  $J$  and  $K$  with respect to the field strength tensors and contains a Levi-Civita tensor. The operators chosen for this basis are

$$\mathcal{O}_{W_2H_41} = \left( \phi^\dagger \phi - \frac{\hat{v}^2}{2} \right)^2 W_{\mu\nu}^I W^{I\mu\nu}, \quad (4.75)$$

$$\mathcal{O}_{W_2H_43} = (\phi^\dagger \tau^I \phi) (\phi^\dagger \tau^J \phi) W_{\mu\nu}^I W^{J\mu\nu}. \quad (4.76)$$

#### 4.2.3.6. $\phi^2 D^6$

The six derivatives in the operator class  $\phi^2 D^6$  can be arranged freely by using IBP and the fact that commutators of derivatives generate lower class operators. Therefore, all operators in this class are linearly dependent up to lower class operators and one can chose

$$\mathcal{O}_{HDDD} = (D_\mu D_\nu D_\alpha \phi)^\dagger D^\mu D^\nu D^\alpha \phi. \quad (4.77)$$

### 4.2.3.7. $\phi^2 D^4 X$

For the operator class  $\phi^2 D^4 X$  one can start with the structure

$$\phi^\dagger \tau^I \phi W_{\mu\nu}^I \quad (4.78)$$

and add the derivatives afterwards. Using IBP one can argue that all derivatives should act on the higgs fields generating three groups of operators

- All derivatives act on the same field.
- Three derivatives act on the same field and one on the other field.
- Two derivatives act on each field.

By using equation (4.24) one can generate a symmetric term in  $D^\mu$  and  $D^\nu$  whenever both of these derivatives act on the same field. Since the field strength tensor is anti symmetric in  $\mu$  and  $\nu$  all of these operators vanish. In the end one is left with two operators in which  $D^\mu$  and  $D^\nu$  act on different fields and no derivatives act on the field strength tensor

$$\mathcal{O}_{HD4W1} = i(D^\alpha D^\mu \phi)^\dagger \tau^I D_\alpha D^\nu \phi W_{\mu\nu}^I, \quad (4.79)$$

$$\mathcal{O}_{HD4W2} = i \left( (D_\alpha D^\alpha D^\nu \phi)^\dagger \tau^I D^\mu \phi - (D^\mu \phi)^\dagger \tau^I D_\alpha D^\alpha D^\nu \phi \right) W_{\mu\nu}^I. \quad (4.80)$$

### 4.2.3.8. $\phi^2 D^2 X^2$

For the operator class  $\phi^2 D^2 X^2$  one wants to create a set of operators that contains the M-operators

$$\mathcal{O}_{M0} = \frac{1}{2} (D_\alpha \phi)^\dagger D^\alpha \phi W_{\mu\nu}^I W^{I\mu\nu}, \quad (4.81)$$

$$\mathcal{O}_{M1} = \frac{1}{2} (D_\mu \phi)^\dagger D^\nu \phi W_{\nu\alpha}^I W^{I\alpha\mu}, \quad (4.82)$$

$$\mathcal{O}_{M7} = \frac{i}{2} \epsilon^{IJK} ((D_\mu \phi)^\dagger \tau^I D^\nu \phi) W_{\nu\alpha}^J W^{K\alpha\mu}. \quad (4.83)$$

Before placing the derivatives one can come up with four structures

$$\phi^\dagger \phi W_{\mu\nu}^I W^{I\mu\nu}, \quad (4.84)$$

$$\phi^\dagger \phi W_{\mu\nu}^I W^{I\mu\alpha}, \quad (4.85)$$

$$\epsilon^{IJK} \phi^\dagger \tau^K \phi W_{\mu\nu}^I W^{J\mu\nu}, \quad (4.86)$$

$$\epsilon^{IJK} \phi^\dagger \tau^K \phi W_{\mu\nu}^I W^{J\mu\alpha}. \quad (4.87)$$

For the derivatives there are the following options

- Both derivatives act on the same field strength tensor.
- One derivative acts on each field strength tensor.
- One derivative acts on a field strength tensor and one on a higgs field.
- Both derivatives act on the same higgs field.
- Both derivatives act on different higgs fields.

The first of these options can always be ignored by using IBP which generates the second and third option. Writing down the possible operators for the first structure one gets

$$\phi^\dagger \phi (D_\alpha W_{\mu\nu})^I (D^\alpha W^{\mu\nu})^I, \quad (4.88)$$

$$\phi^\dagger D_\alpha \phi W_{\mu\nu}^I (D^\alpha W^{\mu\nu})^I, \quad (4.89)$$

$$\phi^\dagger D_\alpha D^\alpha \phi W_{\mu\nu}^I W^{I\mu\nu}, \quad (4.90)$$

$$D^\alpha \phi^\dagger D_\alpha \phi W_{\mu\nu}^I W^{I\mu\nu}. \quad (4.91)$$

Using IBP one can transform the second operator into the third and the fourth which leaves three independent operators for this structure. For the second structure we can use IBP in order to avoid contractions of derivatives with field strength tensors they are acting on. The possible operators for this structure then read

$$\phi^\dagger \phi (D_\alpha W_{\mu\nu})^I (D^\nu W^{\mu\alpha})^I, \quad (4.92)$$

$$\phi^\dagger D^\nu \phi D_\alpha W_{\mu\nu}^I W^{I\mu\alpha}, \quad (4.93)$$

$$\phi^\dagger D_\alpha D^\nu \phi W_{\mu\nu}^I W^{I\mu\alpha}, \quad (4.94)$$

$$D_\alpha \phi^\dagger D^\nu \phi W_{\mu\nu}^I W^{I\mu\alpha}. \quad (4.95)$$

For the first operator we can use the Bianchi identity (4.30)

$$\begin{aligned} \phi^\dagger \phi (D_\alpha W_{\mu\nu})^I (D^\nu W^{\mu\alpha})^I &= -\phi^\dagger \phi (D_\alpha W_{\mu\nu})^I (D^\mu W^{\alpha\nu})^I - \phi^\dagger \phi D_\alpha W_{\mu\nu}^I (D^\alpha W^{\nu\mu})^I \\ &\stackrel{\mu\leftrightarrow\nu}{=} -\phi^\dagger \phi (D_\alpha W_{\nu\mu})^I (D^\nu W^{\alpha\mu})^I - \phi^\dagger \phi (D_\alpha W_{\mu\nu})^I (D^\alpha W^{\nu\mu})^I, \\ 2\phi^\dagger \phi (D_\alpha W_{\mu\nu})^I (D^\nu W^{\mu\alpha})^I &= \phi^\dagger \phi (D_\alpha W_{\mu\nu})^I (D^\alpha W^{\mu\nu})^I, \end{aligned} \quad (4.96)$$

in order to link it to the first structure. For the second operator one can do the same calculation

$$\begin{aligned} \phi^\dagger D_\alpha \phi W_{\mu\nu}^I (D^\nu W^{\mu\alpha})^I &= -\phi^\dagger D_\alpha \phi W_{\mu\nu}^I (D^\mu W^{\alpha\nu})^I - \phi^\dagger D_\alpha \phi W_{\mu\nu}^I (D^\alpha W^{\nu\mu})^I \\ &\stackrel{\mu\leftrightarrow\nu}{=} -\phi^\dagger D_\alpha \phi W_{\nu\mu}^I (D^\nu W^{\alpha\mu})^I - \phi^\dagger D_\alpha \phi W_{\mu\nu}^I (D^\alpha W^{\nu\mu})^I, \\ 2\phi^\dagger D_\alpha \phi W_{\mu\nu}^I (D^\nu W^{\mu\alpha})^I &= \phi^\dagger D_\alpha \phi W_{\mu\nu}^I (D^\alpha W^{\mu\nu})^I, \end{aligned} \quad (4.97)$$

which leaves two operators linearly independent.

As  $\mathcal{O}_{M7}$  belongs to the fourth structure this is the next one to look at. Similarly to the second structure derivatives, acting on field strength tensors they are contracted with, can be avoided using IBP. The possible operators are

$$\epsilon^{IJK} \phi^\dagger \tau^K \phi (D_\alpha W_{\mu\nu})^I (D^\nu W^{\mu\alpha})^J, \quad (4.98)$$

$$\epsilon^{IJK} \phi^\dagger \tau^K D_\alpha \phi W_{\mu\nu}^I (D^\nu W^{\mu\alpha})^J, \quad (4.99)$$

$$\epsilon^{IJK} \phi^\dagger \tau^K D^\nu D_\alpha \phi W_{\mu\nu}^I W^{J\mu\alpha}, \quad (4.100)$$

$$\epsilon^{IJK} D^\nu \phi^\dagger \tau^K D_\alpha \phi W_{\mu\nu}^I W^{J\mu\alpha}. \quad (4.101)$$

By interchanging  $\nu$  and  $\alpha$  for the first operator one can observe, that the two field strength tensors are symmetric under the transformation  $I \leftrightarrow J$ . Due to the Levi-Civita tensor this operator therefore vanishes. The third operator vanishes with the same argument and equation (4.24), leaving two independent operators for this structure.

For the third structure one can again, similarly to the first structure, avoid two derivatives acting on the same field strength tensor by using IBP. The possible operators read

$$\epsilon^{IJK} \phi^\dagger \tau^K \phi (D_\alpha W_{\mu\nu})^I (D^\alpha W^{\mu\nu})^J, \quad (4.102)$$

$$\epsilon^{IJK} \phi^\dagger \tau^K D_\alpha \phi W_{\mu\nu}^I (D^\alpha W^{\mu\nu})^J, \quad (4.103)$$

$$\epsilon^{IJK} \phi^\dagger \tau^K D^\alpha D_\alpha \phi W_{\mu\nu}^I W^{J\mu\nu}, \quad (4.104)$$

$$\epsilon^{IJK} D^\alpha \phi^\dagger \tau^K D_\alpha \phi W_{\mu\nu}^I W^{J\mu\nu}. \quad (4.105)$$

The first, the third and the fourth operator all vanish due to the Levi-Civita tensor being anti symmetric when swapping  $I$  and  $J$ , while the remaining operator is symmetric under this transformation. For the remaining operator one can use the Bianchi identity in order to get

$$\begin{aligned} \epsilon^{IJK} \phi^\dagger \tau^K D_\alpha \phi W_{\mu\nu}^I (D^\alpha W^{\mu\nu})^J &= -\epsilon^{IJK} \phi^\dagger \tau^K D_\alpha \phi W_{\mu\nu}^I (D^\mu W^{\nu\alpha})^J \\ &\quad -\epsilon^{IJK} \phi^\dagger \tau^K D_\alpha \phi W_{\mu\nu}^I (D^\nu W^{\alpha\mu})^J \end{aligned} \quad (4.106)$$

$$\stackrel{\mu \leftrightarrow \nu}{=} -2\epsilon^{IJK} \phi^\dagger \tau^K D_\alpha \phi W_{\mu\nu}^I (D^\mu W^{\nu\alpha})^J \quad (4.107)$$

thereby linking it to the fourth structure.

In total one can find the following seven operators for this class

$$\mathcal{O}_{M0} = \frac{1}{2} (D_\alpha \phi)^\dagger D^\alpha \phi W_{\mu\nu}^I W^{I\mu\nu}, \quad (4.108)$$

$$\mathcal{O}_{M1} = \frac{1}{2} (D_\mu \phi)^\dagger D^\nu \phi W_{\nu\alpha}^I W^{I\alpha\mu}, \quad (4.109)$$

$$\mathcal{O}_{M7} = \frac{i}{2} \epsilon_{IJK} ((D_\mu \phi)^\dagger \tau^I D^\nu \phi) W_{\nu\alpha}^J W^{K\alpha\mu} \quad (4.110)$$

$$\mathcal{O}_{DWH1} = \left( \phi^\dagger \phi - \frac{\hat{v}^2}{2} \right) (D_\alpha W_{\mu\nu})^I (D^\alpha W^{\mu\nu})^I \quad (4.111)$$

$$\mathcal{O}_{DWH2} = ((D_\alpha D^\mu \phi)^\dagger \phi + \phi^\dagger D_\alpha D^\mu \phi) W_{\mu\nu}^I W^{I\alpha\nu} \quad (4.112)$$

$$\mathcal{O}_{DWH3} = ((D_\alpha D^\alpha \phi)^\dagger \phi + \phi^\dagger D_\alpha D^\alpha \phi) W_{\mu\nu}^I W^{I\mu\nu} \quad (4.113)$$

$$\mathcal{O}_{DWH4} = i\epsilon_{IJK} ((D^\mu \phi)^\dagger \tau^I \phi - \phi^\dagger \tau^I D^\mu \phi) W_{\mu\alpha}^J (D_\nu W^{\nu\alpha})^K \quad (4.114)$$

#### 4.2.3.9. $\phi^2 X^3$

The operator class  $\phi^2 X^3$  comes with two possible structures

$$\phi^\dagger \phi \epsilon_{IJK} W_\mu^{I\nu} W_\nu^{J\rho} W_\rho^{K\mu}, \quad (4.115)$$

$$\phi^\dagger \tau^I \phi W_\mu^{I\nu} W_\nu^{J\rho} W_\rho^{J\mu}, \quad (4.116)$$

leaving no free indices for other operators. In the second structure  $W_\nu^{J\rho} W_\rho^{J\mu}$  is symmetric under interchanging  $\mu \leftrightarrow \nu$  which leaves only one operator for this class

$$\mathcal{O}_{W3H21} = \left( \phi^\dagger \phi - \frac{\hat{v}^2}{2} \right) \epsilon_{IJK} W_\mu^{I\nu} W_\nu^{J\rho} W_\rho^{K\mu}. \quad (4.117)$$

#### 4.2.3.10. $D^4X^2$

In the operator class  $D^4X^2$  one is again free to chose the position of the derivatives, as all possibilities are equal (up to lower class operators) using equation (4.24) and IBP. The resulting operator is

$$\mathcal{O}_{D^2W} = (D_\alpha D^\alpha W_{\mu\nu})^I (D_\beta D^\beta W^{\mu\nu})^I. \quad (4.118)$$

#### 4.2.3.11. $D^2X^3$

The  $SU(2)_L$  structure of this operator class is identical to the one of the operator class  $X^3$ . Concerning the lorentz structure there are three groups:

- Both derivatives are connected to the same field strength tensor.
- Both derivatives are connected to each other.
- The derivatives are connected to different field strength tensors.

For the first group the following operators are possible

$$\epsilon_{IJK} (D^\mu D^\nu W_{\mu\nu})^I W_{\rho\sigma}^J W^{K\rho\sigma}, \quad (4.119)$$

$$\epsilon_{IJK} W_{\mu\nu}^I (D^\mu D^\nu W_{\rho\sigma})^J W^{K\rho\sigma}, \quad (4.120)$$

$$\epsilon_{IJK} (D^\mu W_{\mu\nu})^I (D^\nu W_{\rho\sigma})^J W^{K\rho\sigma}, \quad (4.121)$$

$$\epsilon_{IJK} W_{\mu\nu}^I (D^\mu W_{\rho\sigma})^J (D^\nu W^{\rho\sigma})^K. \quad (4.122)$$

Using equation (4.24) the derivatives in the first two operators are symmetric under  $\mu \leftrightarrow \nu$  (up to lower class operators). Due to the field strength tensor  $W_{\mu\nu}^I$  they then vanish. The third operator is proportional to the second one plus the fourth one using IBP for  $D^\mu$ , leaving one independent operator for this group.

For the second group the two derivatives either act on the same field strength tensor or on two different field strength tensors. These two possibilities are connected via IBP:

$$\begin{aligned} & \epsilon_{IJK} (D_\alpha D^\alpha W_{\mu\nu})^I W^{J\nu\rho} W_\rho^{K\mu} \\ \stackrel{\text{IBP}}{=} & - \epsilon_{IJK} (D_\alpha W_{\mu\nu})^I (D^\alpha W^{\nu\rho})^J W_\rho^{K\mu} - \epsilon_{IJK} (D_\alpha W^{\mu\nu})^I W_\nu^{J\rho} (D^\alpha W_{\rho\mu})^K \\ \stackrel{\mu \leftrightarrow \nu}{=} & - \epsilon_{IJK} (D_\alpha W_{\mu\nu})^I (D^\alpha W^{\nu\rho})^J W_\rho^{K\mu} - \epsilon_{IJK} (D_\alpha W^{\nu\mu})^I W_\mu^{J\rho} (D^\alpha W_{\rho\nu})^K \\ = & - 2\epsilon_{IJK} (D_\alpha W_{\mu\nu})^I (D^\alpha W^{\nu\rho})^J W_\rho^{K\mu}. \end{aligned} \quad (4.123)$$

leaving again only one operator for this group.

For the last group there are nine possibilities:

$$\mathcal{O}_1 = \epsilon_{IJK} (D_\sigma D_\mu W^{\mu\nu})^I W_\nu^{J\rho} W_\rho^{K\sigma}, \quad (4.124)$$

$$\mathcal{O}_2 = \epsilon_{IJK} (D^\mu W_{\mu\nu})^I (D_\sigma W^{\nu\rho})^J W_\rho^{K\sigma}, \quad (4.125)$$

$$\mathcal{O}_3 = \epsilon_{IJK} (D_\mu W^{\mu\nu})^I W_\nu^{J\rho} (D^\sigma W_{\rho\sigma})^K, \quad (4.126)$$

$$\mathcal{O}_4 = \epsilon_{IJK} (D_\sigma W_{\mu\nu})^I (D^\mu W^{\nu\rho})^J W_\rho^{K\sigma}, \quad (4.127)$$

$$\mathcal{O}_5 = \epsilon_{IJK} W_{\mu\nu}^I (D_\sigma D^\mu W^{\nu\rho})^J W_\rho^{K\sigma}, \quad (4.128)$$

$$\mathcal{O}_6 = \epsilon_{IJK} W_\mu^{I\nu} (D^\mu W_{\nu\rho})^J (D_\sigma W^{\rho\sigma})^K, \quad (4.129)$$

$$\mathcal{O}_7 = \epsilon_{IJK} (D^\sigma W^{\mu\nu})^I W_\nu^{J\rho} (D_\mu W_{\rho\sigma})^K, \quad (4.130)$$

$$\mathcal{O}_8 = \epsilon_{IJK} W_\mu^{I\nu} (D_\sigma W_{\nu\rho})^J (D^\mu W^{\rho\sigma})^K, \quad (4.131)$$

$$\mathcal{O}_9 = \epsilon_{IJK} W_\mu^{I\nu} W_\nu^{J\rho} (D^\sigma D^\mu W_{\rho\sigma})^K. \quad (4.132)$$

The first operator  $\mathcal{O}_1$  can be linked to the second group in the following way

$$\begin{aligned}
& \epsilon_{IJK} (D_\sigma D^\mu W_{\mu\nu})^I W^{J\nu\rho} W_\rho^{K\sigma} \\
\stackrel{\text{BI}}{=} & -\epsilon_{IJK} (D_\mu D^\mu W_{\nu\sigma})^I W^{J\nu\rho} W_\rho^{K\sigma} - \epsilon_{IJK} (D_\nu D^\mu W_{\sigma\mu})^I W^{J\nu\rho} W_\rho^{K\sigma} \\
\stackrel{\sigma \leftrightarrow \nu}{=} & -\epsilon_{IJK} (D_\mu D^\mu W_{\nu\sigma})^I W^{J\nu\rho} W_\rho^{K\sigma} - \epsilon_{IJK} (D_\sigma D^\mu W_{\nu\mu})^I W^{J\sigma\rho} W_\rho^{K\nu} \\
= & -\epsilon_{IJK} (D_\mu D^\mu W_{\nu\sigma})^I W^{J\nu\rho} W_\rho^{K\sigma} - \epsilon_{IJK} (D_\sigma D^\mu W_{\mu\nu})^I W_\rho^{K\sigma} W^{J\nu\rho} \\
= & -\frac{1}{2} \epsilon_{IJK} (D_\mu D^\mu W_{\nu\sigma})^I W^{J\nu\rho} W_\rho^{K\sigma}. \tag{4.133}
\end{aligned}$$

Using the same ideas the second operator  $\mathcal{O}_2$  can be linked to the second group:

$$\begin{aligned}
& \epsilon_{IJK} (D_\mu W^{\mu\nu})^I (D_\sigma W_{\nu\rho})^J W^{K\rho\sigma} \\
\stackrel{\text{BI}}{=} & -\epsilon_{IJK} (D_\mu W^{\mu\nu})^I (D_\nu W_{\rho\sigma})^J W^{K\rho\sigma} - \epsilon_{IJK} (D_\mu W^{\mu\nu})^I (D_\rho W_{\sigma\nu})^J W^{K\rho\sigma} \\
\stackrel{\sigma \leftrightarrow \rho}{=} & -\epsilon_{IJK} (D_\mu W^{\mu\nu})^I (D_\nu W_{\rho\sigma})^J W^{K\rho\sigma} - \epsilon_{IJK} (D_\mu W^{\mu\nu})^I (D_\sigma W_{\rho\nu})^J W^{K\sigma\rho} \\
= & -\frac{1}{2} \epsilon_{IJK} (D_\mu W^{\mu\nu})^I (D_\nu W_{\rho\sigma})^J W^{K\rho\sigma}. \tag{4.134}
\end{aligned}$$

In a similar fashion one can deal with the fifth operator  $\mathcal{O}_5$

$$\begin{aligned}
& \epsilon_{IJK} W^{I\mu\nu} (D_\sigma D_\mu W_{\nu\rho})^J W^{K\rho\sigma} \\
\stackrel{\text{BI}}{=} & -\epsilon_{IJK} W^{I\mu\nu} (D_\sigma D_\rho W_{\mu\nu})^J W^{K\rho\sigma} - \epsilon_{IJK} W^{I\mu\nu} (D_\sigma D_\nu W_{\rho\mu})^J W^{K\rho\sigma} \\
\stackrel{\nu \leftrightarrow \mu}{=} & -\epsilon_{IJK} W^{I\mu\nu} (D_\sigma D_\rho W_{\mu\nu})^J W^{K\rho\sigma} - \epsilon_{IJK} W^{I\nu\mu} (D_\sigma D_\mu W_{\rho\nu})^J W^{K\rho\sigma} \\
= & -\frac{1}{2} \epsilon_{IJK} W^{I\mu\nu} (D_\sigma D_\rho W_{\mu\nu})^J W^{K\rho\sigma}, \tag{4.135}
\end{aligned}$$

linking it to the first group. For the remaining operators one can use IBP and symmetry arguments

$$\mathcal{O}_3 \stackrel{\text{IBP}}{=} -\mathcal{O}_2 - \mathcal{O}_1, \tag{4.136}$$

$$\mathcal{O}_4 \stackrel{\text{IBP}}{=} -\mathcal{O}_5 - \mathcal{O}_6, \tag{4.137}$$

$$\mathcal{O}_6 \propto \mathcal{O}_2 (\mu \leftrightarrow \sigma, \nu \leftrightarrow \rho), \tag{4.138}$$

$$\mathcal{O}_7 \stackrel{\text{IBP}}{=} -\mathcal{O}_8 - \mathcal{O}_9, \tag{4.139}$$

$$\mathcal{O}_8 \propto \mathcal{O}_4 (\mu \leftrightarrow \sigma, \nu \leftrightarrow \rho), \tag{4.140}$$

$$\mathcal{O}_9 \propto \mathcal{O}_1 (\mu \leftrightarrow \sigma, \nu \leftrightarrow \rho). \tag{4.141}$$

Using all of these equations there are no independent operators left in this group and one is left with two operators for the whole class

$$\mathcal{O}_{DWWW0} = \epsilon_{IJK} (D_\alpha W_{\mu\nu})^I (D^\alpha W^{\nu\rho})^J W_\rho^{K\mu}, \tag{4.142}$$

$$\mathcal{O}_{DWWW1} = \epsilon_{IJK} (D^\alpha W_{\mu\nu})^I (D^\beta W^{\mu\nu})^J W_{\alpha\beta}^K. \tag{4.143}$$

**4.2.3.12.  $X^4$** 

For the last operator class,  $X^4$ , only one  $SU(2)_L$  structure is possible. For the lorentz indices four possibilities can be found. These possibilities are the T-operators

$$\mathcal{O}_{T0} = \frac{1}{4} W_{\mu\nu}^I W^{I\mu\nu} W_{\alpha\beta}^J W^{J\alpha\beta}, \quad (4.144)$$

$$\mathcal{O}_{T1} = \frac{1}{4} W_{\mu\nu}^I W^{I\alpha\beta} W_{\alpha\beta}^J W^{J\mu\nu}, \quad (4.145)$$

$$\mathcal{O}_{T2} = \frac{1}{4} W_{\mu}^{I\nu} W_{\nu}^{I\alpha} W_{\alpha}^{J\beta} W_{\beta}^{J\mu}, \quad (4.146)$$

$$\mathcal{O}_{T3} = \frac{1}{4} W_{\mu\nu}^I W_{\alpha\beta}^I W^{J\nu\alpha} W^{J\beta\mu}. \quad (4.147)$$

### 4.2.4. Renormalization

For the renormalization of the EFT one can go one of two ways

- start with a fully renormalized model (e.g. on-shell renormalized) and do the matching afterwards
- start with a non renormalized theory and perform the renormalization after the matching using the same renormalization criteria.

For a  $\overline{\text{MS}}$ -scheme these methods lead to identical results as all  $\frac{1}{\epsilon}$  poles (and the finite part that comes with them) appear in the coefficients for the SM operators. So it does not matter whether they are subtracted before or after the matching procedure. For other finite renormalizations one needs to be a bit more careful. Starting with the treatment of the higgs tadpoles that can arise from the model discussed in this paper, one can expand the resulting higgs one point function as

$$T = \sum_{n=1}^{\infty} \frac{c_n \hat{v}^{3+(2n-4)}}{\Lambda^{2n-4}}. \quad (4.148)$$

When renormalizing the underlying theory the whole expression for the tadpole is needed for the counterterm. The counterterm operators, being dimension-2 and -4 operators, therefore come with coefficients that are needed in order to cancel higher dimensional operators. When going to the EFT these coefficients are expected to change depending on up to which dimension the matching is performed. In a similar vein the counterterms required for an on-shell renormalization are expected to change between the full model and the EFT.

The counterterms for an on-shell and tadpole free renormalization for the set of operators presented in sec. 4.2.1-4.2.3 in the  $SU_2$ -limit can be calculated using the definitions in equation (3.72), (3.73), (3.79), (3.78), (3.81) and (3.80):

$$\delta_{Z_v} = -c_{\text{kin}} + \frac{g^2 \hat{v}^2 c_{DW}}{\Lambda_{EFT}^2} + \frac{g^4 \hat{v}^4 c_{D2W}}{2\Lambda_{EFT}^4}, \quad (4.149)$$

$$\delta_{Z_W} = -c_{\text{Gauge}} + \frac{2g^2 \hat{v}^2 c_{DW}}{\Lambda_{EFT}^2} + \frac{3g^4 \hat{v}^4 c_{D2W}}{4\Lambda_{EFT}^4} + \frac{g^2 \hat{v}^2 c_{HDD}}{8\Lambda_{EFT}^4}, \quad (4.150)$$

$$\delta_{Z_h} = -c_{\text{kin}} + \frac{-(c_{HD1} + 2c_{HD3})\hat{v}^2 - 4m_h^2 c_{HDD}}{\Lambda_{EFT}^2} \quad (4.151)$$

$$- \frac{m_h^2 (\hat{v}^2 (2c_{H4D41} + c_{H4D43}) + 6m_h^2 c_{HDDD})}{\Lambda_{EFT}^4} \quad (4.152)$$

$$\delta_{\lambda_h} = -c_{H4} + \frac{c_{\text{kin}} m_h^2}{\hat{v}^2} + \frac{m_h^2 (c_{HD1} + 2c_{HD3} - g^2 c_{DW} + 2\lambda_h c_{HDD})}{2\Lambda_{EFT}^2} \\ + \frac{m_h^2 (m_h^2 (8\lambda_h c_{HDDD} + c_{H4D43} + 2c_{H4D41}) - 2g^4 \hat{v}^2 c_{D2W})}{8\Lambda_{EFT}^4}, \quad (4.153)$$

$$\delta_{\mu^2} = -c_{H2} - \frac{m_h^2 c_{\text{kin}}}{2} - \frac{m_h^2 (\hat{v}^2 (c_{HD1} + 2c_{HD3}) + 2m_h^2 c_{HDD})}{4\Lambda_{EFT}^2} \\ - \frac{m_h^4 (4m_h^2 c_{HDDD} + \hat{v}^2 (2c_{H4D41} + c_{H4D43}))}{8\Lambda_{EFT}^4}. \quad (4.154)$$

The explicit counterterms for the EFT can be found in section B.

**Table 4.1.:** Wilson coefficients for dimensions d=2 and d=4 showing the  $m^0$  and  $m^2$  terms.

D2, D4		$c_{\mathcal{O},\epsilon}$	$c_{\mathcal{O}}$
$\mathcal{O}_{H2}$	$-\phi^\dagger\phi$	$\frac{3(2j+1)\lambda^2 m^2}{4\pi^2\epsilon}$	$\frac{(2j+1)\lambda^2 m^2 (3 \log(\frac{\mu^2}{m^2}) + 1)}{4\pi^2}$
$\mathcal{O}_{H4}$	$-(\phi^\dagger\phi)^2$	$\frac{3(2j+1)\lambda^4}{24\pi^2\epsilon}$	$\frac{(2j+1)\lambda^4 (3 \log(\frac{\mu^2}{m^2}) - 8)}{24\pi^2}$
$\mathcal{O}_{\text{Gauge}}$	$\frac{-1}{4} W_{\mu\nu}^I W^{I\mu\nu}$	$\frac{g^2 j^2 (2j+1)}{12\pi^2\epsilon}$	$\frac{g^2 j^2 (2j+1) (\log(\frac{\mu^2}{m^2}))}{12\pi^2}$
$\mathcal{O}_{\text{kin}}$	$(D_\mu\phi)^\dagger D^\mu\phi$	$\frac{3(2j+1)\lambda^2}{24\pi^2\epsilon}$	$\frac{(2j+1)\lambda^2 (3 \log(\frac{\mu^2}{m^2}) - 2)}{24\pi^2}$

### 4.3. Matching

In general the EFT-matching can be done on different levels of the calculation ranging from process by process down to n-point function by n-point function. Matching on the level of whole processes is required when a general basis is used as can be seen in section 4.1.1. Somewhere in between lies the method of integrating out the heavy degrees of freedom. For heavy vector like fermions this tends to be a quite tedious calculation but new studies [51][45] have provided a more straight forward approach to do so on the dimension-6 level. The result of this method is an effective Lagrangian for each operator class. This effective Lagrangian can directly be used for matching or it can be further processed (e.g. EOM, IBP, etc.) in order to fit the chosen operator basis. This procedure however is not readily available for dimension-8 operators stemming from heavy vector like fermions.

Doing the matching for each n-point function is the most straight forward way of calculating the coefficients, once a dedicated basis for the underlying theory is found. Once the basis is known the contribution to each affected n-point function of the underlying theory is calculated as a series in  $\frac{1}{\Lambda_{EFT}}$ . One can further separate the results for each n-point function in terms of lorentz and momentum structures (similar to the structures used for the reduction of one loop tensor functions in section A), in order to arrive at a large linear system of equations.

For the EFT scale of the model in this thesis  $m_\Psi$  is chosen. The other scales, that are supposed to be small in comparison, are the masses of the SM ( $\sim \hat{v}$ ), the mass splitting in the model as well as the momenta involved in the process. This results in the requirements for the expansion parameters

$$\frac{\hat{v}}{m_\Psi} \ll 1, \quad (4.155)$$

$$\frac{\lambda \hat{v}}{\sqrt{2} m_\Psi} \ll 1, \quad (4.156)$$

$$\frac{p_i p_j}{m_\Psi^2} \ll 1. \quad (4.157)$$

Looking at these requirements from the point of view of the EFT, equations (4.155) and (4.156) guarantee that higher dimensional operators with more higgs fields can be neglected, while (4.157) guarantees that higher dimensional operators with more derivatives can be neglected. As field strength tensors can be written as a commutator of derivatives, one can see, that any higher dimensional operator (unless specifically enhanced by an unaccounted effect) should be suppressed, which allows cutting the

EFT expansion after dimension-8.

In tables 4.1, 4.2, 4.3, 4.4 and 4.5 the resulting Wilson coefficients for  $J = 3$  and  $J = 4$  are presented. For the Wilson coefficients of an operator of dimension  $d$  one finds terms that are suppressed by  $\frac{1}{m^{(d-4)}}$ , which is the expected suppression of  $\frac{1}{\Lambda_{EFT}^{(d-4)}}$  as well as terms with additional suppression factors of  $\frac{1}{m}$  i.e.

$$\left( \frac{c_1}{m^2} + \frac{c_2 \lambda^2 \hat{v}^2}{m^4} \right) \mathcal{O}^{(d=6)}. \quad (4.158)$$

These additional  $\frac{1}{m^4}$  terms appear at the same order in the expansion as the dimension 8 operators. Therefore these contributions have to be treated similarly as them. When talking about dimension 6 terms in the EFT one should only consider the  $\frac{1}{m^2}$  part of the Wilson coefficient. Similarly the  $\frac{1}{m^4}$  part of the Wilson coefficient of a dimension 6 operator should be considered when discussing the dimension 8 effects. Going forward, dimension 6 contributions refer to all contributions that are suppressed by  $\frac{1}{m^2}$  while dimension 8 contribution refer to those suppressed by  $\frac{1}{m^4}$ . Studying the structure of the Wilson coefficient, one finds that the isospin dependence comes with a factor of  $2J + 1$  from the multiplicity of the fermions and a polynomial in  $J$  divided by a power of  $J$ . An example would be the operator  $\mathcal{O}_{HD1}$  with the coefficient

$$\frac{c_{HD1}}{\Lambda_{EFT}^2} = \frac{(2J + 1)\lambda^4(7J + 1)}{120J\pi^2 m^2} + \frac{(2J + 1)\lambda^6 \hat{v}^2(214J + 1)}{13440J\pi^2 m^2}. \quad (4.159)$$

In general the power of  $\frac{1}{J}$  stems from the CGC and is present in terms, that come from vector bosons coupling to different multiplets and are accompanied by a polynomial in  $J$  of at least the same order. Further powers of  $J$  in the polynomial in the numerator come from couplings of vector bosons to two fermions of the same multiplet. As a rule two powers of  $J$  are added for every two field strength tensors in the operator. An explicit example for this can be seen in table 4.1 for  $\mathcal{O}_{Gauge}$  where the polynomial is of degree two. For the  $\frac{1}{m^2}$  and  $\frac{1}{m^4}$  terms one finds a polynomial of degree three divided by  $J$ . For the power of  $\lambda$  one finds one power for each higgs field in the operator as well further terms due to the expansion in  $\frac{\lambda \hat{v}}{m}$ .

With the structure of the coefficients understood, one can compare them with the constraints on these operators found in the literature. As one is dealing with a dedicated basis only some of these operators are constrained in the literature, namely the T-, S- and M-operators [4] and a couple of dimension 6 operators, that parameterize aTGC [3] and anomalous higgs couplings [2]. In table 4.6 the current limits are compared with the coefficients as they appear in the EFT of the proposed model. The coefficients of the model are calculated for two sets of parameters,  $m = 700$  GeV,  $J = 3$ ,  $\lambda = 1$  and  $m = 1100$  GeV,  $J = 4$ ,  $\lambda = 3$ , which represent one point with  $gJ \gg \lambda$  and one point with  $gJ \sim \lambda$ . For  $gJ \gg \lambda$  one finds a mild conflict for  $c_{\mathcal{T}_1}$  and  $c_{\mathcal{T}_2}$ . Whether this conflict results in a possible exclusion of the set of parameters however, depends on the interference pattern of the operators (the bounds are only single operator bounds) and whether the operators actually describe the model in the region of phase space that is responsible for the limit. In the previous study for one multiplet [19] the total EFT contribution was found to be smaller compared to the single operator contribution of the dominant T-operator. Therefore this set of parameters is expected to be allowed from the side of experimental bounds on the EFT.

For the second set of parameters with  $\lambda = 3$ , one can observe violations for the three bounds set by anomalous higgs couplings ( $c_{HD1}$ ,  $c_{HD3}$  and  $c_{HW}$ ), with the strongest violation appearing in  $c_{HD1} + 2c_{HD3} = -c_{H\Box}$ . This combination gives contributions to the higgs 2-point 3-point and 4-point function. As such it appears in the renormalization of the higgs field  $\delta_{Z_h}$  which cancels most of their impact. The remaining impact will be analyzed in 5.4. The limit on  $c_{HD1}$  can be ignored altogether as  $c_{HD1}$  only ever appears in  $SU(2)_C$  conserving combination  $c_{HD1} + 2c_{HD3}$ . For  $c_{HW}$  the one sigma limit is broken by a factor of five. As this operator does not impact a propagator there is no counterterm from the renormalization. There is however possible correlation with other operators, which might decrease the impact, so that it is fine with the two sigma bounds. Lastly the operators  $\mathcal{O}_{M_0}$  exceeds the limit for its Wilson coefficient while the T-operators are below their limits. This implies that it is possible that the M-operators give the dominant contribution for VBS processes. Unfortunately one has to keep in mind that there are a total of seven operators in the operator class  $\phi^2 D^2 X^2$  that can theoretically destructively interfere with  $\mathcal{O}_{M_0}$ . In order to solve the question of which operators are dominant one has to run the full VBS simulation which will be done in section 5.5.1.2.

Lastly one can discuss the range of validity of the EFT based on the expansion made in equations (4.155)-(4.157) and the setups in table 4.6. Equation (4.155) should pose no problem, as fermion masses of  $m \geq 700$  GeV are considered. For equation (4.156) one finds a mass splitting of  $\Delta m = 174$  GeV for  $\lambda = 1$  and  $\Delta m = 522$  GeV for  $\lambda = 3$ . These are considerable smaller than the original masses of the fermions and one shouldn't get into trouble using these sets of parameters. Lastly equation (4.157) suggests that the EFT is only valid up to  $\sqrt{s} = m$ . In the previous study [19] a range of validity up to  $\sqrt{s} \leq 1.3 m$  was found. A similar analysis is performed in section 5.5.1.3.

**Table 4.2.:** Wilson coefficients for dimensions  $d=2$ ,  $d=4$  and  $d=6$  for  $J = 3$  and  $J = 4$ . Only the  $\frac{1}{m^2}$  and  $\frac{1}{m^4}$  are shown.

dimension 2 and 4 operators		$c_{\mathcal{O}}(J = 3)$	$c_{\mathcal{O}}(J = 4)$
$\mathcal{O}_{H2}$	$-\phi^\dagger\phi$	$\frac{-7\lambda^6\hat{v}^4}{160\pi^2m^2} - \frac{\lambda^8\hat{v}^6}{160\pi^2m^4}$	$\frac{-63\lambda^6\hat{v}^4}{1120\pi^2m^2} - \frac{9\lambda^8\hat{v}^6}{1120\pi^2m^4}$
$\mathcal{O}_{H4}$	$-(\phi^\dagger\phi)^2$	$\frac{84\lambda^6\hat{v}^2}{960\pi^2m^2} + \frac{9\lambda^8\hat{v}^4}{960\pi^2m^4}$	$\frac{252\lambda^6\hat{v}^2}{2240\pi^2m^2} + \frac{27\lambda^8\hat{v}^4}{2240\pi^2m^4}$
$\mathcal{O}_{\text{Gauge}}$	$\frac{-1}{4}W_{\mu\nu}^I W^{I\mu\nu}$	$\frac{2242g^2\lambda^2\hat{v}^2}{11520\pi^2m^2} + \frac{5593g^2\lambda^4\hat{v}^4}{11520\pi^2m^4}$	$\frac{78484g^2\lambda^2\hat{v}^2}{17920\pi^2m^2} + \frac{19573g^2\lambda^4\hat{v}^4}{17920\pi^2m^4}$
$\mathcal{O}_{\text{kin}}$	$(D_\mu\phi)^\dagger D^\mu\phi$	$\frac{56\lambda^4\hat{v}^2}{5760\pi^2m^2} - \frac{13\lambda^6\hat{v}^4}{2240\pi^2m^4}$	$\frac{336\lambda^4\hat{v}^2}{17920\pi^2m^2} - \frac{51\lambda^6\hat{v}^4}{17920\pi^2m^4}$
operator class: $\phi^6$		$\frac{c_{\mathcal{O}}}{\Lambda_{EFT}^2}(J = 3)$	$\frac{c_{\mathcal{O}}}{\Lambda_{EFT}^2}(J = 4)$
$\mathcal{O}_{H6}$	$(\phi^\dagger\phi - \frac{\hat{v}^2}{2})^3$	$\frac{-16\lambda^6}{240\pi^2m^2} - \frac{3\lambda^8\hat{v}^2}{240\pi^2m^4}$	$\frac{-42\lambda^6}{560\pi^2m^2} - \frac{9\lambda^8\hat{v}^2}{560\pi^2m^4}$
operator class: $\phi^4 D^2$			
$\mathcal{O}_{HD1}$	$((D_\mu\phi)^\dagger\phi)(\phi^\dagger D^\mu\phi)$	$\frac{2464\lambda^4}{5760\pi^2m^2} + \frac{643\lambda^6\hat{v}^2}{5760\pi^2m^4}$	$\frac{9744\lambda^4}{17920\pi^2m^2} + \frac{2571\lambda^6\hat{v}^2}{17920\pi^2m^4}$
$\mathcal{O}_{HD2}$	$(\phi^\dagger\phi - \frac{\hat{v}^2}{2})((D_\mu\phi)^\dagger D^\mu\phi)$	$\frac{28\lambda^4}{1440\pi^2m^2} - \frac{13\lambda^6\hat{v}^2}{1440\pi^2m^4}$	$\frac{168\lambda^4}{4480\pi^2m^2} - \frac{51\lambda^6\hat{v}^2}{4480\pi^2m^4}$
$\mathcal{O}_{HD3}$	$((D_\mu\phi)^\dagger\phi)((D_\mu\phi)^\dagger\phi) + h.c.$	$\frac{2464\lambda^4}{11520\pi^2m^2} + \frac{643\lambda^6\hat{v}^2}{11520\pi^2m^4}$	$\frac{9744\lambda^4}{35840\pi^2m^2} + \frac{2571\lambda^6\hat{v}^2}{35840\pi^2m^4}$
operator class: $\phi^2 D^4$			
$\mathcal{O}_{HDD}$	$(D_\mu D^\mu\phi)^\dagger(D_\nu D^\nu\phi)$	$\frac{42\lambda^2}{480\pi^2m^2} + \frac{7\lambda^4\hat{v}^2}{480\pi^2m^4}$	$\frac{252\lambda^2}{2240\pi^2m^2} + \frac{45\lambda^4\hat{v}^2}{2240\pi^2m^4}$
operator class: $\phi^2 D^2 X$			
$\mathcal{O}_{HDDW}$	$i((D^\mu\phi)^\dagger\tau^I D^\nu\phi)W_{\mu\nu}^I$	$\frac{2394g\lambda^2}{17280\pi^2m^2} + \frac{3493g\lambda^4\hat{v}^2}{17280\pi^2m^4}$	$\frac{1596g\lambda^2}{8960\pi^2m^2} + \frac{2967g\lambda^4\hat{v}^2}{8960\pi^2m^4}$
operator class: $\phi^2 X^2$			
$\mathcal{O}_{HW}$	$(\phi^\dagger\phi - \frac{\hat{v}^2}{2})W_{\mu\nu}^I W^{I\mu\nu}$	$\frac{-22442g^2\lambda^2}{23040\pi^2m^2} - \frac{11207g^2\lambda^4\hat{v}^2}{23040\pi^2m^4}$	$\frac{-78484g^2\lambda^2}{35840\pi^2m^2} - \frac{39191g^2\lambda^4\hat{v}^2}{35840\pi^2m^4}$
operator class: $D^2 X^2$			
$\mathcal{O}_{DW}$	$(D_\alpha W_{\mu\nu})^I (D^\alpha W^{\mu\nu})^I$	$\frac{-2016g^2}{7680\pi^2m^2} - \frac{2273g^2\lambda^2\hat{v}^2}{7680\pi^2m^4}$	$\frac{-10752g^2}{17920\pi^2m^2} - \frac{11859g^2\lambda^2\hat{v}^2}{17920\pi^2m^4}$
operator class: $X^3$			
$\mathcal{O}_W$	$\epsilon_{IJK}W_\mu^{I\nu}W_\nu^{J\rho}W_\rho^{K\mu}$	$\frac{819g^3}{1440\pi^2m^2} + \frac{923g^3\lambda^2\hat{v}^2}{1440\pi^2m^4}$	$\frac{2912g^3}{2240\pi^2m^2} + \frac{3211g^3\lambda^2\hat{v}^2}{2240\pi^2m^4}$

**Table 4.3.:** Wilson coefficients for dimensions  $d=8$ , for operators with four, six or eight higgs fields for  $J = 3$  and  $J = 4$

operator class: $\phi^8$		$\frac{c_{\mathcal{O}}}{\Lambda_{EFT}^4}(J = 3)$	$\frac{c_{\mathcal{O}}}{\Lambda_{EFT}^4}(J = 4)$
$\mathcal{O}_{H8}$	$(\phi^\dagger\phi - \frac{\hat{v}^2}{2})^4$	$\frac{-\lambda^8}{160\pi^2 m^4}$	$\frac{-9\lambda^8}{1120\pi^2 m^4}$
operator class: $\phi^6 D^2$			
$\mathcal{O}_{H61}$	$(\phi^\dagger\phi - \frac{\hat{v}^2}{2})^2 ((D_\mu\phi)^\dagger D^\mu\phi)$	$\frac{-13\lambda^6}{1440\pi^2 m^4}$	$\frac{-51\lambda^6}{4480\pi^2 m^4}$
$\mathcal{O}_{H62}$	$(\phi^\dagger\phi - \frac{\hat{v}^2}{2}) ((D_\mu\phi)^\dagger\phi)(\phi^\dagger D^\mu\phi)$	$\frac{643\lambda^6}{2880\pi^2 m^4}$	$\frac{2571\lambda^6}{8960\pi^2 m^4}$
$\mathcal{O}_{H63}$	$(\phi^\dagger\phi - \frac{\hat{v}^2}{2}) ((D_\mu\phi)^\dagger\phi(D^\mu\phi)^\dagger\phi) + h.c.$	$\frac{643\lambda^6}{5760\pi^2 m^4}$	$\frac{2571\lambda^6}{17920\pi^2 m^4}$
operator class: $\phi^4 D^4$			
$\mathcal{O}_{S0}$	$((D_\mu\phi)^\dagger D^\nu\phi)((D_\mu\phi)^\dagger D^\nu\phi)$	$\frac{3773\lambda^4}{25920\pi^2 m^4}$	$\frac{4957\lambda^4}{26880\pi^2 m^4}$
$\mathcal{O}_{S1}$	$((D_\mu\phi)^\dagger D^\mu\phi)((D_\nu\phi)^\dagger D^\nu\phi)$	$\frac{-217\lambda^4}{6480\pi^2 m^4}$	$\frac{-101\lambda^4}{2688\pi^2 m^4}$
$\mathcal{O}_{S2}$	$((D_\mu\phi)^\dagger D^\nu\phi)((D_\nu\phi)^\dagger D^\mu\phi)$	$\frac{3773\lambda^4}{25920\pi^2 m^4}$	$\frac{4957\lambda^4}{26880\pi^2 m^4}$
$\mathcal{O}_{H4D41}$	$\frac{1}{2}((D_\mu D^\nu\phi)^\dagger\phi(D^\mu D_\nu\phi)^\dagger\phi) + h.c.$	$\frac{7\lambda^4}{60\pi^2 m^4}$	$\frac{333\lambda^4}{2240\pi^2 m^4}$
$\mathcal{O}_{H4D42}$	$(\phi^\dagger\phi - \frac{\hat{v}^2}{2}) ((D_\mu D^\nu\phi)^\dagger D^\mu D_\nu\phi)$	$\frac{7\lambda^4}{240\pi^2 m^4}$	$\frac{9\lambda^4}{224\pi^2 m^4}$
$\mathcal{O}_{H4D43}$	$\frac{1}{2}((D_\mu D^\nu\phi)^\dagger\phi\phi^\dagger(D^\mu D_\nu\phi))$	$\frac{7\lambda^4}{30\pi^2 m^4}$	$\frac{333\lambda^4}{2240\pi^2 m^4}$
$\mathcal{O}_{H4D44}$	$\frac{1}{2}((D_\mu D^\nu\phi)^\dagger D^\mu\phi\phi^\dagger D_\nu\phi) + h.c.$	$\frac{1057\lambda^4}{4320\pi^2 m^4}$	$\frac{1423\lambda^4}{4480\pi^2 m^4}$
$\mathcal{O}_{H4D45}$	$\frac{1}{2}((D_\mu D^\nu\phi)^\dagger D^\mu\phi(D_\nu\phi)^\dagger\phi) + h.c.$	$\frac{1057\lambda^4}{4320\pi^2 m^4}$	$\frac{1423\lambda^4}{4480\pi^2 m^4}$
$\mathcal{O}_{H4D46}$	$\frac{1}{2}((D_\mu\phi)^\dagger D_\nu\phi) ((D^\mu D^\nu\phi)^\dagger\phi + \phi^\dagger D^\mu D^\nu\phi)$	$\frac{959\lambda^4}{2160\pi^2 m^4}$	$\frac{253\lambda^4}{448\pi^2 m^4}$
operator class: $\phi^4 D^2 X$			
$\mathcal{O}_{HHDDW1}$	$i(\phi^\dagger\phi - \frac{\hat{v}^2}{2}) ((D^\mu\phi)^\dagger\tau^I D^\nu\phi)W_{\mu\nu}^I + h.c.$	$\frac{-889g\lambda^4}{4320\pi^2 m^4}$	$\frac{-753g\lambda^4}{2240\pi^2 m^4}$
$\mathcal{O}_{HHDDW2}$	$i([(D^\mu\phi)^\dagger\tau^I\phi][(D^\nu\phi)^\dagger\phi])W_{\mu\nu}^I + h.c.$	$\frac{217g\lambda^4}{1920\pi^2 m^4}$	$\frac{3821g\lambda^4}{17920\pi^2 m^4}$
$\mathcal{O}_{HHDDW3}$	$i([(D^\mu\phi)^\dagger\tau^I\phi][\phi^\dagger D^\nu\phi])W_{\mu\nu}^I + h.c.$	$\frac{217g\lambda^4}{1920\pi^2 m^4}$	$\frac{3821g\lambda^4}{17920\pi^2 m^4}$
operator class: $\phi^4 X^2$			
$\mathcal{O}_{W2H41}$	$(\phi^\dagger\phi - \frac{\hat{v}^2}{2})^2 W_{\mu\nu}^I W^{I\mu\nu}$	$\frac{-2807g^2\lambda^4}{5760\pi^2 m^4}$	$\frac{-9809g^2\lambda^4}{8960\pi^2 m^4}$
$\mathcal{O}_{W2H43}$	$(\phi^\dagger\tau^I\phi)(\phi^\dagger\tau^J\phi)W_{\mu\nu}^I W^{J\mu\nu}$	0	0

**Table 4.4.:** Wilson coefficients for dimensions  $d=8$ , for operators with two higgs fields for  $J = 3$  and  $J = 4$ 

operator class: $\phi^2 D^6$		$\frac{c_{\mathcal{O}}}{\Lambda_{EFT}^4} (J = 3)$	$\frac{c_{\mathcal{O}}}{\Lambda_{EFT}^4} (J = 4)$
$\mathcal{O}_{HDDD}$	$(D_\mu D_\nu D_\alpha \phi)^\dagger D^\mu D^\nu D^\alpha \phi$	$\frac{\lambda^2}{160\pi^2 m^4}$	$\frac{9\lambda^2}{1120\pi^2 m^4}$
operator class: $\phi^2 D^4 X$			
$\mathcal{O}_{HD4W1}$	$i(D^\alpha D^\mu \phi)^\dagger \tau^I D_\alpha D^\nu \phi W_{\mu\nu}^I$	$\frac{17g\lambda^2}{720\pi^2 m^4}$	$\frac{17g\lambda^2}{560\pi^2 m^4}$
$\mathcal{O}_{HD4W2}$	$i\left((D_\alpha D^\alpha D^\nu \phi)^\dagger \tau^I D^\mu \phi\right) W_{\mu\nu}^I + h.c.$	$\frac{-g\lambda^2}{48\pi^2 m^4}$	$\frac{-3g\lambda^2}{112\pi^2 m^4}$
operator class: $\phi^2 D^2 X^2$			
$\mathcal{O}_{M0}$	$\frac{1}{2}(D_\alpha \phi)^\dagger D^\alpha \phi W_{\mu\nu}^I W^{I\mu\nu}$	$\frac{14291g^2\lambda^2}{8640\pi^2 m^4}$	$\frac{24791g^2\lambda^2}{6720\pi^2 m^4}$
$\mathcal{O}_{M1}$	$\frac{1}{2}(D_\mu \phi)^\dagger D^\nu \phi W_{\nu\alpha}^I W^{I\alpha\mu}$	$\frac{7891g^2\lambda^2}{4320\pi^2 m^4}$	$\frac{13771g^2\lambda^2}{3360\pi^2 m^4}$
$\mathcal{O}_{M7}$	$\frac{i}{2}\epsilon_{IJK}((D_\mu \phi)^\dagger \tau^I D^\nu \phi) W_{\nu\alpha}^J W^{K\alpha\mu}$	$\frac{17g^2\lambda^2}{240\pi^2 m^4}$	$\frac{51g^2\lambda^2}{560\pi^2 m^4}$
$\mathcal{O}_{DWH1}$	$\left(\phi^\dagger \phi - \frac{\hat{v}^2}{2}\right) (D_\alpha W_{\mu\nu})^I (D^\alpha W^{\mu\nu})^I$	$\frac{-2273g^2\lambda^2}{3840\pi^2 m^4}$	$\frac{-11859g^2\lambda^2}{8960\pi^2 m^4}$
$\mathcal{O}_{DWH2}$	$\left((D_\alpha D^\mu \phi)^\dagger \phi + \phi^\dagger D_\alpha D^\mu \phi\right) W_{\mu\nu}^I W^{I\alpha\nu}$	$\frac{-97g^2\lambda^2}{960\pi^2 m^4}$	$\frac{-501g^2\lambda^2}{2240\pi^2 m^4}$
$\mathcal{O}_{DWH3}$	$\left((D_\alpha D^\alpha \phi)^\dagger \phi + \phi^\dagger D_\alpha D^\alpha \phi\right) W_{\mu\nu}^I W^{I\mu\nu}$	$\frac{253g^2\lambda^2}{512\pi^2 m^4}$	$\frac{3957g^2\lambda^2}{3584\pi^2 m^4}$
$\mathcal{O}_{DWH4}$	$i\epsilon_{IJK} \left((D^\mu \phi)^\dagger \tau^I \phi - \phi^\dagger \tau^I D^\mu \phi\right) W_{\mu\alpha}^J (D_\nu W^{\nu\alpha})^K$	$\frac{-11g^2\lambda^2}{1152\pi^2 m^4}$	$\frac{-11g^2\lambda^2}{896\pi^2 m^4}$
operator class: $\phi^2 X^3$			
$\mathcal{O}_{W3H21}$	$\left(\phi^\dagger \phi - \frac{\hat{v}^2}{2}\right) \epsilon_{IJK} W_\mu^{I\nu} W_\nu^{J\rho} W_\rho^{K\mu}$	$\frac{923g^3\lambda^2}{720\pi^2 m^4}$	$\frac{3211g^3\lambda^2}{1120\pi^2 m^4}$

**Table 4.5.:** Wilson coefficients for dimensions  $d=8$ , for operators with no higgs fields for  $J = 3$  and  $J = 4$ 

operator class: $D^4X^2$		$\frac{c_{\mathcal{O}}}{\Lambda_{EFT}^4}(J = 3)$	$\frac{c_{\mathcal{O}}}{\Lambda_{EFT}^4}(J = 4)$
$\mathcal{O}_{D2W}$	$(D_\alpha D^\alpha W_{\mu\nu})^I (D_\beta D^\beta W^{\mu\nu})^I$	$\frac{-9g^2}{320\pi^2 m^4}$	$\frac{-9g^2}{140\pi^2 m^4}$
operator class: $D^2X^3$			
$\mathcal{O}_{DWWW0}$	$\epsilon_{IJK} (D_\alpha W_{\mu\nu})^I (D^\alpha W^{\nu\rho})^J W_\rho^{K\mu}$	$\frac{24g^3}{35\pi^2 m^4}$	$\frac{3g^3}{10\pi^2 m^4}$
$\mathcal{O}_{DWWW1}$	$\epsilon_{IJK} (D^\alpha W_{\mu\nu})^I (D^\beta W^{\mu\nu})^J W_{\alpha\beta}^K$	$\frac{g^3}{40\pi^2 m^4}$	$\frac{2g^3}{35\pi^2 m^4}$
operator class: $X^4$			
$\mathcal{O}_{T0}$	$\frac{1}{4} W_{\mu\nu}^I W^{I\mu\nu} W_{\alpha\beta}^J W^{J\alpha\beta}$	$\frac{-2551g^4}{2880\pi^2 m^4}$	$\frac{-5863g^4}{1680\pi^2 m^4}$
$\mathcal{O}_{T1}$	$\frac{1}{4} W_{\mu\nu}^I W^{I\alpha\beta} W_{\alpha\beta}^J W^{J\mu\nu}$	$\frac{-613g^4}{360\pi^2 m^4}$	$\frac{-5731g^4}{840\pi^2 m^4}$
$\mathcal{O}_{T2}$	$\frac{1}{4} W_\mu^{I\nu} W_\nu^{I\alpha} W_\alpha^{J\beta} W_\beta^{J\mu}$	$\frac{1441g^4}{360\pi^2 m^4}$	$\frac{7289g^4}{420\pi^2 m^4}$
$\mathcal{O}_{T3}$	$\frac{1}{4} W_{\mu\nu}^I W_{\alpha\beta}^I W^{J\nu\alpha} W^{J\beta\mu}$	$\frac{4673g^4}{1440\pi^2 m^4}$	$\frac{9677g^4}{840\pi^2 m^4}$

**Table 4.6.:** Limits on Wilson coefficients from anomalous higgs couplings [2] (one sigma), aTGC [3] (95% CL) and aQGC [4] (95% CL) compared with the coefficients for the model for two sets of parameters. Setup 1:  $m = 700$  GeV,  $J = 3$ ,  $\lambda = 1$ ; setup 2:  $m = 1100$  GeV,  $J = 4$ ,  $\lambda = 3$ 

Wilson coefficient $c_{\mathcal{O}}$	Observed	Setup 1	Setup 2
$\frac{-c_{HD1}-2c_{HD3}}{\Lambda_{EFT}^2} (\text{TeV}^{-2})$	[-0.41,0.47]	-0.18	-8.252
$\frac{c_{HD1}}{\Lambda_{EFT}^2} (\text{TeV}^{-2})$	[-4.94,0.26]	0.091	4.126
$\frac{c_{HW}}{\Lambda_{EFT}^2} (\text{TeV}^{-2})$	[-0.16,0.19]	-0.093	-0.880
$\frac{4c_W}{g^3\Lambda_{EFT}^2} (\text{TeV}^{-2})$	[-1.44,1.47]	0.536	0.651
$\frac{c_{HDDW}}{g\Lambda_{EFT}^2} (\text{TeV}^{-2})$	[-2.45,2.08]	0.033	0.184
$\frac{c_{S0}}{\Lambda_{EFT}^4} (\text{TeV}^{-4})$	[-2.7,2.7]	0.055	1.035
$\frac{c_{S1}}{\Lambda_{EFT}^4} (\text{TeV}^{-4})$	[-3.4,3.4]	-0.014	-0.211
$\frac{c_{M0}}{\Lambda_{EFT}^4} (\text{TeV}^{-4})$	[-0.69,0.70]	0.304	1.000
$\frac{c_{M1}}{\Lambda_{EFT}^4} (\text{TeV}^{-4})$	[-2.0,2.1]	0.336	1.112
$\frac{c_{M7}}{\Lambda_{EFT}^4} (\text{TeV}^{-4})$	[-3.4,3.4]	0.013	0.025
$\frac{c_{T0}}{\Lambda_{EFT}^4} (\text{TeV}^{-4})$	[-0.12,0.11]	-0.071	-0.046
$\frac{c_{T1}}{\Lambda_{EFT}^4} (\text{TeV}^{-4})$	[-0.12,0.13]	-0.136	-0.089
$\frac{c_{T2}}{\Lambda_{EFT}^4} (\text{TeV}^{-4})$	[-0.28,0.28]	0.321	0.228

## 5. Results

For the analysis of the proposed model and its impact on VBS we will restrict ourselves to a couple of parameter points, in order to understand the behavior of the model when varying the three parameters  $J$ ,  $\lambda$  and  $m_\Psi$ . These exemplary model parameters should not be in conflict with the present data. As such a model has not been analyzed at the LHC there are no direct limits to draw upon from the ATLAS or CMS collaborations. We will therefore base the selection for these exemplary parameter points on the previous study for one multiplet and  $\lambda = 0$  [19], and quick analyses of non-VBS processes to arrive at reasonable parameter choices for our model. The limits on the parameters that arise from these considerations should however not be mistaken as stringent limits on the model, which can only be set by a full experimental analysis of this model, which is beyond the scope of the presented thesis

Starting with the case of  $\lambda = 0$  one can use the results of [19] in order to set a lower limit on the mass and an upper limit on the isospin. The upper limit for the isospin of  $J \leq 4$  in [19] is mainly chosen based on the analysis of perturbative unitarity of  $VV \rightarrow VV$  processes. In this analysis  $J = 5$  was found to be just outside of the perturbative region while  $J = 4$  was well within that region. For the model discussed in this thesis this implies that choosing one multiplet with  $J = 4$  and two multiplets with  $J = 3.5$  still produces a model that can be analyzed perturbatively.

The lower limit on the mass of  $m_\Psi \geq 600$  GeV in [19] is based on the current limits on anomalous triple gauge couplings (aTGC), anomalous quartic gauge couplings (aQGC) and limits on four fermion vertices stemming from Drell-Yan production of two fermions at the LHC. Again this limit applies similarly to the model discussed here, but probably needs to be slightly raised to the presence of three multiplets compared to one.

Leaving the case  $\lambda = 0$  behind one has to wonder how larger values of  $\lambda$  influence these limits. In [19] the perturbative limit for  $J$  was analyzed for purely transverse scattering, as this was the channel in which almost all of the contribution of the model was situated. When increasing  $\lambda$  these purely transverse channels are not expected to change significantly, thereby leaving the limit on  $J$  from [19] intact.

With respect to the  $m_\Psi$  limit one now has to deal with the fact, that the multiplet with the smallest mass becomes lighter as  $\lambda$  increases. As the limit from [19] mainly depends on the energy of the two particle production threshold the limit for the mass has to be adjusted accordingly

$$m_\Psi - \frac{\lambda \hat{v}}{\sqrt{2}} \gtrsim 600 \text{ GeV}. \quad (5.1)$$

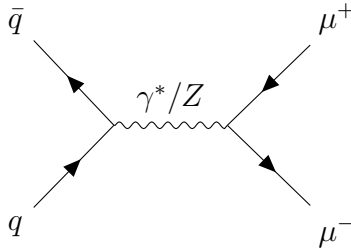


**Figure 5.1.:** Drell-Yan:  $q\bar{q} \rightarrow \mu^+\mu^-$

In order to study the region  $\lambda \leq 1$  the two sets of multiplets that will be investigated are

$$(J, Y) = \left\{ \left( \frac{5}{2}, -\frac{1}{2} \right); (3, 0); \left( \frac{5}{2}, \frac{1}{2} \right) \right\} \quad m_\Psi = 700 \text{ GeV}, \quad (5.2)$$

$$(J, Y) = \left\{ \left( \frac{7}{2}, -\frac{1}{2} \right); (4, 0); \left( \frac{7}{2}, \frac{1}{2} \right) \right\} \quad m_\Psi = 700 \text{ GeV}. \quad (5.3)$$

For larger values of the coupling the mass is chosen as  $m_\Psi = 1100 \text{ GeV}$  which allows for  $\lambda \leq 3$  when requiring the lightest mass to be above 500 GeV.

Using these parameter points one can now study the effect of this model on the Drell-Yan production of fermions (section 5.1 and 5.2), on vector boson production (section 5.3), on the HVV coupling (section 5.4), on on-shell VBS (section 5.5.1) and on higgs pair production from two vector bosons (section 5.6). The goal within these sections is to assess possible signals for the model and expected limits from present LHC data on the allowed parameter range. In these sections the full model will be compared to its EFT, which leads to the discussion of the possibility of finding BSM contributions first in M-operators.

## 5.1. Production of opposite sign SM fermions

The first process to look at is the Drell-Yan production of a muon pair (fig. 5.1). In [19] one multiplet with  $J = 4$  and  $m = 600 \text{ GeV}$  was found to be on the verge of being excluded based on the search for resonant and nonresonant phenomena in dilepton final states [52]. As a quick comparison one can look at the change in the transverse part of the Dyson-resummed Z boson propagator

$$\Pi = \frac{i}{p^2 - m_Z^2 - \Pi_T(m_\Psi, \lambda, J, p^2)}, \quad (5.4)$$

and compare it to the SM

$$\frac{\Pi(Full)^2}{\Pi(SM)^2} = \frac{(p^2 - m_Z^2)^2}{(p^2 - m_Z^2 - \Pi_T(m_\Psi, \lambda, J, p^2))^2}. \quad (5.5)$$

This ratio gives a good idea of how the production cross section changes. One has to keep in mind however, that in the SM both a photon and a Z boson mediate this process while only the  $W^3$  boson propagator, with  $W^3$  only coupling to left chiral SM fermions, is significantly influenced by the new fermions. The absolute value of the ratio therefore overestimates the impact on the whole process. One can however still use this ratio in order to compare different parameter choices with the limit

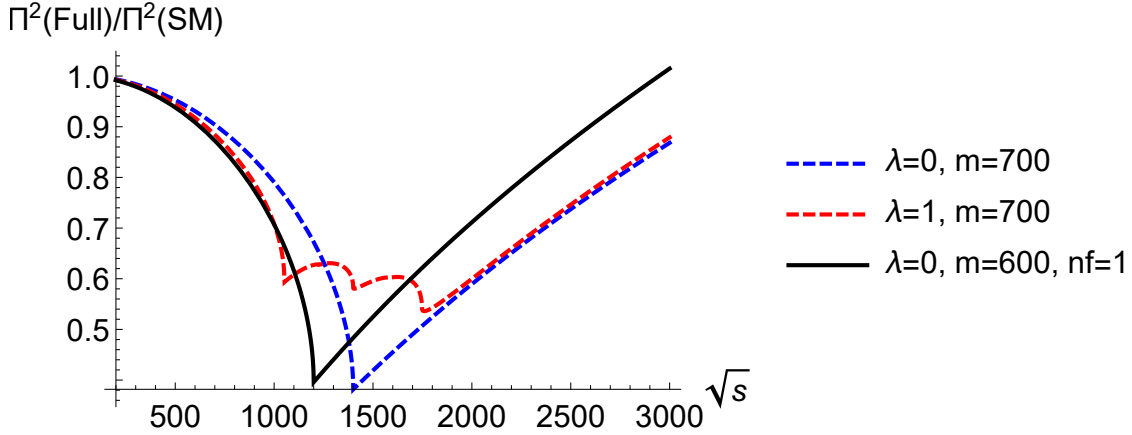


**Figure 5.2.:** Ratio of  $\frac{\Pi(\text{Full})^2}{\Pi(\text{SM})^2}$  from equation (5.5) for the case of one multiplet with a mass of  $m = 600$  GeV and an isospin of  $J = 4$  (black) and for the case of three multiplets with  $J = 3, J = 2.5, J = 2.5$  with a mass of  $m = 700$  GeV and a coupling of  $\lambda = 0$  (blue, dashed) and  $\lambda = 1$  (red, dashed)

found in [19].

In figure 5.2 the ratio is shown for the parameter choice from the previous work [19] and one multiplet (black) as well as the first parameter choice for this paper  $m = 700$  GeV and  $J = 3$  (blue and red). Comparing the two cases without coupling, one can observe that both curves have a similar shape, with the blue curve being shifted to larger energies. This behavior can be understood when looking at the isospin dependence of the propagator correction

$$\Pi_T(J, p, m) = \sum \frac{J_f(J_f + 1)(2J_f + 1)}{3} \Pi_T(p, m) = T_J \Pi_T(p, m). \quad (5.6)$$

This isospin factor is 60 for one multiplet with  $J = 4$  and 63 for one multiplet with  $J = 3$  and two with  $J = 2.5$ . This explains the similar shape and the shift is simply explained by the slightly larger mass of  $m = 700$  GeV. Going to the case of  $\lambda = 1$  one can see that the single dip at  $\sqrt{s} = 1400$  GeV  $= 2m$  has been split into three dips at  $\sqrt{s} \approx 1050$  GeV  $= 2m_{\chi_2}$ ,  $\sqrt{s} = 1400$  GeV  $= 2m_{\chi_1}$  and  $\sqrt{s} = 1750$  GeV  $\approx 2m_{\chi_3}$ . This leads to a stronger deviation from the SM around the first dip and a smaller deviation around the second dip compared to the  $\lambda = 0$  case. Since the threshold region is mostly responsible for the limit on  $J$ , one can say that larger  $\lambda$  give weaker bounds on  $J$ . This trend however has a limit as the position of the threshold is linearly dependent on  $\lambda$  while the amplitude stays almost unchanged once the thresholds are far enough separated (which will be shown later on). Compared to the case with one multiplet it now becomes apparent why the mass for the three multiplets is chosen slightly larger in comparison as now the curves of the two cases align up to  $\sqrt{s} \approx 1050$  GeV. This implies that for both, smaller masses and larger couplings, the deviation from the SM in the region before the first threshold become larger than in the case of only one multiplet. As this case was already on the edge of being ruled out (or even slightly over it) one can conclude that for  $J = 3$  the combination  $m = 700$  GeV,  $\lambda = 1$  is on the edge of the allowed parameter space.

Figure 5.3 shows a similar situation as figure 5.2 with the only change being a larger isospin for the three multiplets ( $J = 4$ ). Starting again with the case of no coupling

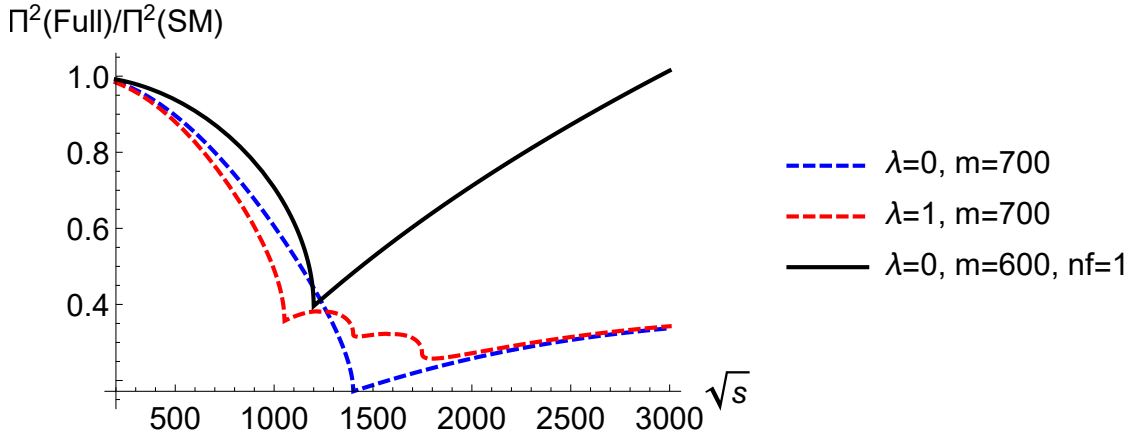


**Figure 5.3.:** Ratio of  $\frac{\Pi(\text{Full})^2}{\Pi(\text{SM})^2}$  from equation (5.5) for the case of one multiplet with a mass of  $m = 600$  GeV and an isospin of  $J = 4$  (black) and for the case of three multiplets with  $J = 4, J = 3.5, J = 3.5$  with a mass of  $m = 700$  GeV and a coupling of  $\lambda = 0$  (blue, dashed) and  $\lambda = 1$  (red, dashed)

(blue), one can see that, up to the threshold of the single multiplet  $\sqrt{s} = 1200$  GeV, both models give somewhat similar deviation from the SM. Going further to the pair production threshold of the three multiplets the deviation from the SM rises further, which, assuming the peak of the black curve is somewhat the limit, implies that evidence for this model should have been detected.

Going to  $\lambda = 1$  improves the situation slightly as the maximum deviation from the SM is smaller. Still with a similar threshold at slightly smaller energies and a lot larger deviations above  $\sqrt{s} = 1200$  GeV this model should already be detectable. Therefore a multiplets with  $J = 4$  and two multiplets with  $J = 3.5$  and a mass of  $m = 700$  GeV can be ruled out no matter the choice of the coupling parameter  $\lambda$ . In order to explore larger values of  $J$  and  $\lambda$  a mass of  $m = 1100$  GeV is chosen for the third comparison. In figure 5.4 this comparison is shown for the single multiplet (black) and for three multiplets with a mass of  $m = 1100$  GeV, a largest isospin of  $J = 4$ , and a coupling of  $\lambda = 2$  (blue) and  $\lambda = 3$  (red). When comparing the threshold position for the  $\lambda = 2$  and the  $\lambda = 3$  case as well as the deviation at the threshold, one can see that an increase in  $\lambda$  no longer significantly lowers the deviation but only shifts the position of the threshold. When comparing the  $\lambda = 3$  case with the case of one lighter multiplet one can observe quite a similar behavior up to  $\sqrt{s} = 1500$  GeV which is due to the quite similar masses,  $m = 600$  GeV and  $m_{\chi_2} = 578$  GeV. Starting at  $\sqrt{s} = 1500$  GeV the effects of the other multiplets become apparent and the deviations from the SM becomes larger again. As uncertainties on the LHC data side grow with increasing energy these deviations might be compatible with the SM.

As the main focus of this thesis lies on studying the impact of this model on VBS and whether it can produce large M-operators, this short study of the effect of the model on the Z boson propagator in Drell-Yan production of two muons will suffice for now, as it already gives a good qualitative picture of the effects. From the figures 5.2, 5.3 and 5.4 one can see, that the parameter points  $J = 3, m = 700$  GeV,  $\lambda = 1$  and  $J = 4, m = 1100$  GeV,  $\lambda = 3$  are both limits on how far one can push the parameters before definitely being observable in muon pair production.

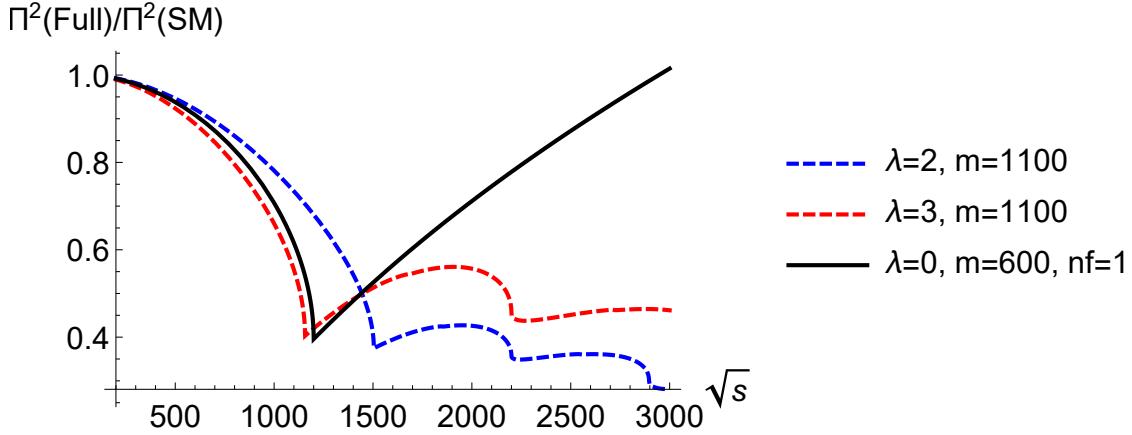


**Figure 5.4.:** Ratio of  $\frac{\Pi(\text{Full})^2}{\Pi(\text{SM})^2}$  from equation (5.5) for the case of one multiplet with a mass of  $m = 600$  GeV and an isospin of  $J = 4$  (black) and for the case of three multiplets with  $J = 4, J = 3.5, J = 3.5$  with a mass of  $m = 1100$  GeV and a coupling of  $\lambda = 2$  (blue, dashed) and  $\lambda = 3$  (red, dashed)

## 5.2. Production of same sign SM fermions

At high enough  $\sqrt{s}$  a virtual W, which is produced by  $q\bar{q}$  annihilation, can directly decay into a pair of the new heavy fermions. These fermions then decay via Z and W boson emission to the lightest state,  $\chi_2^0$ . The first decays within this decay chain are between different multiplets due to the larger mass splitting between the multiplets (of the order of 100 GeV for sizable values of  $\lambda$ ) compared to the small mass splitting within a multiplet (of the order of 100 MeV to 1 GeV). The later decays therefore produce Pions with a couple of hundred MeV of energy which are useless for the event reconstruction and can be ignored. The vector bosons from the first decay however can carry a couple of hundred GeV of energy (depending on  $\lambda$ ), which produce hadronic jets or fermions that could be well detectable. As these events require vector bosons with an energy larger than  $2m_\chi$  in order to produce SM quarks or leptons with 100 GeV of energy, one can usually ignore their contribution compared to the standard model. Some signals, like same sign leptons without any jets, are however rare in the standard model. Sticking with the production of a muon pair (this time with the same charge), one can investigate how many of these events can be expected from the model. The production of such events can be seen in figure 5.5, where a Z boson is produced and decays into two fermions of a heavier multiplet, which then further decay into fermions of the lightest multiplet and W bosons. As the charge of the fermions in the lightest multiplet does not matter (these decay to the neutral one anyways), this process can also be mediated by a W boson instead of the Z boson. Looking at the decay side it is also possible to emit both W bosons sequentially from the same fermion line as can be seen in figure 5.6.

Looking at the possible number of events for such processes one can come up with three scenarios

- Only very few events (if any) are expected which allows for no further limitations on the model
- Quite a few events are expected and it is not clear whether the excess is detectable compared to the SM background. This means, that only full analysis

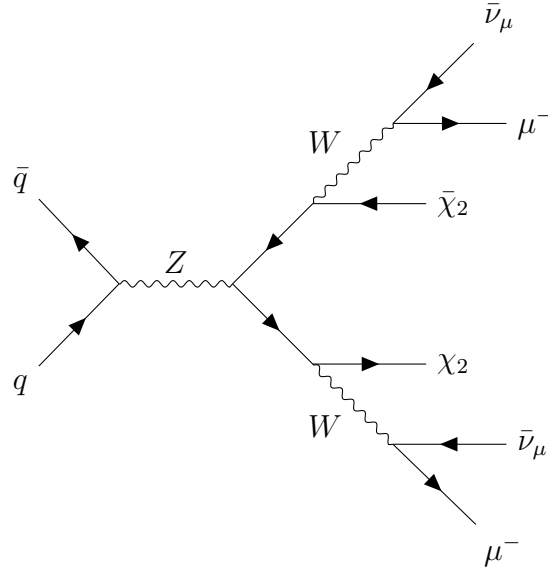


**Figure 5.5.:** Drell-Yan production of a same sign lepton pair. The charges of the final new fermions are suppressed as these decay to the neutral state anyways.

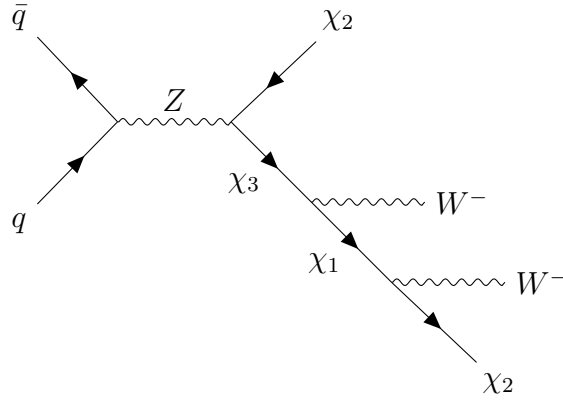


**Figure 5.6.:** Drell-Yan production of a same sign W pair. The charge of the final new fermions is suppressed as these decay to the neutral state anyways.

of both the model and possible backgrounds can determine limitations for the model

- A lot of events compared to the SM background are expected. This requires the events to be hard to detect or undetectable. This can be done by limiting  $\lambda$  to the point, where the W bosons, and therefore the muons, don't carry enough energy in order to be triggered on. This is achieved by requiring  $\lambda \ll 1$ .

In order to know which scenario one has to deal with a rough approximation of the number of events should suffice. For this purpose the processes can be separated into a production cross section for two new on shell fermions and a decay part. Starting with the production one can make the approximation

$$\frac{d\sigma(pp \rightarrow W^3 \rightarrow \chi\bar{\chi})}{dQ(W^3)} \approx \frac{d\sigma(pp \rightarrow \gamma^*/Z \rightarrow \mu^+\mu^-)}{dQ(Z)} \cdot \frac{2\sigma(u\bar{u} \rightarrow W^3 \rightarrow \chi\bar{\chi}) + \sigma(d\bar{d} \rightarrow W^3 \rightarrow \chi\bar{\chi})}{2\sigma(u\bar{u} \rightarrow \gamma^*/Z \rightarrow \mu^+\mu^-) + \sigma(d\bar{d} \rightarrow \gamma^*/Z \rightarrow \mu^+\mu^-)}, \quad (5.7)$$

where the production is expected to be similar to the SM fermions times the ratio between the cross sections of the hard processes. The factor of two accounts for the factor between the up- and down-quark parton density functions for large momentum fractions  $x$ . In a similar vein the production via  $W^\pm$  bosons can be approximated as

$$\frac{d\sigma(pp \rightarrow W \rightarrow \chi\bar{\chi})}{dQ(W)} \approx \frac{d\sigma(pp \rightarrow W^3 \rightarrow \chi\bar{\chi})}{dQ(W^3)} \cdot \frac{2\sigma(u\bar{d} \rightarrow W^+ \rightarrow \chi\bar{\chi}) + \sigma(d\bar{u} \rightarrow W^- \rightarrow \chi\bar{\chi})}{2\sigma(u\bar{u} \rightarrow W^3 \rightarrow \chi\bar{\chi}) + \sigma(d\bar{d} \rightarrow W^3 \rightarrow \chi\bar{\chi})}. \quad (5.8)$$

The relevant cross sections in the limit of zero fermion masses for the SM, equal masses for the new fermions and  $\sqrt{s} \gg m_z$  read

$$\sigma(u\bar{u} \rightarrow \gamma^*/Z \rightarrow \mu^+\mu^-) = \frac{g^4}{64\pi s} \frac{(88 \sin(\theta_w)^4 - 12 \sin(\theta_w)^2 + 9)}{324 \cos(\theta_w)^4}, \quad (5.9)$$

$$\sigma(d\bar{d} \rightarrow \gamma^*/Z \rightarrow \mu^+\mu^-) = \frac{g^4}{64\pi s} \frac{(40 \sin(\theta_w)^4 - 24 \sin(\theta_w)^2 + 9)}{324 \cos(\theta_w)^4}, \quad (5.10)$$

$$\sigma(u\bar{u} \rightarrow W^3 \rightarrow \chi_i\bar{\chi}_j) = \frac{2g^4 \mathcal{T}_{Z,ij}^2 \sqrt{1 - \frac{4m_\chi^2}{s}} (2m_\chi^2 + s)}{64\pi s \cdot 9s}, \quad (5.11)$$

$$\sigma(d\bar{d} \rightarrow W^3 \rightarrow \chi_i\bar{\chi}_j) = \frac{2g^4 \mathcal{T}_{Z,ij}^2 \sqrt{1 - \frac{4m_\chi^2}{s}} (2m_\chi^2 + s)}{64\pi s \cdot 9s}, \quad (5.12)$$

$$\sigma(u\bar{d} \rightarrow W^+ \rightarrow \chi_i\bar{\chi}_j) = \frac{4g^4 V_{ud}^* \mathcal{T}_{W^+,ij}^2 \sqrt{1 - \frac{4m_\chi^2}{s}} (2m_\chi^2 + s)}{64\pi s \cdot 9s}, \quad (5.13)$$

$$\sigma(d\bar{u} \rightarrow W^- \rightarrow \chi_i\bar{\chi}_j) = \frac{4g^4 V_{ud} \mathcal{T}_{W^-,ij}^2 \sqrt{1 - \frac{4m_\chi^2}{s}} (2m_\chi^2 + s)}{64\pi s \cdot 9s}. \quad (5.14)$$

Using the  $SU(2)$ -limit and large  $\sqrt{s}$  one can approximate the Z boson with the  $W^3$  state from the unbroken theory. Having a closer look at the squared coupling factors  $\mathcal{T}_{ij}^2$ , one finds that they are identical for W and Z, when summing over all particles within the same multiplet

$$\sum_{T_3(i), T_3(j)} T_{J;(\chi_i, T_3(i)), (\chi_j, T_3(j))}^Z = \sum_{T_3(i), T_3(j)} T_{J;(\chi_i, T_3(i)), (\chi_j, T_3(j))}^W. \quad (5.15)$$

This can be used to find

$$\frac{d\sigma(pp \rightarrow W \rightarrow \chi\bar{\chi})}{dQ(W)} = \frac{d\sigma(pp \rightarrow W^3 \rightarrow \chi\bar{\chi})}{dQ(W^3)} \cdot 2. \quad (5.16)$$

One further finds that this sum is way larger when both particles belong to the same multiplet compared to them belonging to different multiplets. This implies that processes like in figure 5.6 are suppressed compared to figure 5.5. On the decay side of things the branching ratios for the new fermions and for the W boson are needed

$$\frac{\Gamma(W^+ \rightarrow \mu^+\nu)}{\Gamma(W)} = 0.106 \quad (5.17)$$

$$\frac{\Gamma(\chi_i \rightarrow W^+ \chi_j)}{\Gamma(\chi_i)} \approx \frac{1}{3}. \quad (5.18)$$

**Table 5.1.:** Values for the  $pp \rightarrow \gamma^*/Z \rightarrow \mu^+\mu^-$  cross section for different virtualities, extracted from [53]

$Q(Z)$	1.4 TeV	2.0 TeV	2.2 TeV	2.5 TeV
$\frac{d\sigma(pp \rightarrow \gamma^*/Z \rightarrow \mu^+\mu^-)}{dQ(Z)}$	$3 \frac{\text{ab}}{\text{GeV}}$	$0.5 \frac{\text{ab}}{\text{GeV}}$	$0.3 \frac{\text{ab}}{\text{GeV}}$	$0.1 \frac{\text{ab}}{\text{GeV}}$

This results in a total factor of

$$2 \left( \frac{\Gamma(W^+ \rightarrow \mu^+\nu)}{\Gamma(W)} \right)^2 \left( \frac{\Gamma(\chi_i \rightarrow W^+\chi_j)}{\Gamma(\chi_i)} \right)^2 \approx \frac{1}{400} \quad (5.19)$$

for the decay. Lastly the muon production cross section is needed which can be extracted from recent publications (e.g [53] or [54]) and is shown for some points in table 5.1. With this information it is now possible to estimate the expected number of events for the production of two muons with the same charge until the end of the high luminosity program at the LHC

$$N \approx 3 \text{ ab}^{-1} \int dQ(W^3) \frac{d\sigma(pp \rightarrow W^3 \rightarrow \chi\bar{\chi})}{dQ(W^3)} \cdot 3 \cdot \frac{1}{400}. \quad (5.20)$$

As the  $\frac{\sigma(pp \rightarrow \gamma^*/Z \rightarrow \mu^+\mu^-)}{dQ(Z)}$  distribution is steeply falling and the ratio between the di-muon production and the production of a pair of new fermions is increasing towards a constant for larger virtualities, it is sufficient to only consider a small region of  $Q$  above the production threshold of two fermions of the multiplet with the medium mass. With the  $\frac{\sigma(pp \rightarrow \gamma^*/Z \rightarrow \mu^+\mu^-)}{dQ(Z)}$  distribution halving roughly every 200 GeV one can make the approximation

$$\begin{aligned} N &\approx 3 \text{ ab}^{-1} \left. \frac{d\sigma(pp \rightarrow W^3 \rightarrow \chi\bar{\chi})}{dQ(W^3)} \right|_{Q=2m_\chi} \cdot 200 \text{ GeV} \cdot 3 \cdot \frac{1}{400} \\ &\leq 3 \text{ ab}^{-1} \left( \left. \frac{d\sigma(pp \rightarrow \gamma^*/Z \rightarrow \mu^+\mu^-)}{dQ(Z)} \right) \right|_{Q=2m_\chi} \\ &\cdot \left. \frac{2\sigma(u\bar{u} \rightarrow W^3 \rightarrow \chi\bar{\chi}) + \sigma(d\bar{d} \rightarrow W^3 \rightarrow \chi\bar{\chi})}{2\sigma(u\bar{u} \rightarrow \gamma^*/Z \rightarrow \mu^+\mu^-) + \sigma(d\bar{d} \rightarrow \gamma^*/Z \rightarrow \mu^+\mu^-)} \right|_{Q=2m_\chi+200 \text{ GeV}} \\ &\cdot 200 \text{ GeV} \cdot 3 \cdot \frac{1}{400}. \end{aligned} \quad (5.21)$$

For the two masses of  $m_\chi = 700 \text{ GeV}$  and  $m_\chi = 1100 \text{ GeV}$  and an isospin of  $J = 3$  and  $J = 4$  respectively one finds

$$N(m_\chi = 700 \text{ GeV}, J = 3) \approx 3 \text{ ab}^{-1} 3 \frac{\text{ab}}{\text{GeV}} 20,7 \frac{3 \text{ GeV}}{2} \approx 326, \quad (5.22)$$

$$N(m_\chi = 1100 \text{ GeV}, J = 4) \approx 3 \text{ ab}^{-1} 0,3 \frac{\text{ab}}{\text{GeV}} 55 \frac{3 \text{ GeV}}{2} \approx 87. \quad (5.23)$$

These numbers of events now have to be compared with the SM background. This background was calculated in the context of studying supersymmetry events with two same-sign leptons [55]. After some preselection (sufficient  $p_T$  for the leptons, rapidity cut to account for the detector and spatial isolation of jets and leptons) 7273 SM events at  $200 \text{ pb}^{-1}$  and  $\sqrt{s} = 10 \text{ TeV}$  or roughly  $10^9$  events for  $3 \text{ ab}^{-1}$ , ignoring the increase in center of mass energy, are expected. This number of course



Following the original parameterization of the three boson vertex [56] one can write the CP-even part of the effective Lagrangian for the vertex in the SU(2)-limit as

$$\begin{aligned}\mathcal{L}_{WWZ} = & ig(g_1^V((\partial_\mu W_\nu^\dagger - \partial_\nu W_\mu^\dagger)W^\mu Z^\nu - (\partial_\mu W_\nu - \partial_\nu W_\mu)W^{\dagger\mu} Z^\nu) \\ & + \kappa_V W_\mu^\dagger W_\nu (\partial^\mu Z^\nu - \partial^\nu Z^\mu) \\ & + \frac{\lambda_V}{m_W^2} (\partial_\mu W_\nu^\dagger - \partial_\nu W_\mu^\dagger)(\partial^\rho W_\rho - \partial_\rho W^\nu)(\partial^\rho Z^\mu - \partial^\mu Z^\rho)).\end{aligned}\quad (5.26)$$

In terms of the vertex this leads to the following expression

$$\begin{aligned}\Gamma^{\mu\nu\rho}(p, q, P) = & g(g_1^Z + \frac{s}{2m_W^2}\lambda_Z)(p - q)^\rho g^{\mu\nu} - \frac{\lambda_Z}{m_W^2}(p - q)^\rho P^\mu P^\nu \\ & + (g_1^Z + \kappa_Z + \lambda_Z)(P^\mu g^{\rho\nu} - P^\nu g^{\rho\mu}).\end{aligned}\quad (5.27)$$

For the model we will consider the dimension 6 EFT contributions to the vertex and the transverse part of the off-shell propagator (the on-shell contributions as well as the longitudinal ones vanish). Comparing this to equation (5.27) one finds the following relations

$$g_1^Z + \frac{s}{2m_W^2}\lambda_Z = \frac{-16g^2\hat{v}^2 c_{DW} + g^2\hat{v}^2 c_{HDD} - 4g\hat{v}^2 c_{HDDW}}{16\Lambda_{EFT}^2} + s \frac{3c_W + 6gc_{DW}}{g\Lambda_{EFT}^2},\quad (5.28)$$

$$\frac{\lambda_V}{m_W^2} = \frac{12gc_{DW} + 6c_W}{g\Lambda_{EFT}^2},\quad (5.29)$$

$$\begin{aligned}g_1^Z + \kappa_Z + \Lambda_Z = & \frac{-16g^2\hat{v}^2 c_{DW} + g^2\hat{v}^2 c_{HDD} - 4g\hat{v}^2 c_{HDDW} + 48m_W^2(2gc_{DW} + \frac{c_W}{g})}{8\Lambda_{EFT}^2} \\ = & 2 \frac{-16g^2\hat{v}^2 c_{DW} + g^2\hat{v}^2 c_{HDD} - 4g\hat{v}^2 c_{HDDW}}{16\Lambda_{EFT}^2} + m_W^2 \frac{6c_W + 12gc_{DW}}{g\Lambda_{EFT}^2},\end{aligned}\quad (5.30)$$

which results in

$$\begin{aligned}g_1^Z = & \frac{-16g^2\hat{v}^2 c_{DW} + g^2\hat{v}^2 c_{HDD} - 4g\hat{v}^2 c_{HDDW}}{16\Lambda_{EFT}^2} \\ = & \frac{(2j + 1)\hat{v}^2(64g^4 j^2 - 7g^2 \lambda^2)}{960\pi^2 m^2},\end{aligned}\quad (5.31)$$

$$\begin{aligned}\lambda_Z = & m_W^2 \frac{12gc_{DW} + 6c_W}{g\Lambda_{EFT}^2} \\ = & \frac{g^3 j^2 (2j + 1) m_W^2}{240\pi^2 m^2},\end{aligned}\quad (5.32)$$

$$\kappa_Z = g_1^Z.\quad (5.33)$$

Using these equations the LHC CMS limits [3] and LEP limits [11] can be compared to the proposed model. In table 5.2 the LHC and LEP limits on the three anomalous triple gauge coupling parameters at 95% confidence level are shown alongside the values calculated for the BSM model for two parameter setups. The first setup is for the lower mass of  $m = 700$  GeV with the maximal allowed isospin of  $J = 3$  and the maximal allowed coupling  $\lambda = 1$  and the second setup is for the larger mass of  $m = 1100$  GeV with an isospin of  $J = 4$  and a coupling of  $\lambda = 3$ . Looking at the

**Table 5.2.:** Limits on the anomalous triple gauge couplings from CMS [3] and LEP [11] compared to the expected values for the presented model. The parameter points for the setups are: 1:  $m = 700$  GeV,  $J = 3$ ,  $\lambda = 1$ ; 2:  $m = 1100$  GeV,  $J = 4$ ,  $\lambda = 3$

	CMS(WV) $35.9 \text{ fb}^{-1}$	LEP	setup 1	setup 2
$\kappa_Z$	$[-0.0079, 0.0082]$	$[-0.074, 0.051]$	0.0005	0.0012
$\lambda_Z$	$[-0.0065, 0.0066]$	$[-0.059, 0.017]$	0.0002	0.0001
$g_1^Z$	$[-0.0061, 0.0074]$	$[-0.054, 0.021]$	0.0005	-0.0001

values one can see that for either of the these parameter choices the proposed model would be far below the current experimental limits This behavior aligns with the  $\lambda = 0$  case studied in [19] where it was shown that the coefficients of the operators  $\mathcal{O}_W$  and  $\mathcal{O}_{DW}$  destructively interfere and mostly cancel each other. Comparing these results one has to keep in mind, that the model presented here has three multiplets and therefore the factor  $T_R$  has to be replaced. Using equation 3.41 one finds

$$T_R(J) + 2T_R(J - \frac{1}{2}) = J^2(2J + 1). \quad (5.34)$$

As the aTGC parameters are well within the experimentally allowed range, no limit on the parameters of the model will be set going forward.

**Table 5.3.:** Limits on the anomalous higgs couplings from CMS ([2], one sigma bounds) compared to the expected values for the presented model. The parameter points for the setups are: 1:  $m = 700$  GeV,  $J = 3$ ,  $\lambda = 1$ ; 2:  $m = 1100$  GeV,  $J = 4$ ,  $\lambda = 3$ .

	CMS(HVV) 137 fb <sup>-1</sup>	setup 1	setup 2
$\delta c_z$	[-0.28, 0.03]	0.018	0.103
$c_{ZZ}$	[-0.09, 0.12]	0.05	0.41
$c_{z\Box}$	[-0.06, 0.02]	-0.002	0.002

## 5.4. Anomalous Higgs Boson Couplings

For the anomalous higgs boson coupling to vector bosons one can look at the HVV vertex and the effects of the dimension 6 operators on this vertex. Using the commonly used so-called higgs basis [57] the relevant part of the effective Lagrangian in the SU(2)-limit can be written as

$$\begin{aligned}
\mathcal{L}_{HVV} = & \frac{h}{v} \left( \delta c_z \frac{g^2 \hat{v}^2}{4} Z_\mu Z^\mu + c_{zz} \frac{g^2}{4} (\partial_\mu Z_\nu - \partial_\nu Z_\mu) (\partial^\mu Z^\nu - \partial^\nu Z^\mu) \right. \\
& + c_{z\Box} g^2 Z_\mu \partial_\nu (\partial^\mu Z^\nu - \partial^\nu Z^\mu) \\
& + \delta c_W \frac{g^2 \hat{v}^2}{2} W_\mu^+ W^{-\mu} + c_{WW} \frac{g^2}{2} (\partial_\mu W_\nu^+ - \partial_\nu W_\mu^+) (\partial^\mu W^{-\nu} - \partial^\nu W^{-\mu}) \\
& \left. + c_{W\Box} g^2 W_\mu^- \partial_\nu (\partial^\mu W^{+\nu} - \partial^\nu W^{+\mu}) \right). \tag{5.35}
\end{aligned}$$

Focusing on the HZZ vertex one can again compare the coefficients and finds

$$\begin{aligned}
\delta c_z = & - \frac{\hat{v}^2 (6g^2 c_{DW} + c_{HD1} - 2c_{HD2} + 2c_{HD3}) + 4c_{HDD} (m_H^2 - m_W^2)}{4\Lambda_{EFT}^2} \\
= & \frac{(2j+1)g^4 j^2 \hat{v}^2}{160\pi^2 m^2} - \frac{(2j+1)(2j\lambda^2(2\lambda^2 \hat{v}^2 + m_H^2 - m_W^2) + 2\lambda^4 \hat{v}^2)}{160\pi^2 j m^2}, \tag{5.36}
\end{aligned}$$

$$\begin{aligned}
c_{ZZ} = & - \frac{\hat{v}^2 (g^2 c_{HDD} - 2g c_{HDDW} + 8c_{HW})}{2g^2 \Lambda_{EFT}^2} \\
= & - \frac{(160j^3 + 160j^2 + 2j - 19)\lambda^2 \hat{v}^2}{1440\pi^2 m^2}, \tag{5.37}
\end{aligned}$$

$$c_{z\Box} = - \frac{\kappa_Z + g_1^Z}{g}. \tag{5.38}$$

For these three parameters and the two parameter choices for the BSM model (first setup:  $m = 700$  GeV,  $J = 3$ ,  $\lambda = 1$ ; second setup:  $m = 1100$  GeV,  $J = 4$ ,  $\lambda = 3$ ) the expected values from the model and the experimental (one sigma) limits [2] can be compared. Looking at those values one sees that the first setup is well within the allowed limits, while the second setup exceeds the bound on  $c_{ZZ}$  and  $\delta c_z$ . The exceeded limit in  $\delta c_z$  is driven by  $\mathcal{O}_{HD1}$  and  $\mathcal{O}_{HD3}$ , but is comparatively a lot smaller than for the combination  $-c_{HD1} - 2c_{HD3}$  in table 4.6. This implies that the renormalization plays a sizable effect for these considerations. When considering correlation it is possible that the value for  $\delta c_z$  falls within the two sigma band allowing us to move forward with this setup.

Investigating  $c_{ZZ}$  further one finds that the operator  $\mathcal{O}_{HW}$  is mostly responsible for this value in the model. In the model with  $\lambda = 0$  the dimension 6 operators could be

neglected, as these would only scale with  $J^3$  (stemming from the trace over three generators) compared to the  $J^5$  scaling of the dimension 8 operators. For the  $VVH$  vertex one can still find up to three powers of  $J$ , stemming from two couplings and a sum over the members of the multiplets, one power of  $\lambda$  from the higgs coupling and additional powers of  $\lambda$  from the mass splitting in the propagators. Going back to the operator  $\mathcal{O}_{HW}$  one then finds

$$\frac{c_{HW}}{\Lambda_{EFT}^2} = \frac{g^2(2J+1)(-160J^2 - 80J + 77)\lambda^2}{11520\pi^2 m^2} \propto \frac{g^2 J^3 \lambda^2}{m^2}. \quad (5.39)$$

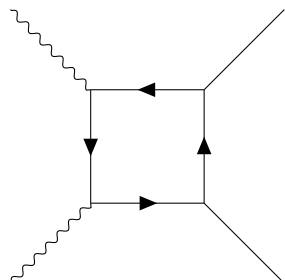
This is the same scaling behavior with respect to  $J$  and  $\lambda$  as one would expect for the M-operators and for  $gJ = \lambda$  the same scaling behavior as the T-operators. With respect to  $m$  this operator is only suppressed by  $m^2$  compared to the  $m^4$  one finds for the dimension 8 operators. Therefore, for values of  $\lambda$  of the order of  $gJ$  the dimension 6 operators can give sizable contributions. Considering the fact that the bounds in table 5.3 are one sigma bounds and taking into account the possible correlation between these observables, one can conclude that the parameter point  $\lambda = 3$ ,  $m = 1100$  GeV and  $J = 4$  is on the edge of what is experimentally allowed with respect to  $c_{ZZ}$  and  $\delta c_z$ . We will therefore only consider  $\lambda \leq 3$  for  $m = 1100$  GeV and  $J = 4$ .

## 5.5. On-Shell Four Particle Scattering

For probing the influence of the model on four point functions, and thereby investigating the possibility of large M-operators, one can look at the different  $2 \rightarrow 2$  processes for vector bosons and higgs bosons. These different processes were implemented into a custom program, that uses LoopTools [35] for the numerical evaluation of the one loop integrals as well as Cuba [58] for the integration over the phase space (see section 2.4). The incoming and outgoing particles are implemented as on-shell. The squared amplitude is calculated as

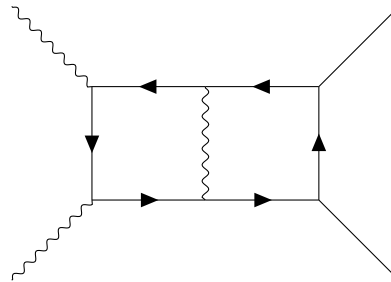
$$|M|^2 = |M_{SM} + M_{BSM}|^2 = |M_{SM}|^2 + 2\text{Re}(M_{SM}M_{BSM}^*) + |M_{BSM}|^2 \quad (5.40)$$

which includes the interference as well as the squared amplitudes for the SM and the new model. As  $M_{BSM}$  is by construction a one loop quantity one can argue that only the interference term and the SM term should be considered since  $|M_{BSM}|^2$  would be of the same order as possible two loop graphs. For this issue one can look at the  $\lambda$  and  $J$  dependence of the one loop and possible two loop graphs for four external particles. Taking the process  $VV \rightarrow HH$  one finds one power of  $\lambda$  at each higgs vertex and, depending on which fermions propagate, either one power of  $J$  at each vector boson vertex or at least one power of  $\lambda$  from one of the attached fermion propagators. Additionally one power of  $J$  can be found when summing over all particles of the multiplets. In total this gives five powers of  $J$  or  $\lambda$



$$\propto J \cdot J^2 \cdot \lambda^2. \quad (5.41)$$

Looking at a two loop graph one has two additional vertices which leads to two additional factors of  $J$  or  $\lambda$



$$\propto J \cdot J^4 \cdot \lambda^2. \quad (5.42)$$

Comparing  $|M_{BSM}|^2$  to the interference term of the two loop amplitude with the SM one finds ten powers of the coupling coefficients for one loop squared compared to only seven at two loop. This implies that the one loop squared contribution is expected to be quite a bit larger than the two loop mixed contribution which justifies equation 5.40. The BSM contributions are then implemented purely at one loop, therefore having only one vertex or one propagator affected at a time. For the EFT the same approach is taken.

When trying to estimate the effects of the model for LHC processes like  $pp \rightarrow VVjj$  one has to consider the fact that some of the vector bosons in these processes can be highly virtual. For vector boson scattering the incoming vector bosons can have virtualities of a couple of hundred GeV while the outgoing ones are in good approximation on-shell. For the on-shell ones there is no contribution to the outgoing vector boson propagator while the incoming ones are expected to get contributions. Since the virtualities are still small compared to the production threshold of two new fermions and additionally negative one wouldn't expect much of an influence there either (see section 5.1). This implies that studying the effects of the new model on on-shell  $VV \rightarrow VV$  scattering gives a good understanding of the effects of the model on  $pp \rightarrow VVjj$ .

Lastly some comments on the scattering angle are needed. While the new model is relatively flat in the scattering angle the SM contribution is strongly peaked for forward and backward scattering due to the strong enhancements to the t- or u-channels at these angles. At the LHC the visible scattering angle is limited by the geometry of the detectors. Therefore scattering along the beam axis (at angles close to  $0^\circ$  or  $180^\circ$ ) can't be observed. For the on-shell scattering this means that a cut on the scattering angle is acceptable in order to enhance the relative contribution of the new fermions. For this purpose a cut of  $5^\circ \leq \theta \leq 175^\circ$  is applied for all on-shell cross sections.

### 5.5.1. VBS

For the VBS processes in the SU(2)-limit five processes are relevant:

- scattering of same sign W bosons:  $W^+W^+ \rightarrow W^+W^+$
- scattering of opposite sign W bosons:  $W^+W^- \rightarrow W^+W^-$
- scattering of one W and one Z boson:  $W^+Z \rightarrow W^+Z$
- scattering of two Z bosons:  $ZZ \rightarrow ZZ$
- production of two Z bosons from two W bosons (or vice versa):  $W^+W^- \rightarrow ZZ$

For these processes the cross section for the full model and its EFT can be studied and compared.

#### 5.5.1.1. Full Model

Starting with the lower mass for the new fermions,  $m = 700$  GeV, one can study the effects of the isospin and the coupling  $\lambda$  on the five processes as well as the interference pattern between the SM and the BSM model. For this purpose the  $J = 4$  case, which is excluded following the argumentation in section 5.1, is also shown in order to see the size of the impact of choosing larger isospins. Starting with  $W^+W^+ \rightarrow W^+W^+$  in figure 5.8 the SM (black) and the BSM cross section for  $J = 3$  (red, blue) and  $J = 4$  (green, orange) are shown. In the region  $\sqrt{s} > 2$  TeV one finds an increase in the cross section due to the new fermions by about 20% for  $J = 3$  and about 100% for  $J = 4$ . This increase is independent of the choices of  $\lambda$ , that are allowed following section 5.1. This strong dependence on the isospin is due to the four point function being proportional to  $J^5$ , stemming from four couplings to vector bosons and a sum over all particles of the multiplets. The second region of importance is the threshold region around  $\sqrt{s} = 2m = 1.4$  TeV which is shown in figure 5.8b. In this region one can observe a destructive interference between the SM and the BSM model, which causes decreases of 10% ( $J = 3$ ) to 20% ( $J = 4$ ) for the cross section. At around  $\sqrt{s} = 2m = 1.4$  TeV the imaginary part of the BSM amplitude, stemming from two fermions being on-shell in s-channel loops, starts rising and compensating for the destructive interference in the real part of the amplitude. Lastly one can investigate the  $\lambda$  dependence of the cross section. When comparing  $\lambda = 1$  and  $\lambda = 0$  one can observe three threshold regions  $\sqrt{s} = 2(m - \frac{\lambda \hat{v}}{\sqrt{2}}) = 1.05$  TeV,  $\sqrt{s} = 2m = 1.4$  TeV and  $\sqrt{s} = 2(m + \frac{\lambda \hat{v}}{\sqrt{2}}) = 1.75$  TeV, that are caused by the three masses of the mass eigenstate multiplets. At these thresholds the slope of the BSM cross section peaks which is again more prominent in the  $J = 4$  case and hardly visible in the  $J = 3$  case.

Going to the next process,  $W^+W^- \rightarrow W^+W^-$ , in figure 5.9 one can observe a slightly different picture. For this process the interference between the SM and the BSM model is constructive which leads to a different behavior around the thresholds for pair production. For all cases of isospin and  $\lambda$  a peak in the cross section can be observed (again for  $J = 3$  these are hardly visible). This constructive interference around the threshold region also results in larger differences between the SM and the BSM cross section for  $J = 4$  and similar differences for  $J = 3$ . Above the thresholds the difference between the cross sections of SM and of the BSM model for  $J = 3$  shrinks and finally vanishes. This can be explained by destructive

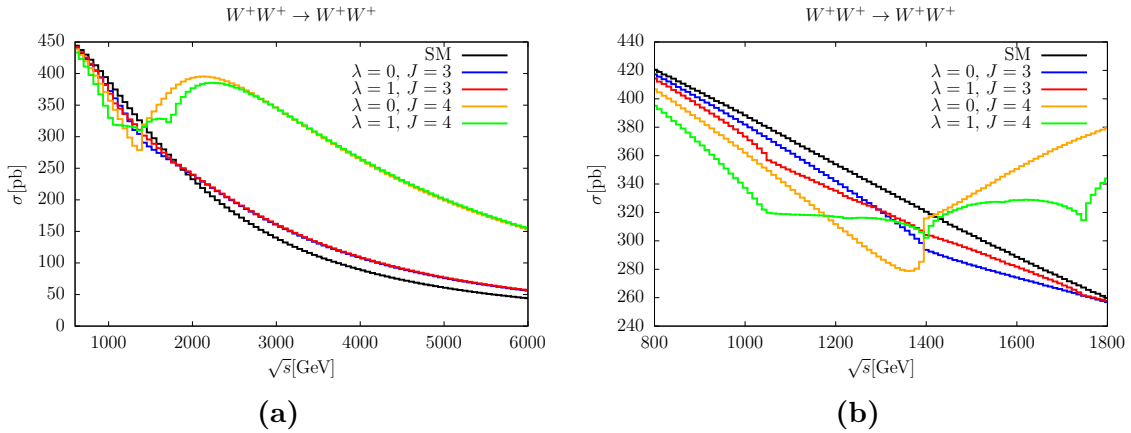


**Figure 5.8.:** Cross section of the full model with  $m = 700$  GeV for  $W^+W^+ \rightarrow W^+W^+$  for different invariant masses of the vector boson pair. 5.8b provides a closer look at the threshold region. The SM distribution (black) and the full model distributions for  $J = 3, 4$  and  $\lambda = 0, 1$  (blue, red, yellow, green) are shown.

interference between the real parts of the amplitude from the new fermions and the SM which is compensated by the remaining imaginary part of the BSM amplitude.

For  $W^+W^- \rightarrow ZZ$  in figure 5.10 one finds the same general behavior as for  $W^+W^- \rightarrow W^+W^-$ , when it comes to the interference between the SM and the BSM model. The striking feature in comparison is simply the size of the contribution, which is substantially smaller than in the case of scattering of opposite sign W bosons. This leads to overall smaller differences in the cross sections for all  $J$  and  $\lambda$ .

For the next process,  $W^+Z \rightarrow W^+Z$ , in figure 5.11 one finds structurally similar behavior as for the scattering of same sign W bosons. Again one can observe destructive interference in the threshold region but with slightly smaller BSM contributions.

Lastly for  $ZZ \rightarrow ZZ$  in figure 5.12 the SM contribution is considerably smaller than for the other processes. For small energies one still finds a constructive interference and at the difference between the full cross section and the SM one finds a similar behavior as for  $W^+W^- \rightarrow W^+W^-$ .

For all of these processes one can make the following general statements

- For  $J = 4$  the deviations from the SM can be quite sizable and the different masses of the mass eigenstate multiplets can be observed. This case is however ruled out in section 5.1.
- For  $J = 3$  the deviations from the SM are of the order of 10% and the different masses of the mass eigenstate multiplets are hardly noticeable. Furthermore the  $\lambda = 1$  and  $\lambda = 0$  case mostly differ by the position of the first threshold, while the general shape of the cross section is mostly similar (but shifted).

In order to study larger couplings, the second parameter point of  $m = 1100$  GeV and  $J = 4$  can be studied for the same processes. Although  $\lambda = 3$  is disfavored due to the HVV parameters in section 5.4 it is included in order to see an upper limit of the effects that large couplings can cause. In figure 5.13 and 5.14 the cross

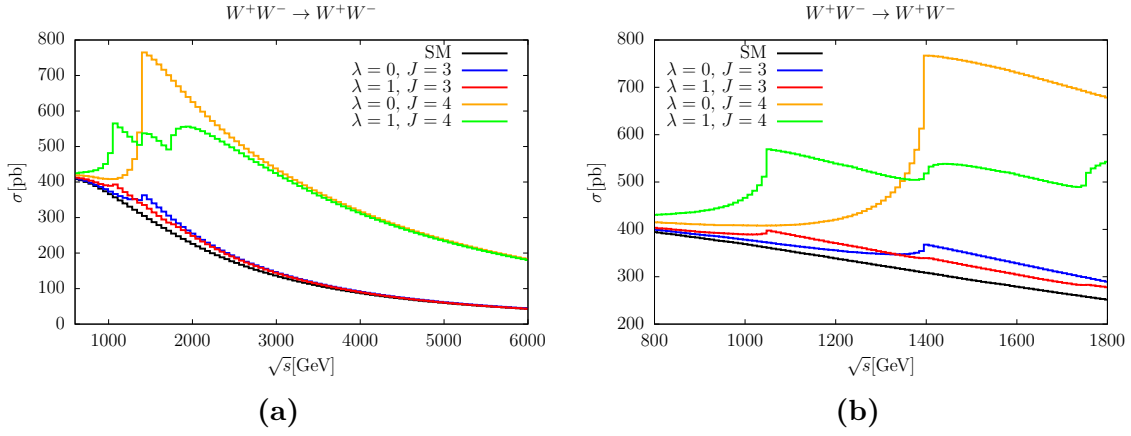


**Figure 5.9.:** Cross section of the full model with  $m = 700$  GeV for  $W^+W^- \rightarrow W^+W^-$  for different invariant masses of the vector boson pair. 5.9b provides a closer look at the threshold region. The SM distribution (black) and the full model distributions for  $J = 3, 4$  and  $\lambda = 0, 1$  (blue, red, yellow, green) are shown.

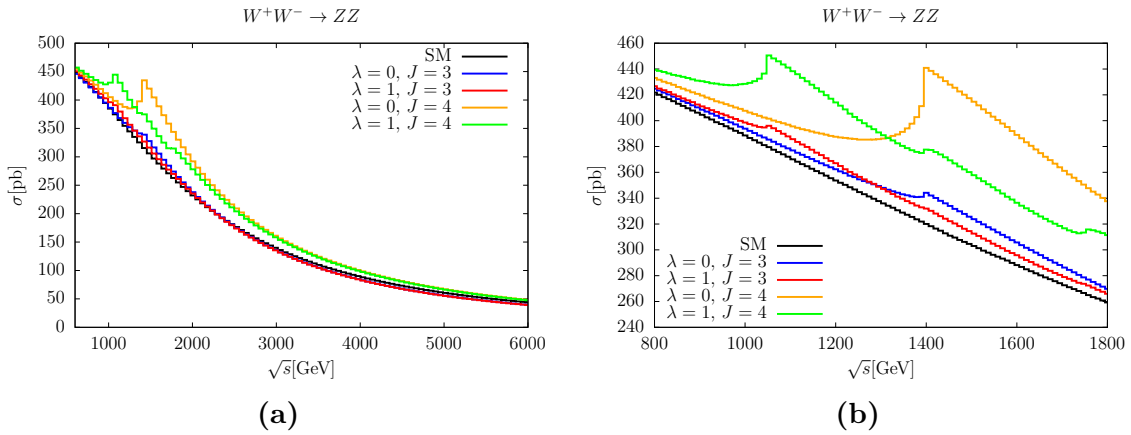


**Figure 5.10.:** Cross section of the full model with  $m = 700$  GeV for  $W^+W^- \rightarrow ZZ$  for different invariant masses of the vector boson pair. 5.10b provides a closer look at the threshold region. The SM distribution (black) and the full model distributions for  $J = 3, 4$  and  $\lambda = 0, 1$  (blue, red, yellow, green) are shown.

sections for  $\lambda = 0$  (orange),  $\lambda = 1$  (green),  $\lambda = 2$  (red),  $\lambda = 3$  (blue) and the SM (black) are shown for the processes  $W^+W^+ \rightarrow W^+W^+$  and  $W^+W^- \rightarrow W^+W^-$ . As little further insight can be gained by the remaining processes, they will no longer be discussed. For completeness the figures for these processes can be found in the appendix in figures C.1, C.2 and C.3. The  $\lambda = 0$  and  $\lambda = 1$  distributions follow the same shape as for the  $m = 700$  case thereby not producing any new phenomenology. For  $\lambda = 2$  in figure 5.14b one can observe the two particles production thresholds at  $\sqrt{s} = 2.2$  TeV and  $\sqrt{s} \approx 1.5$  TeV from the two lighter multiplets. Additionally a slight bump in the cross section at  $\sqrt{s} \approx 1.85$  TeV can be seen which stems from the on-shell production of one particle from the light and one from the medium multiplet. This bump becomes more pronounced when going to  $\lambda = 3$ . This implies that the cross section at these mixed thresholds depends stronger on the coupling and less on the isospin compared to the cross section at the production threshold of two particles of the same multiplet. Concerning the size of the excess over the SM, one finds that  $\lambda = 0$ ,  $\lambda = 1$  and  $\lambda = 2$  all produce a similar amount of excess (but shifted due to the

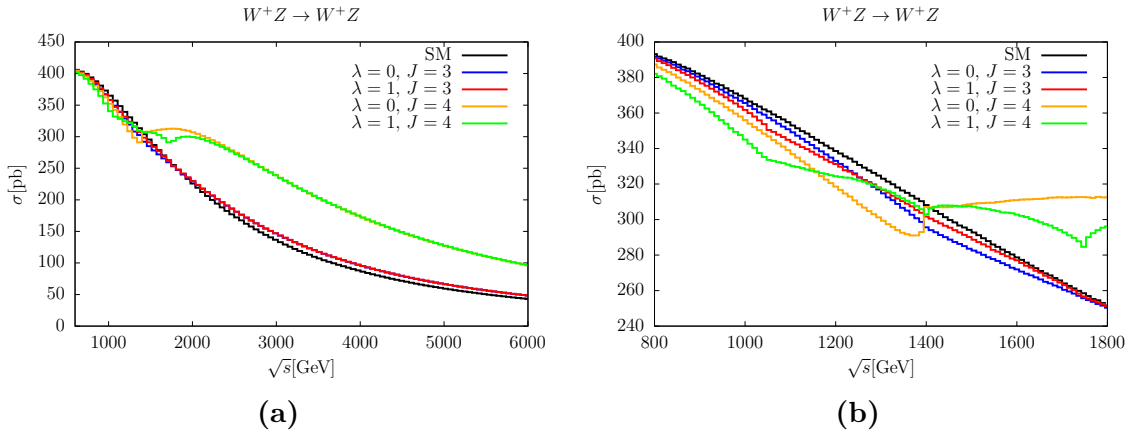


**Figure 5.11.:** Cross section of the full model with  $m = 700$  GeV for  $W^+Z \rightarrow W^+Z$  for different invariant masses of the vector boson pair. 5.11b provides a closer look at the threshold region. The SM distribution (black) and the full model distributions for  $J = 3, 4$  and  $\lambda = 0, 1$  (blue, red, yellow, green) are shown.

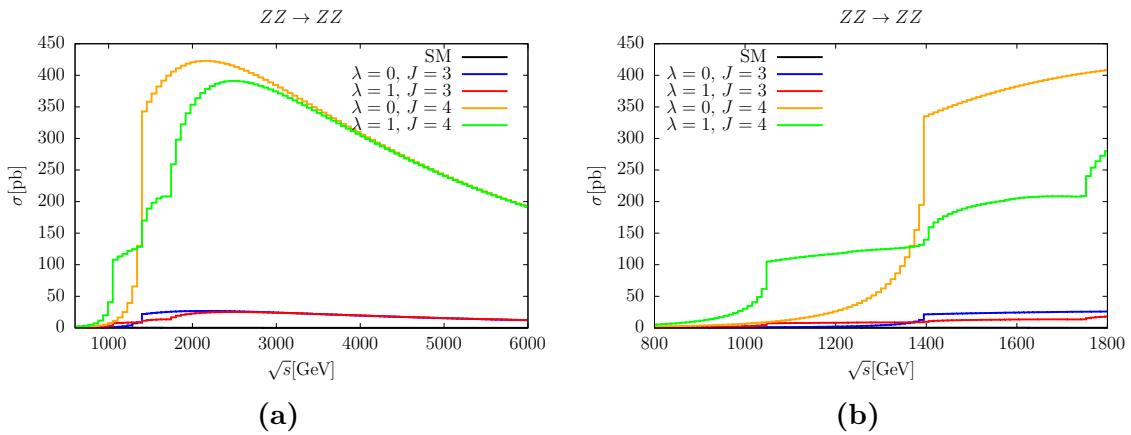


**Figure 5.12.:** Cross section of the full model with  $m = 700$  GeV for  $ZZ \rightarrow ZZ$  for different invariant masses of the vector boson pair. 5.12b provides a closer look at the threshold region. The SM distribution (black) and the full model distributions for  $J = 3, 4$  and  $\lambda = 0, 1$  (blue, red, yellow, green) are shown.

different threshold positions) while  $\lambda = 3$  generates overall a larger excess. As the onset of this increase can also be observed for  $\lambda = 2$  one can make the assumption that this increase is caused by absorptive contributions from particles from different multiplets.

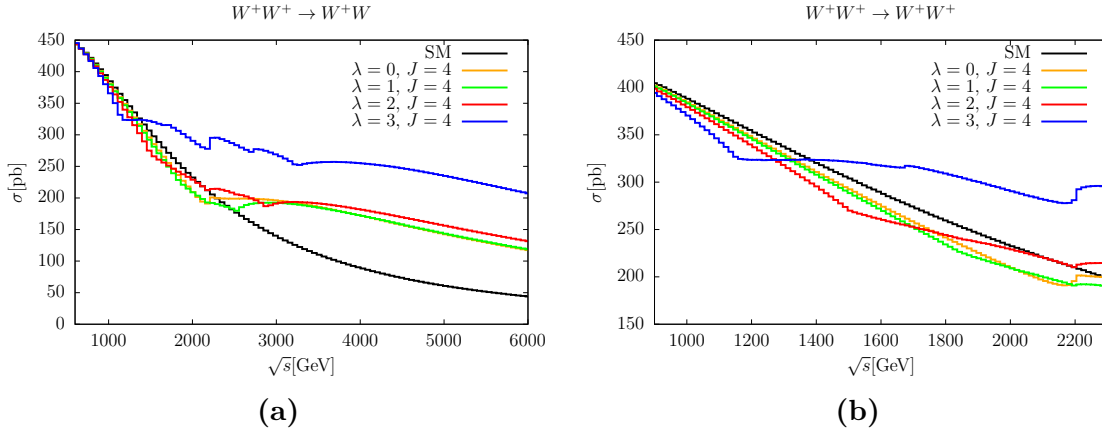


**Figure 5.13.:** Cross section of the full model with  $m = 1100$  GeV for  $W^+W^+ \rightarrow W^+W^+$  for different invariant masses of the vector boson pair. 5.13b provides a closer look at the threshold region. The SM distribution (black) and the full model distributions for  $J = 4$  and  $\lambda = 0, 1, 2, 3$  (yellow, green, red, blue) are shown.

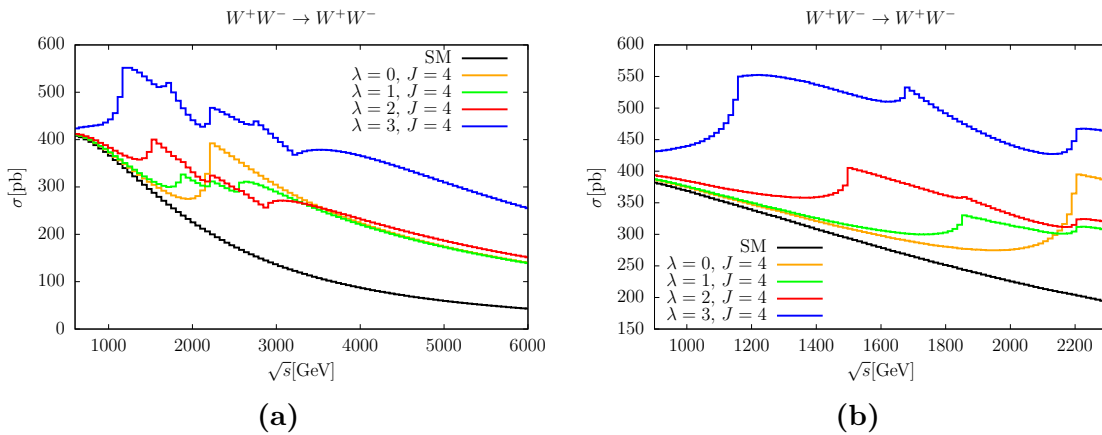


**Figure 5.14.:** Cross section of the full model with  $m = 1100$  GeV for  $W^+W^- \rightarrow W^+W^-$  for different invariant masses of the vector boson pair. 5.14b provides a closer look at the threshold region. The SM distribution (black) and the full model distributions for  $J = 4$  and  $\lambda = 0, 1, 2, 3$  (yellow, green, red, blue) are shown.

### 5.5.1.2. EFT

Looking at the EFT side of things there are mainly three things to investigate:

- Do dimension 6 operators give a sizable contribution
- How do the contributions of T- and M- operators compare
- How much do the contributions from the M-operators depend on the definition of the other operators (see sections 4.2.3.6 - 4.2.3.9).

For the M-operators and operators that behave similarly one has to remember that the choice of operators within the classes in sections 4.2.3.6 - 4.2.3.9 is not unique. Therefore a different choice of operators, while keeping the M-operators, can be achieved by using the allowed tools (total derivatives, replacing commutators etc.). During this process contributions proportional to the M-operators can appear, which results in different Wilson coefficients for the M-operators between different sets of operators making them somewhat arbitrary. What is however invariant under changing the basis, is the total contribution stemming from all operator classes that are connected via the tools presented section 2.2.1.1. The common part of all of these operator classes is the presence of two higgs fields, as these can't be transformed away without equations of motion. Transformations after which the two higgs fields only appear as  $\frac{\hat{v}^2}{2}$  in the Wilson coefficient are however possible. As both higgs fields and factors of  $\hat{v}$  always appear together with a factor of  $\lambda$  one can group all of these contributions together as contributions that are proportional to  $\frac{\lambda^2}{m^4}$ . In a similar vein one can group contributions that behave like T-operators as  $\frac{\lambda^0}{m^4}$  and contributions that behave like S-operators as  $\frac{\lambda^4}{m^4}$ .

With these definitions out of the way one can now study the EFT contributions for the two sets of parameters,  $m = 700$  GeV,  $J = 3$ ,  $\lambda = 1$  and  $m = 1100$  GeV,  $J = 4$ ,  $\lambda = 3$ , for the processes  $W^+W^+ \rightarrow W^+W^+$  and  $W^+W^- \rightarrow W^+W^-$  in figures 5.15 - 5.18 (with the remaining processes found in the appendix in figures C.4- C.9). Subplot (a) of each plot shows the comparison of dimension 6 and dimension 8 contributions. For the  $\lambda = 1$  case the dimension 6 contribution is almost completely vanishing while for the  $\lambda = 3$  case one can find similarly large contributions from both, dimension 6 and dimension 8, up until  $\sqrt{s} = 2m = 2.2$  TeV. This increase in contributions from dimension 6 can be understood by looking at the VVV and HVV couplings in section 5.3 and 5.4. There it was found that the VVV-vertex has rather small contributions at dimension 6 level while the HVV-vertex gets sizable contributions for larger values of  $\lambda$ . Additionally the dimension 6 operators that first appear in the VVV-vertex depend on  $J^3$  while the dimension 8 operators that only affect the four particle vertex (like the T-operators) grow with  $J^5$ . For the M-operators one finds a factor of  $\lambda^2 J^3$  which is identical to the dominant dimension 6 operator in HVV:  $\mathcal{O}_{HW}$ . One can therefore conclude that there is no mechanism in this model, that suppresses dimension 6 operators compared to dimension 8 operators for growing  $\lambda$ . The next study (b) of the plots shows the comparison between the contribution coming from T-operators and from M-operators. For the  $\lambda = 1$  case the M-operators can be neglected compared to the T-operators, which are responsible for most of the EFT cross section. Going to larger couplings of  $\lambda = 3$  this behavior seems to turn around as the dimension 8 EFT cross section is now dominated by the M-operators. This is however only half of the truth, as when comparing the M-operators to the full set of contributions proportional to  $\frac{\lambda^2}{m^4}$  (c), one finds that the full set produces way

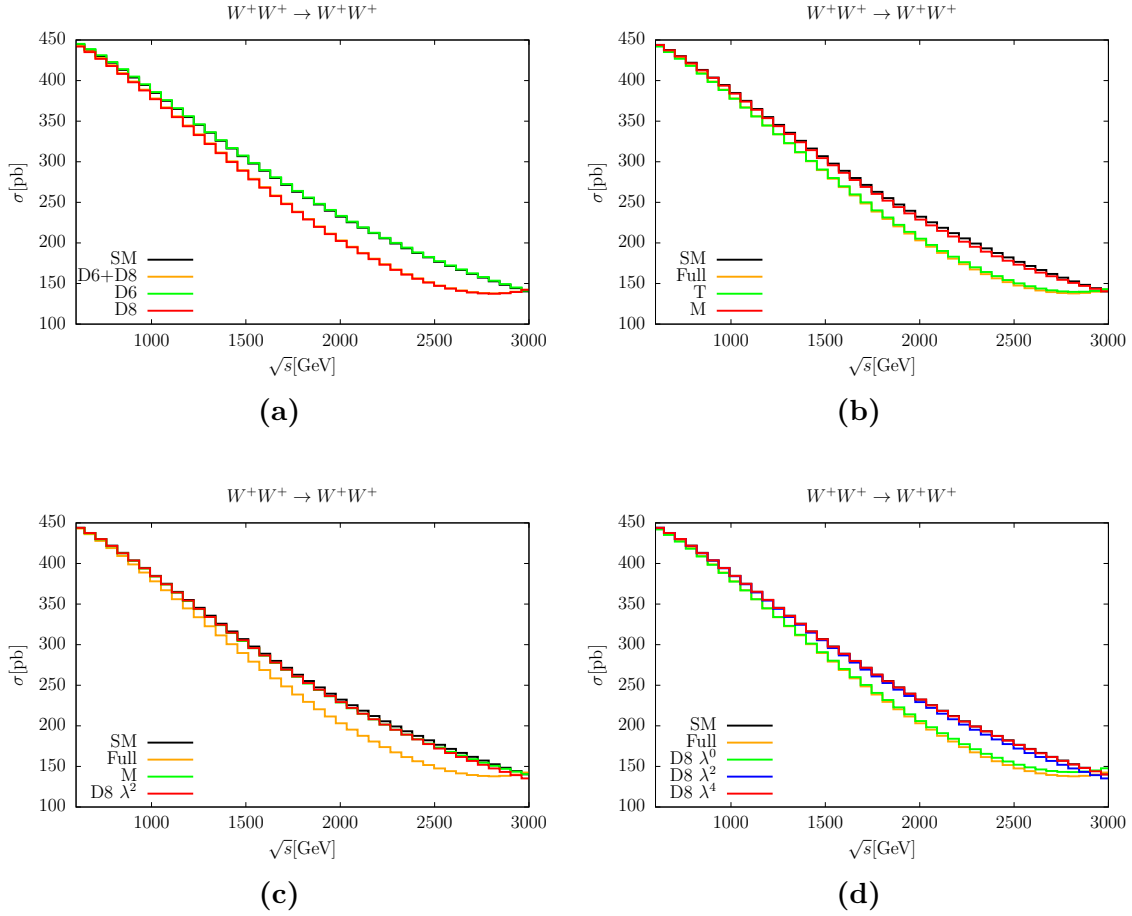


**Figure 5.15.:** Cross section of the EFT for  $m = 700$  GeV,  $J = 3$  and  $\lambda = 1$  for  $W^+W^+ \rightarrow W^+W^+$  for different invariant masses of the vector boson pair. 5.15a shows the SM (black) the full EFT (yellow) the dimension 6 (green) and the dimension 8 (red) contributions. 5.15b shows the SM (black) the full EFT (yellow) the contributions from the T-operators (green) and the M-operators (red). In 5.15c the contribution from the M-operators (green) is compared to the one from all connected operators (red). 5.15d shows the contribution from the T-like operators (green), M-like operators (blue) and the T-like operators (red).

smaller cross sections compared to the M-operators. This implies strong destructive interference between different contributions within this set of operators.

Lastly one can investigate, how the three complete sets of contributions ( $\frac{\lambda^0}{m^4}$ ,  $\frac{\lambda^2}{m^4}$ ,  $\frac{\lambda^4}{m^4}$ ) behave for  $\lambda = 1$  and  $\lambda = 3$  (d). For  $\lambda = 1$ , as expected,  $\frac{\lambda^0}{m^4}$  gives the dominant contribution while for  $\lambda = 3$  it is quite unclear and process dependent.

With all these comparison done one still has to keep in mind that the EFT has a finite range of validity and results beyond  $\sqrt{s} = 2m$  are expected to have little to do with the actual model. Still one can make the following generalized conclusions

- For  $\lambda = 1$  (so  $\lambda \ll gJ$ ) the EFT is dominated by the dimension 8 T-operators.
- For  $\lambda = 3$  (so  $\lambda \sim gJ$ ) both dimension 8 and dimension 6 operators give sizable contributions to the EFT cross section.
- There can be strong destructive interference within groups of operators (e.g.  $\frac{\lambda^2}{m^4}$  operators)

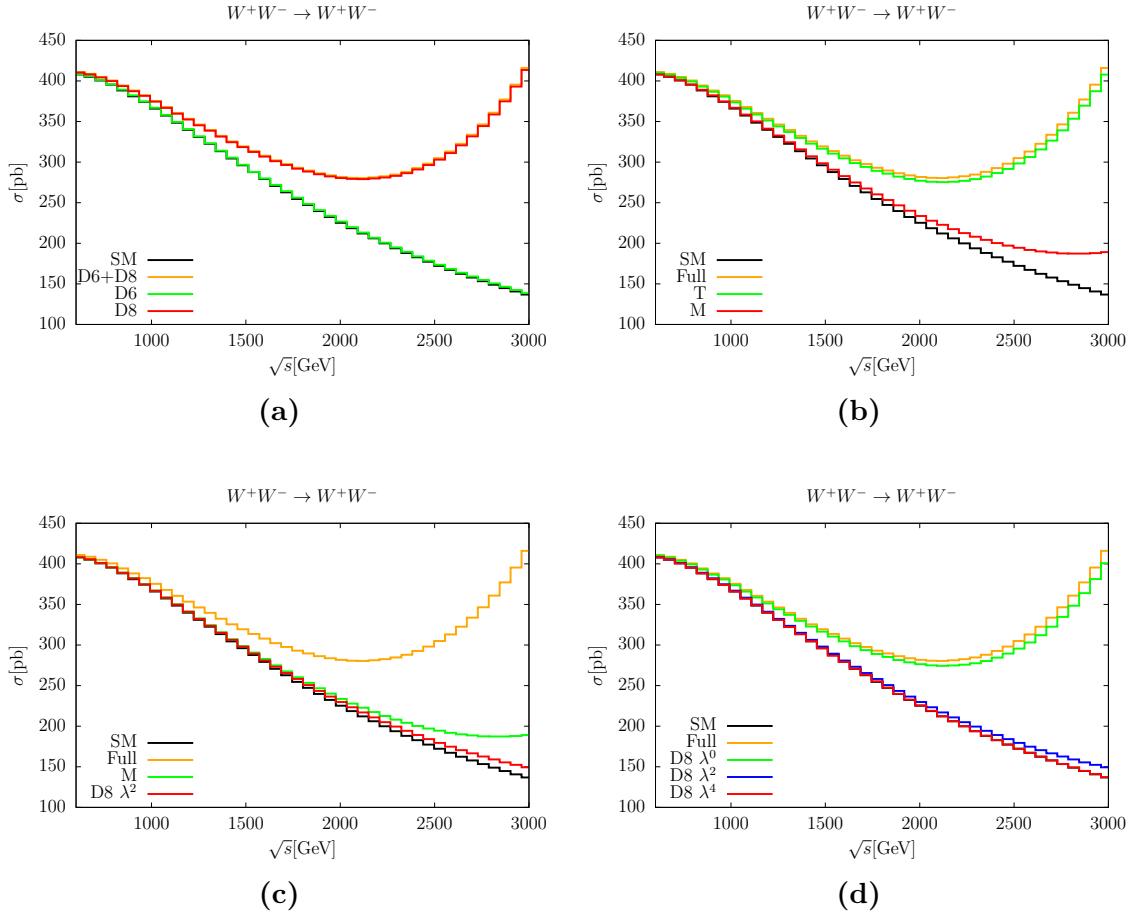


**Figure 5.16.:** Cross section of the EFT for  $m = 700$  GeV,  $J = 3$  and  $\lambda = 1$  for  $W^+W^- \rightarrow W^+W^-$  for different invariant masses of the vector boson pair. 5.16a shows the SM (black) the full EFT (yellow) the dimension 6 (green) and the dimension 8 (red) contributions. 5.16b shows the SM (black) the full EFT (yellow) the contributions from the T-operators (green) and the M-operators (red). In 5.16c the contribution from the M-operators (green) is compared to the one from all connected operators (red). 5.16d shows the contribution from the T-like operators (green), M-like operators (blue) and the T-like operators (red).

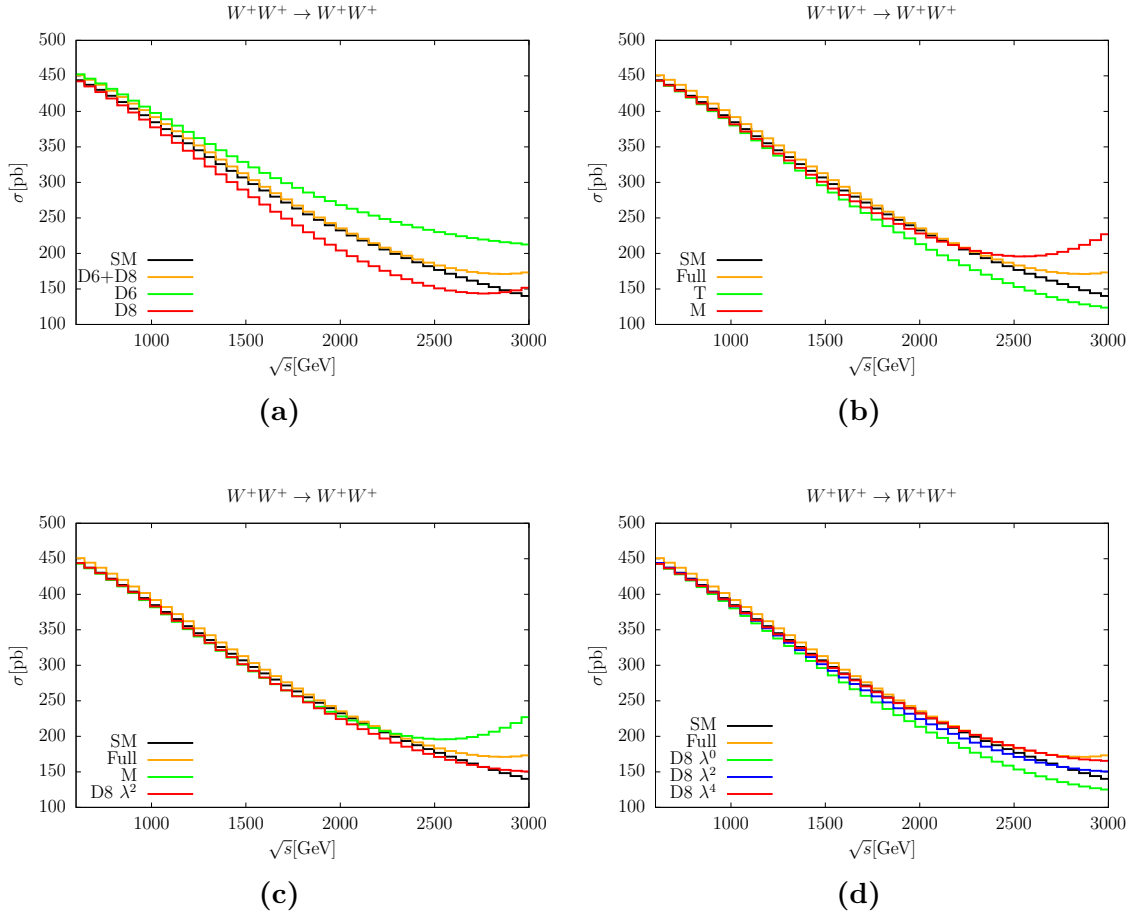


**Figure 5.17.:** Cross section of the EFT for  $m = 1100$  GeV,  $J = 4$  and  $\lambda = 3$  for  $W^+W^+ \rightarrow W^+W^+$  for different invariant masses of the vector boson pair. 5.17a shows the SM (black) the full EFT (yellow) the dimension 6 (green) and the dimension 8 (red) contributions. 5.17b shows the SM (black) the full EFT (yellow) the contributions from the T-operators (green) and the M-operators (red). In 5.17c the contribution from the M-operators (green) is compared to the one from all connected operators (red). 5.17d shows the contribution from the T-like operators (green), M-like operators (blue) and the T-like operators (red).

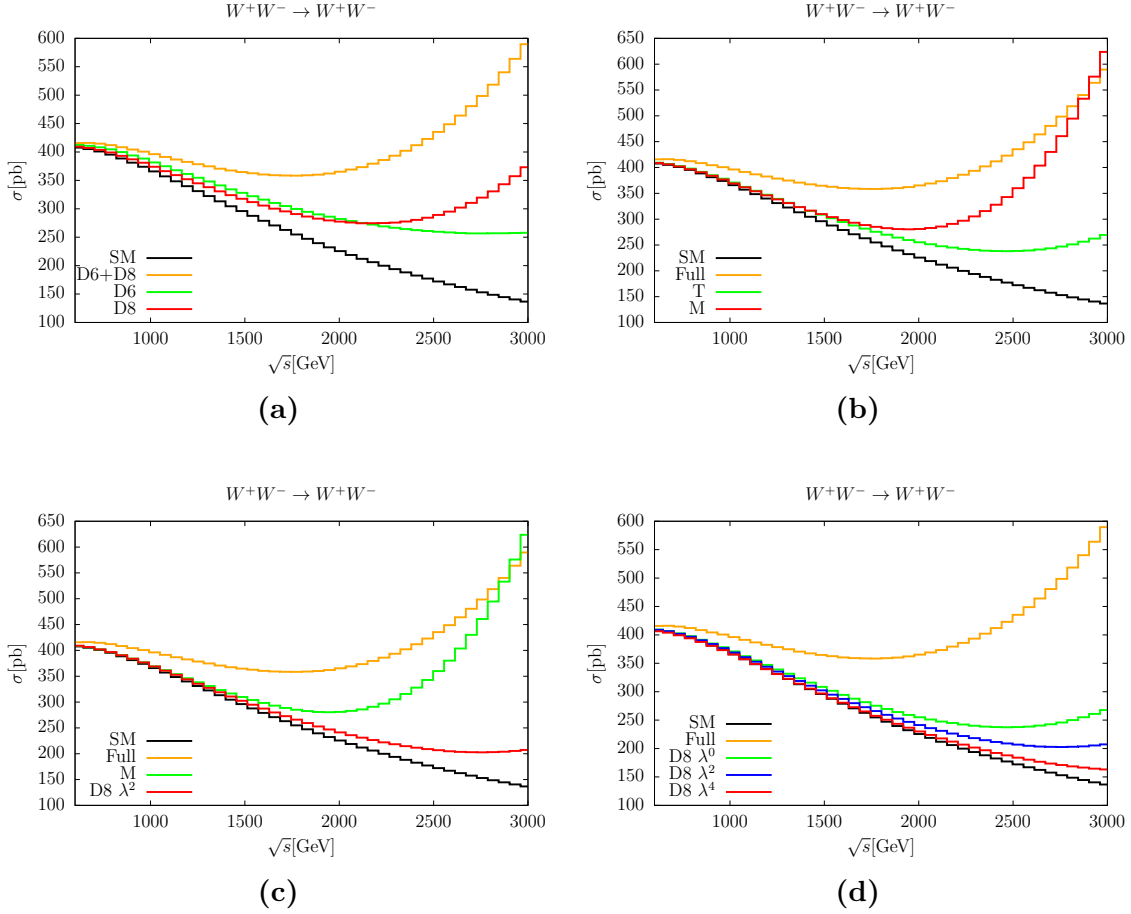


**Figure 5.18.:** Cross section of the EFT for  $m = 1100$  GeV,  $J = 4$  and  $\lambda = 3$  for  $W^+W^- \rightarrow W^+W^-$  for different invariant masses of the vector boson pair. 5.18a shows the SM (black) the full EFT (yellow) the dimension 6 (green) and the dimension 8 (red) contributions. 5.18b shows the SM (black) the full EFT (yellow) the contributions from the T-operators (green) and the M-operators (red). In 5.18c the contribution from the M-operators (green) is compared to the one from all connected operators (red). 5.18d shows the contribution from the T-like operators (green), M-like operators (blue) and the T-like operators (red).

### 5.5.1.3. Model vs EFT

With the cross section of the full model and of its EFT analyzed, one can now compare the two of them in order to figure out, how well the EFT actually captures the features of the full model. This is done for the case of  $\lambda = 0$ , which was studied in [19], and the cases of  $\lambda = 1$  and  $\lambda = 3$  for  $J = 3$  and  $J = 4$  respectively. Similarly to the previous sections the main features can be captured by studying  $W^+W^+ \rightarrow W^+W^+$  (figure 5.19) and  $W^+W^- \rightarrow W^+W^-$  (figure 5.20). The left side of these plots (a) show the cross sections for  $m = 700$  GeV and  $J = 3$  for the two cases  $\lambda = 0$  and  $\lambda = 1$  for the full model (red, blue) and the EFT (orange, green). In the lower part of these plots the difference in cross section from the SM normalized to the SM  $((\sigma - \sigma_{SM})/\sigma_{SM})$  is shown to illustrate the relative deviation from the SM. In the  $\lambda = 0$  case the EFT can describe the full model up to  $\sqrt{s} \approx 1$  TeV and in the  $\lambda = 1$  case up to  $\sqrt{s} \approx 0.75$  TeV. For both cases this means that the EFT can reproduce the full model up to masses of 1.5 times the lightest fermion. For these invariant masses the deviations from the SM are of the order of 5% or smaller, which makes seeing any deviation there close to impossible.

In order to see a sizable deviation one can go to the right side of the figures (b), where the cases of  $m = 1100$  GeV and  $J = 4$  for  $\lambda = 0$  and  $\lambda = 3$  are depicted, again for the full model (red, blue) and the EFT (orange, green). Starting with  $W^+W^+ \rightarrow W^+W^+$  and  $\lambda = 0$  one can find a good agreement between the EFT and the model up to the threshold for pair production of  $\sqrt{s} \approx 2.2$  TeV. This is a better agreement than in the lower mass case. For the  $\lambda = 3$  case however one finds, that the EFT gives no increase in cross section up to  $\sqrt{s} \approx 2.5$  TeV and is therefore unable to reproduce the full model anywhere. In order to understand this one can look at the polarized cross sections which will be done in section 5.5.1.4.

For the  $W^+W^- \rightarrow W^+W^-$  cross section for  $\lambda = 0$  one finds a good agreement up to  $\sqrt{s} = 1.5m$  between the EFT and the full model. Still in this region the deviation from the SM is only a few percent. For the  $\lambda = 3$  case one finds again no region where the EFT is a good approximation of the full model. As a summary one can say

- For  $\lambda = 0$  and  $\lambda = 1$  one can achieve a good agreement between the EFT and the full model up to about  $\sqrt{s} = 1.5m$
- For  $\lambda = 3$  one finds no region above  $\sqrt{s} = 0.6$  TeV where the full model is well described by the EFT

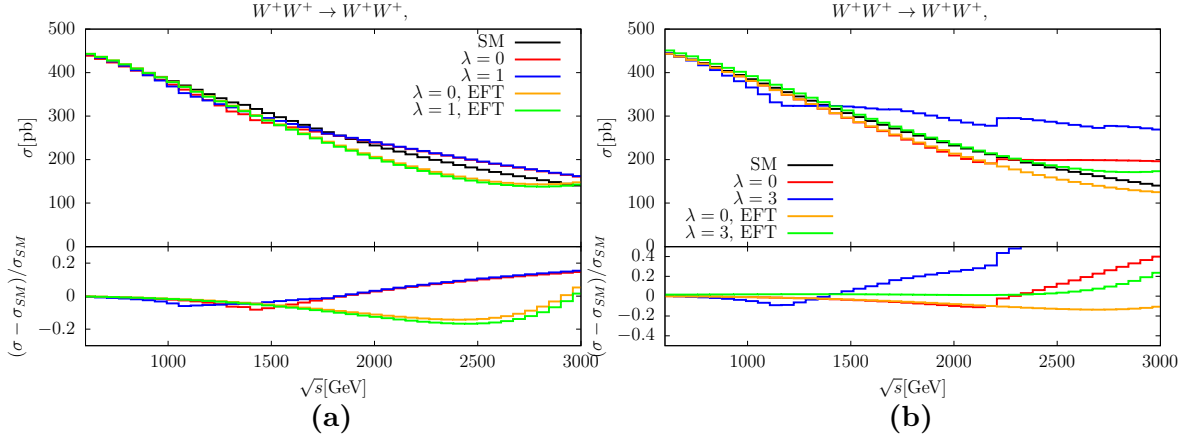


**Figure 5.19.:** Cross section of the full model (red, blue) and the EFT (yellow, green) for  $m = 700$  GeV,  $J = 3$  and  $\lambda = 0, 1$  (5.19a) and for  $m = 1100$  GeV,  $J = 4$  and  $\lambda = 0, 3$  (5.19b) for  $W^+W^+ \rightarrow W^+W^+$  for different invariant masses of the vector boson pair. The lower part shows the difference from the SM distribution normalized by the SM.

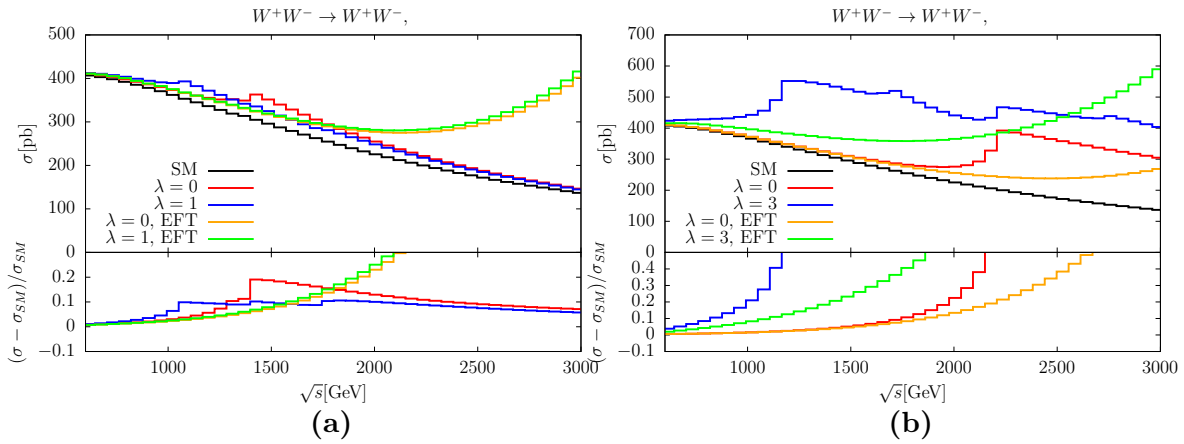


**Figure 5.20.:** Cross section of the full model (red, blue) and the EFT (yellow, green) for  $m = 700$  GeV,  $J = 3$  and  $\lambda = 0, 1$  (5.20a) and for  $m = 1100$  GeV,  $J = 4$  and  $\lambda = 0, 3$  (5.20b) for  $W^+W^- \rightarrow W^+W^-$  for different invariant masses of the vector boson pair. The lower part shows the difference from the SM distribution normalized by the SM.

### 5.5.1.4. Polarized Cross Sections

In order to further investigate which features of the model for larger values of  $\lambda$  can be modeled by the EFT and which can't one can study polarized cross sections. For this purpose the difference between the cross section of the full model (a) or the EFT (b) and the SM is shown in figures 5.21 and 5.22 as well as C.13-C.15. The cross sections of only transversely polarized particles (red), two transverse and two longitudinal particles (blue), four longitudinal particles (orange) and the remaining possible polarizations (green) can be found in each plot. In the lower parts of the plots the ratio between the difference of the full model and the EFT as a fraction of the difference between the model and the SM

$$\frac{\sigma_{BSM} - \sigma_{EFT}}{\sigma_{BSM} - \sigma_{SM}} = 1 - \frac{\sigma_{EFT} - \sigma_{SM}}{\sigma_{BSM} - \sigma_{SM}}, \quad (5.43)$$

are shown. Values above one imply different interference patterns with the SM, values between zero and one represent stronger deviations from the SM in the full model and negative values represent stronger deviations for the EFT. As larger deviations from the SM make it easier to understand their structure, only the point  $m = 1.1$  TeV,  $J = 4$ ,  $\lambda = 3$  is investigated.

Starting with the process  $W^+W^+ \rightarrow W^+W^+$  in figure 5.21 one can find a slowly increasing purely longitudinal component (orange) that, for small values of  $\sqrt{s}$ , is counteracted by a purely transverse component (red). For the purely transverse component one finds two thresholds around  $\sqrt{s} = 2(m - \frac{3\hat{v}}{\sqrt{2}}) \approx 1.15$  TeV and  $\sqrt{s} = 2m = 2.2$  TeV, which stem from the production of two on-shell fermions of the same multiplet. For the mixed component (blue) one also finds two threshold regions in this plot, one at  $\sqrt{s} = (2m - \frac{3\hat{v}}{\sqrt{2}}) \approx 1.70$  TeV and one at  $\sqrt{s} = 2m = 2.2$  TeV. The first threshold can be attributed to the production of one light and one medium on-shell fermion in the loops while the origin of the second threshold is less clear, as it can come from two medium fermions or one heavy and one light. As there is no visible threshold behavior at twice the light mass for the TTLL case, there is good reason to believe that there is also no such behavior stemming from two medium fermions being on-shell. For the comparison with the EFT of the purely transverse component one finds a ratio close to 1 for most of the available values of  $\sqrt{s}$ , the only exception being around  $\sqrt{s} = 1.5$  TeV where  $\sigma_{BSM} - \sigma_{SM}$  becomes zero. For the mixed contributions one can ignore the region before  $\sqrt{s} = 1.6$  TeV as there is close to no contribution from either the model or the EFT. For larger energies the approximation is somewhat good but again not capturing the threshold behavior. For the purely longitudinal contribution one can find good agreement up to  $\sqrt{s} = 2.5$  TeV. From this perspective it also becomes clear why the total EFT contribution almost vanishes up to  $\sqrt{s} = 2.0$  TeV as the TTTT and LLLL contributions cancel each other out.

For the scattering of opposite sign W bosons,  $W^+W^- \rightarrow W^+W^-$  in figure 5.22 one finds the same general behavior in the threshold regions, this time with constructive interference between the full model and the SM in the TTTT channel. For the mixed contribution one can already find sizable contributions around the production threshold of two light fermions. This excess can partially be explained as an onset of the threshold behavior at  $\sqrt{s} = (2m - \frac{3\hat{v}}{\sqrt{2}}) \approx 1.70$  TeV but not completely, as there seems to be a slight bump at  $\sqrt{s} = 1.2$  GeV. Comparing the full model with the EFT one again finds an abysmal description in the TTTT channel and somewhat of

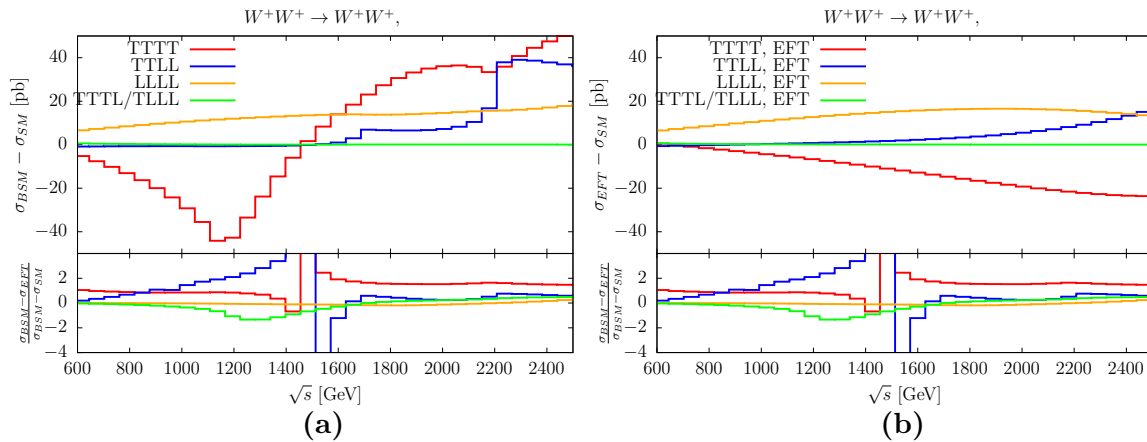


**Figure 5.21.:** Polarized cross section of the full model (5.21a) and the EFT (5.21b) for  $m = 1100$  GeV,  $J = 4$  and  $\lambda = 3$  for  $W^+W^+ \rightarrow W^+W^+$  for different invariant masses of the vector boson pair. The purely transverse (red), the mixed (TTLL, blue), purely longitudinal (yellow) and the remaining (green) contributions are shown. The lower part shows the difference between the full model and the EFT normalized by the difference of the full model from SM.

a fine description in the TTLL and LLLL channels up to  $\sqrt{s} = 1.2$  GeV. Coming back to the different behavior of TTLL for same sign and opposite sign W boson scattering, one can further investigate the Feynman diagrams in which two internal fermions can become on-shell at the same time, in order to see where this behavior can come from. For the same sign case one has a contribution to the four particle vertex and contributions to the t- and u-channel exchange of Z or higgs bosons. With t and u being negative there is no production threshold in these diagrams, leaving only four boson vertex. For the opposite sign case one has an s-channel higgs and Z exchange, giving possible threshold behavior from both the three particles vertices and the propagators. In section 5.3 it was shown that the VVV vertex is only marginally affected by large values of  $\lambda$ , while in section 5.4 it was shown that the HVV vertex gains considerable contributions for large  $\lambda$ , giving rise to the operator  $\mathcal{O}_{HW}$ . This operator increases the coupling of two transverse vector bosons to the higgs boson, which then can decay into two longitudinal vector bosons, thus giving rise to TTLL contributions around the  $\sqrt{s} = 2(m - \frac{3\hat{v}}{\sqrt{2}}) \approx 1.15$  TeV threshold. When pushing the limits one might try to make the TTLL contribution dominant by decreasing  $J$  while increasing  $\lambda$  at the same time. While this would work for VBS one would run into huge trouble in the higgs sector by exceeding the EFT bounds there.

Lastly the abysmal description of purely transverse scattering needs an explanation as for  $\lambda = 0$  and  $\lambda = 1$  it is at least working up to  $\sqrt{s} = 1.5m$ . For this one can look at the coefficients of the T-operators which are mainly responsible for this behavior. As they are dimension 8 operators and contain no higgs field their coefficients do not depend on  $\lambda$ . Therefore their contribution tries to match the onset of the threshold at  $\sqrt{s} = 2m$  but not the one at  $\sqrt{s} = 2(m - \frac{\lambda\hat{v}}{\sqrt{2}})$ . This problem can also be understood by using a different parameterization of the model. Instead of using  $m$  and  $\lambda$  one can use  $m_{new} = m - \frac{\lambda\hat{v}}{\sqrt{2}}$  and  $\lambda$ . With this parameterization the position of the first threshold stays unchanged with increasing  $\lambda$  and the coefficients of the T-operators would be proportional to  $\frac{1}{m_{new}^4}$  instead of  $\frac{1}{m^4}$ . This results in  $\frac{m^4}{m_{new}^4} \approx 16$  times larger

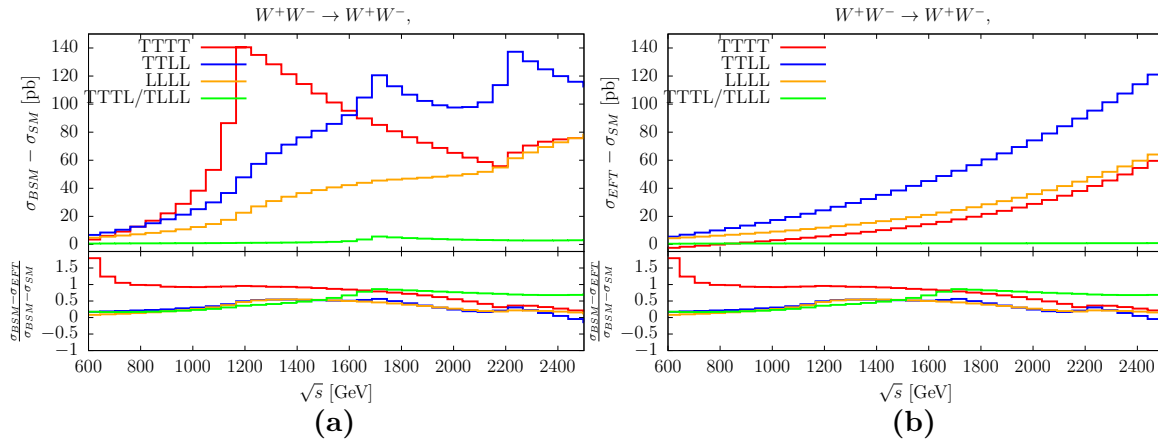


**Figure 5.22.:** Polarized cross section of the full model (5.22a) and the EFT (5.22b) for  $m = 1100$  GeV,  $J = 4$  and  $\lambda = 3$  for  $W^+W^- \rightarrow W^+W^-$  for different invariant masses of the vector boson pair. The purely transverse (red), the mixed (TTLL, blue), purely longitudinal (yellow) and the remaining (green) contributions are shown. The lower part shows the difference between the full model and the EFT normalized by the difference of the full model from SM.

T-operators while parameterizing the same model. As a result the TTTT channels would be better aligned but a different problem would be introduced. For this parameterization going to large values in the coupling is impossible when requiring  $\frac{\lambda\hat{v}}{\sqrt{2}} \ll m_{new}$ . This renders this solution worthless in our situation. Another solution would be the inclusion of additional factors of  $\frac{\lambda\hat{v}}{\sqrt{2}m}$  in the Wilson coefficient of the T-operators in order to parameterize the shift in the threshold position. This however would introduce terms that are suppressed by  $m^6$  and are therefore of the same size as possible dimension 10 operators leaving an inconsistency in the matching procedure to the EFT. With no direct solution in sight one can try to estimate how well a perfect solution would be able to reproduce the full model. From the  $\lambda = 0$  case in [19] one can make the statement that any solution would only be able to reproduce the full mode below the threshold and therefore only in a region where the deviation from the SM is relatively small compared to the deviation at the threshold.

In order to increase the relative contribution from mixed scattering, one might try to decrease the isospin in order to decrease the purely transverse contribution. In figure 5.23 this is shown for  $J = 3$  compared to the  $J = 4$  in figure 5.22. One can observe that both the purely transverse as well as the mixed contributions drastically decrease (by a factor of four in the peaks), while the purely longitudinal is decreased by roughly a factor of two. For this choice of parameters the LLLL channel is now the dominant helicity combination for all values of  $\sqrt{s}$  except around the first threshold. This factor of two implies that the amplitude is proportional to  $J$  which stems from the sum over the third component of the isospin. As vector bosons couple to fermions of the same multiplet proportional to  $J$ , one can assume that for purely longitudinal scattering, the BSM contribution stems either from vector bosons coupling to fermions of different multiplets or from corrections to the higgs graphs.

The last scenario that needs to be discussed is choosing one multiplet with  $J = 3$  and two multiplets with  $J = 3.5$  to start with. This results in one multiplet with nine states and two multiplets with seven states, or in terms of isospin, two multiplets that behave similarly to  $J = 3$  and one similar to  $J = 4$ . For this combination one

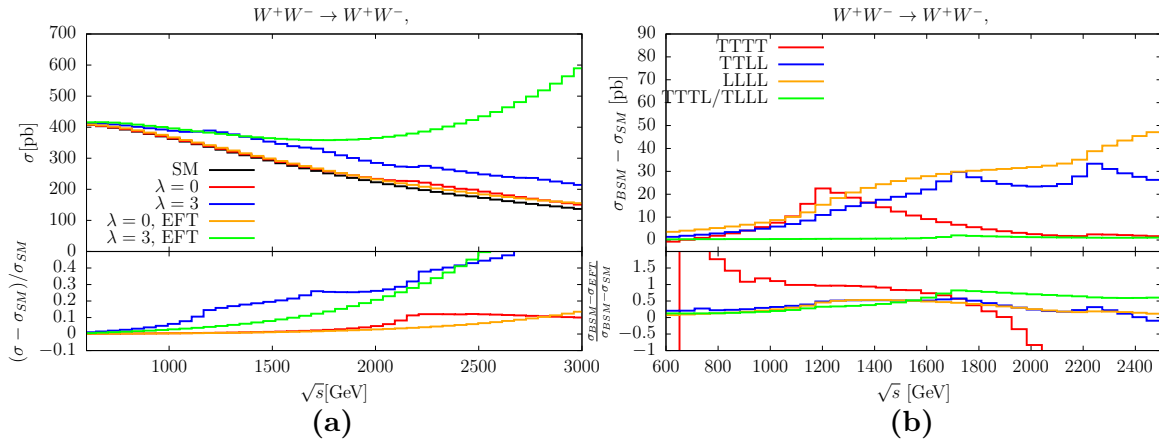


**Figure 5.23.:** 5.23a shows the cross sections of the full model (red, blue) and the EFT (yellow, green) for  $m = 1100$  GeV,  $J = 3$  and  $\lambda = 0, 3$  for  $W^+W^- \rightarrow W^+W^-$  for different invariant masses of the vector boson pair. The lower part shows the difference between the distributions and the SM distribution, normalized to the SM distribution. 5.23b shows the corresponding polarized cross sections for  $\lambda = 3$  for the purely transverse (red), the mixed (TTLL, blue), the purely longitudinal (yellow) and the remaining (green) contributions. The lower part shows the difference between the full model and the EFT normalized by the difference of the full model from SM.

would expect the contributions to be a mixture of the cases  $J = 4$  and  $J = 3$ , that were discussed beforehand. As the lightest multiplet has seven states the first peak for purely transverse scattering is expected to be closer to the  $J = 3$  case in figure 5.23. In contrast to the  $J = 3$  case one would expect a stronger second peak for purely transverse scattering (similar relative excess as the first peak in figure 5.22. For the mixed contributions one would expect a larger excess than in the  $J = 3$  case yet not as large as in the  $J = 4$  case. Altogether this leaves a model in which mixed scattering can be dominant around the peak at  $\sqrt{s} = 2m - \frac{\lambda \hat{v}}{\sqrt{2}}$  but not around the first peak of transverse scattering at  $\sqrt{s} = 2(m - \frac{\lambda \hat{v}}{\sqrt{2}})$ .

As a summary from the study of polarized cross sections one can make the following statements

- The EFT is not able to reproduce the shift of the production threshold for two of the light fermions due to increasing  $\lambda$  for TTTT.
- The EFT can describe both, purely longitudinal and mixed scattering, quite well up to  $\sqrt{s} = 1.5m$
- Even though the TTLL contribution can be the dominant one in the EFT (and therefore suggest dominant M-operators), the full model is dominated by the TTTT channel until after the first threshold at  $\sqrt{s} = 2(m - \frac{\lambda \hat{v}}{\sqrt{2}})$  (at least for reasonable values of  $\lambda$ ). For  $gJ < \lambda$  the whole distribution can become dominated by the purely longitudinal contribution.

## 5.6. Higgs Pair Production From Two Vector Bosons

For the higgs pair production from two vector bosons we will study the process  $W^+W^- \rightarrow hh$  which, in the SU(2) limit, gives identical results for the model as the other possible process  $ZZ \rightarrow hh$ . In figure 5.24 the isospin dependence of the cross section for  $m = 700$  GeV and  $\lambda = 1$  (a) and for  $m = 1100$  GeV and  $\lambda = 3$  (b) is shown. In the bottom figure (c) the  $\lambda$  dependence of the cross section is shown for  $m = 1100$  GeV and  $J = 4$ . For the isospin dependence one finds a factor of roughly two between the  $J = 3$  and  $J = 4$  cases. For the  $\lambda$  dependence one finds a factor of about five between the cross sections in their peaks. This aligns well with the expected  $\lambda^4$  dependence, which stem from two couplings to the higgs boson and the squaring of the amplitude. For the threshold at  $\sqrt{s} = 2(m - \frac{\lambda \hat{v}}{\sqrt{2}})$  one finds the strongest rise of the cross section at this point while the peak of the cross section is reached at slightly larger energies. This behavior is consistent with the threshold behavior of  $ZZ \rightarrow ZZ$  in figure 5.12a, which also has a comparatively small SM contribution. Comparing the additional cross section due to the BSM model in the TLL and LLL channels for  $VV \rightarrow VV$  one finds less excess than in  $VV \rightarrow hh$  which becomes even more prominent when considering  $J = 3$  and  $\lambda = 3$ . Additionally the mixed excess in the  $VV \rightarrow VV$  processes is mostly linked to the thresholds at  $\sqrt{s} = 2m - \frac{\lambda \hat{v}}{\sqrt{2}}$  and  $\sqrt{s} = 2m$  while the excess in the  $VV \rightarrow hh$  processes is tied to the threshold at  $\sqrt{s} = 2(m - \frac{\lambda \hat{v}}{\sqrt{2}})$ . As a result  $VV \rightarrow hh$  is a strong contender when searching for models with additional fermions with smaller isospin  $J \leq 3$  and large couplings  $\lambda \gg gJ$  to the higgs field.

### 5.6.1. Implications for LHC Searches

As a summary we will discuss which processes can give the first signs of the proposed model depending on the choice of the parameters. For all discussed isospins and couplings to the higgs boson, a mass for the lightest multiplet of around  $m \sim 700$  GeV was proposed. Going significantly lower drastically limits the possible values of the isospin due to the quite strong bounds in the dilepton final states (section 5.1 and [52]). At the same time masses above  $m = 1.2$  TeV for the lightest multiplet would require quite a large isospin or coupling in order to produce any significant excess in the currently experimentally accessible  $m_{ll}$  [52],  $m_{VV}$  [4] and  $m_{hh}$  [59, 2] regions. For the parameter choice  $g \cdot J \gg \lambda$  the main constraints come from the dilepton production (section 5.1) and VBS (section 5.5.1). For  $m = 700$  GeV the constraints on dilepton production require  $J \leq 3$  which results in only 10 – 20% deviation in the VBS channels, making the dilepton channel the most prominent channel to find this model. This marks a deviation from the case of only one multiplet in [19] for which  $J = 4$  is still possible. This larger isospin made VBS, due to the  $J^5$  scaling of the amplitude, a strong contender for finding this kind of model. Vector boson pair production from  $q\bar{q}$  annihilation plays no significant role when looking for additional fermions with large isospin due to destructive interference between different contributions (section 5.3).

For  $g \cdot J \sim \lambda$  the deviations in the invariant mass distributions split up due to the mass splitting between the different multiplets. This results in  $J = 4$  still being somewhat fine with the dilepton production analysis, which then results in a similar excess for VBS compared to [19]. In addition to these channels the contributions to anomalous higgs couplings and the higgs boson pair production become sizable.

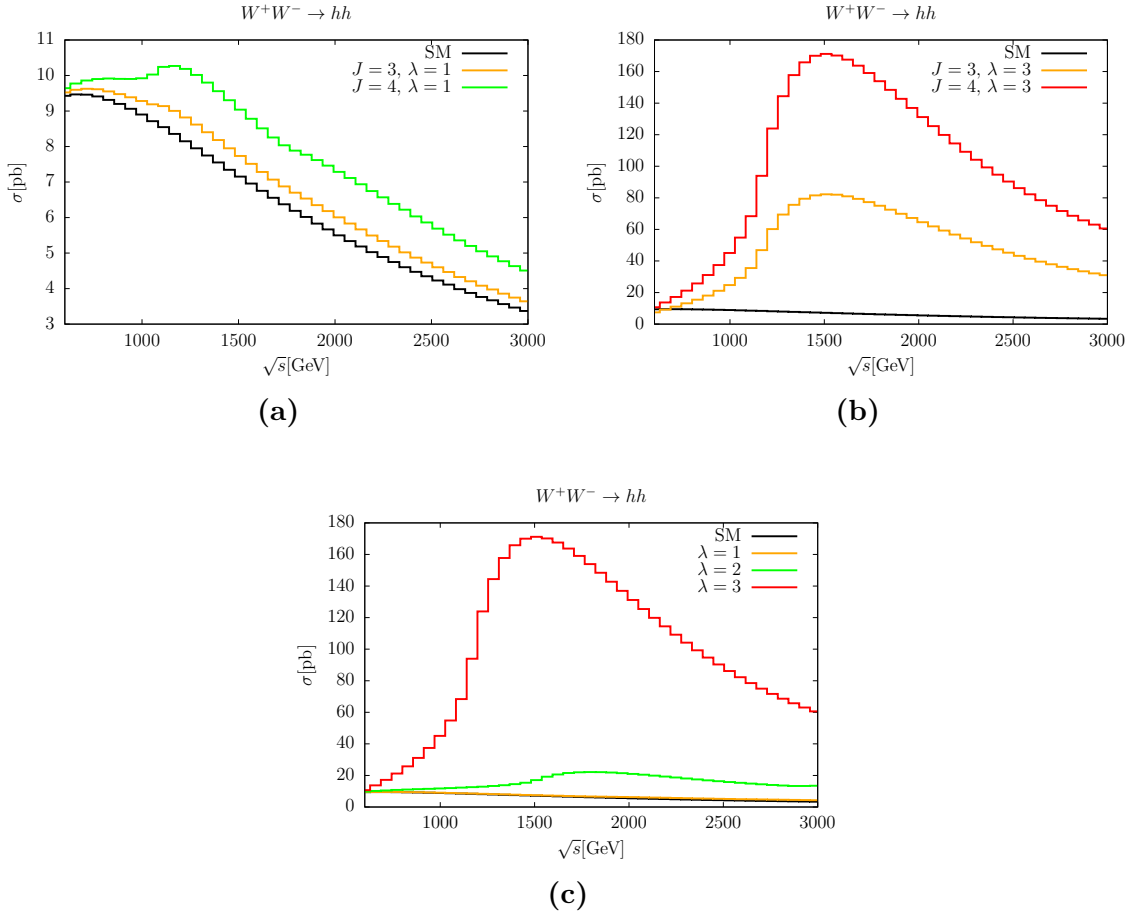


**Figure 5.24.:** Cross section of the full model for  $m = 700$  GeV and  $\lambda = 1$  (5.24a), for  $m = 1100$  GeV and  $\lambda = 3$  (5.24b) and for  $m = 1100$  GeV and  $J = 4$  (5.24c) for  $W^+W^- \rightarrow hh$  for different invariant masses of the vector boson pair. In 5.24a and 5.24b  $J = 3$  (yellow) and  $J = 4$  (red/green) are shown alongside the SM (black). In 5.24c the coupling  $\lambda$  is varied (1: yellow, 2: green, 3: red).

As two higgs bosons tend to be the more challenging final state compared to two vector bosons (especially due to the access to fully- and semi-leptonic final states) one would still expect VBS to be a more relevant channel compared to higgs boson pair production. Searches for anomalous higgs couplings can prove to be a powerful tool when looking for large values of  $\lambda$ , as has been shown in section 5.4, and are expected to see this kind of model at a similar time as dilepton production and VBS for  $gJ \sim \lambda$ .

Lastly the region  $g \cdot J < \lambda$  was only briefly mentioned in section 5.5.1 as it is of less interest for this study. For these parameters the new fermions mainly couple to the higgs boson and effects in VBS come mostly from longitudinal scattering. This kind of signature can also be achieved by other models that generate these kind of contributions already at leading order, e.g. an extended higgs sector.

## 6. Conclusions

The goal of this thesis is studying BSM models that are capable of producing sizable M-operators of the Éboli basis in its EFT. For this purpose the class of models that introduce new, heavy, non-chiral fermions, that couple to vector bosons and the higgs field are studied. By requiring the isospin of the new fermions to be larger than one, coupling to the SM fermions is prohibited, which implies that effects on SM processes can only be seen at the one loop level in the BSM model. As coupling to the higgs field changes the isospin of the fermions at least two fermionic multiplets are needed. These multiplets then mix due to the interaction with the higgs field, which is shown to introduce a mass splitting between and within the multiplets, depending on the parameters. As stable charged fermions would be directly detectable at the LHC all charged particles are required to be able to decay, leaving only neutral stable particles. This requirement is shown to be fulfilled by three multiplets with isospins and hypercharges of  $J, 0$ ,  $J \pm \frac{1}{2}, \pm \frac{1}{2}$  and  $J \pm \frac{1}{2}, \mp \frac{1}{2}$  where the latter two have the same mass. As  $J \gg Y$  is considered for this class of models, it is argued that the coupling to the photon can be omitted. This leads to most calculations being done in the SU(2)-limit ( $g' \rightarrow 0$ ). A quick analysis of extensions to this model was done and it was concluded that CP conserving alterations of the presented model (more/less multiplets, different masses) would either produce a similar phenomenology or charged stable particles. Therefore the most simple implementation of this model, with identical masses for the three multiplets and identical couplings to the higgs field, was deemed sufficient for further analyses.

In order to study the effects of this model the one loop contributions of new fermions to propagators, three particles vertices and four particle vertices were calculated, depending on the remaining three parameters of the model: the mass of the multiplets  $m$ , the isospin of the single multiplet  $J$  and the coupling of the fermions to the higgs field  $\lambda$ . For further implementation the one loop contributions were renormalized on-shell.

For the comparison with its EFT a complete set of operators at dimension 6 and dimension 8 was required. The existing complete sets of operators rely on equations of motion in order to reduce the number of operators and to make sure no redundancies appear. These equations of motion however have been shown to push effects from the sector where the coupling happens (in this case the vector boson and higgs sector) to sectors that shouldn't be affected by the model (in this case the fermionic sector). In order to avoid this issue, a dedicated basis was constructed. While constructing this set of operators, it was shown, that this set is indeed complete and that no redundancies occur. The coefficients for the different operators were then calculated by expanding the one loop n-point functions of the model in terms of  $\frac{p_i p_j}{m^2}$  and  $\frac{\lambda^2 \hat{v}^2}{m^2}$ , and comparing them to the n-point functions of the EFT operators.

For further analyses two sets of parameter points, one for  $g \cdot J \gg \lambda$  and one for  $g \cdot J \sim \lambda$ , were chosen such that contributions from the new fermions are on the edge of what is experimentally allowed in the  $pp \rightarrow V \rightarrow l\bar{l}$  channel. For these sets of parameters the impact on anomalous triple gauge couplings and anomalous higgs couplings was studied, finding little impact on the former and substantial impact on the latter for the case of  $g \cdot J \sim \lambda$ .

For on-shell vector boson scattering it was found that for three multiplets  $J = 4$  is required in order to make VBS a competitive channel when searching for this type of model as  $J = 3$  would only yield 10 – 20% deviation from the SM. For  $g \cdot J \gg \lambda$  the VBS cross sections showed only little difference in shape compared to the  $\lambda = 0$ . This implies that for  $g \cdot J \gg \lambda$  the model can be approximated by three non interacting multiplets with slightly shifted masses.

In the region  $g \cdot J \sim \lambda$  analyzing the different polarized cross sections showed, that the model is still dominated by purely transverse scattering until after the pair production threshold of two fermions of the lightest multiplet. For larger energies the mixed contributions (two longitudinal and two transverse vector bosons) and the purely longitudinal contributions have been shown to be the most important ones. Lastly when going to  $g \cdot J < \lambda$  it was shown that purely longitudinal scattering becomes the dominant contribution. As mixed and purely longitudinal scattering become more important, it was shown that also on-shell higgs boson pair production gets a larger contribution from the proposed model, making it a strong contender when searching in the parameter region  $g \cdot J \leq \lambda$ .

The comparison with the EFT showed that the EFT hardly ever is a good description of the model. For  $g \cdot J \gg \lambda$  the EFT can capture effects up to roughly  $\sqrt{s} \sim 1.5m$ . As effects in this region are only of the order of 5 – 10% compared to up to 100% around  $\sqrt{s} \sim 2m$  one would expect first signs of this model in the threshold region and not the lead up to it. For  $g \cdot J \sim \lambda$  the EFT does a good job capturing the purely longitudinal and mixed contributions but does worse for the purely transverse part. Even though the M-operators can become the dominant dimension 8 contribution one has to take into account that purely transverse scattering is still dominant in the full model and that dimension 6 operators play a significant role for this choice of parameters. This leads to the conclusion that M-operators never show first hints for this class of models as they never parameterize the dominant contribution of the model in the region of  $\sqrt{s}$  where one would expect first signs for this class of models. As this class of models captures most models that are capable of producing dominant M-operators, this result questions searching for M-operators altogether.

Additionally significant destructive interference within the set of operators, that are complete under the presented transformations, to which the M-operators belong, was found. This again stresses the importance of multi operator searches. At the same time it limits the importance of bounds on dimension-8 Wilson coefficients, stemming from searches using incomplete sets of operators or single operators.

Lastly addressing the prospect of EFT searches for this class of models one has to admit that the EFT is quite a bad description of the model overall. Instead of using an EFT, when searching for this class of models in VBS for  $g \cdot J \gg \lambda$ , one could search for the first threshold using the model for  $\lambda = 0$  utilizing the position of the threshold ( $2m$ ) and an effective isospin (to account for mixing of multiplets) as a parameterization. For  $g \cdot J \sim \lambda$  one would expect effects in higgs pair production, VBS, anomalous higgs couplings and dilepton production at the same time making a multiprocess analysis of the full model for  $g \cdot J = \lambda$  a possible way forward. For

---

$g \cdot J \ll \lambda$  one would expect first signs of this model in higgs observables rather than VBS.



# Appendix

## A. Coefficient Functions for Passarino-Veltman-Reduction

In the equations (A.1)-(A.11) the decomposition of the one loop tensor functions in terms of momenta, metric tensors and scalar coefficients is shown.

$$B_\mu = p_{1\mu} B_1 \quad (\text{A.1})$$

$$B_{\mu\nu} = g_{\mu\nu} B_{00} + p_{1\mu} p_{1\nu} B_{11} \quad (\text{A.2})$$

$$C_\mu = \sum_{i=1}^2 p_{i\mu} C_i \quad (\text{A.3})$$

$$C_{\mu\nu} = g_{\mu\nu} C_{00} + \sum_{i,j=1}^2 p_{i\mu} p_{j\nu} C_{ij} \quad (\text{A.4})$$

$$C_{\mu\nu\rho} = \sum_{i=1}^2 (g_{\mu\nu} p_{i\rho} + g_{\nu\rho} p_{i\mu} + g_{\rho\mu} p_{i\nu}) C_{00i} + \sum_{i,j,k=1}^2 p_{i\mu} p_{j\nu} p_{k\rho} C_{ijk} \quad (\text{A.5})$$

$$D_\mu = \sum_{i=1}^3 p_{i\mu} D_i \quad (\text{A.6})$$

$$D_{\mu\nu} = g_{\mu\nu} D_{00} + \sum_{i,j=1}^3 p_{i\mu} p_{j\nu} D_{ij} \quad (\text{A.7})$$

$$D_{\mu\nu\rho} = \sum_{i=1}^3 (g_{\mu\nu} p_{i\rho} + g_{\nu\rho} p_{i\mu} + g_{\rho\mu} p_{i\nu}) D_{00i} + \sum_{i,j,k=1}^3 p_{i\mu} p_{j\nu} p_{k\rho} D_{ijk} \quad (\text{A.8})$$

$$D_{\mu\nu\rho\sigma} = (g_{\mu\nu} g_{\rho\sigma} + g_{\mu\rho} g_{\nu\sigma} + g_{\mu\sigma} g_{\rho\nu}) D_{0000} + \sum_{i,j,k,l=1}^3 p_{i\mu} p_{j\nu} p_{k\rho} p_{l\sigma} D_{ijkl} \quad (\text{A.9})$$

$$+ \sum_{i,j=1}^3 (g_{\mu\nu} p_{i\rho} p_{j\sigma} + g_{\mu\rho} p_{i\nu} p_{j\sigma} + g_{\mu\sigma} p_{i\rho} p_{j\nu} + g_{\nu\rho} p_{i\mu} p_{j\sigma} \quad (\text{A.10})$$

$$+ g_{\nu\sigma} p_{i\rho} p_{j\mu} + g_{\rho\sigma} p_{i\mu} p_{j\nu}) D_{00ij} \quad (\text{A.11})$$

## B. Counterterms for the Renormalization of the EFT

The counterterms for the EFT in terms of  $\lambda$ ,  $J$  and  $m$  read

$$\begin{aligned} \delta_{Z_v} = & -\frac{(2J+1)\lambda^2(3\log(\frac{\mu^2}{m^2}) + \frac{3}{\epsilon} - 2)}{24\pi^2} \\ & -\frac{J^2(2J+1)m_W^2g^2}{60\pi^2m^2} - \frac{(2J+1)(J-2)\hat{v}^2\lambda^4}{240J\pi^2m^2} \\ & -\frac{J^2(2J+1)g^2m_W^4}{280\pi^2m^4} - \frac{\lambda^2(2J+1)(224J^2m_W^4 + 112Jm_W^4 - 79m_W^4)}{3360\pi^2m^4} \\ & + \frac{(2J+1)\lambda^6\hat{v}^4(4J+1)}{13440\pi^2Jm^4} \end{aligned} \quad (\text{B.1})$$

$$\begin{aligned} \delta_{Z_W} = & -\frac{g^2J^2(2J+1)(\log(\frac{\mu^2}{m^2}) + \frac{1}{\epsilon})}{12\pi^2} \\ & -\frac{g^2J^2(2J+1)m_W^2}{30\pi^2m^2} - \frac{g^2\lambda^2\hat{v}^2(2J+1)(80J^2 + 40J - 43)}{2880\pi^2m^2} \\ & -\frac{3g^2J^2(2J+1)m_W^4}{560\pi^2m^4} - \frac{g^2\lambda^2\hat{v}^2m_W^2(2J+1)(224J^2 + 112J - 79)}{6720\pi^2m^4} \\ & -\frac{g^2\lambda^4\hat{v}^4(2J+1)(140J^3 + 70J^2 - 85J + 24)}{20160\pi^2Jm^4} \end{aligned} \quad (\text{B.2})$$

$$\begin{aligned} \delta_{Z_h} = & -\frac{(2j+1)\lambda^2(3\log(\frac{\mu^2}{m^2}) + \frac{3}{\epsilon} - 2)}{24\pi^2} \\ & -\frac{(2J+1)\lambda^2m_W^2}{40\pi^2m^2} - \frac{(2J+1)\lambda^4\hat{v}^2}{16\pi^2m^2} \\ & -\frac{3(2J+1)\lambda^2m_W^4}{1120\pi^2m^4} - \frac{3(2J+1)\lambda^4\hat{v}^2m_W^2}{80\pi^2m^4} - \frac{(2J+1)\lambda^6\hat{v}^4}{64\pi^2m^4} \end{aligned} \quad (\text{B.3})$$

$$\begin{aligned} \delta_{\lambda_h} = & \frac{(2J+1)\lambda^2\hat{v}^2m_h^2(3\log(\frac{\mu^2}{m^2}) + \frac{3}{\epsilon} - 2)}{24\pi^2\hat{v}^4} - \frac{(2J+1)\lambda^4\hat{v}^4(3\log(\frac{\mu^2}{m^2}) + \frac{3}{\epsilon} - 8)}{24\pi^2\hat{v}^4} \\ & + \frac{J^2(2J+1)m_W^4m_h^2}{30\pi^2m^2\hat{v}^4} + \frac{(2J+1)\lambda^2\hat{v}^2m_h^4}{160\pi^2m^2\hat{v}^4} + \frac{(2J+1)\lambda^4\hat{v}^4m_h^2(16J-2)}{480\pi^2m^2J\hat{v}^4} - \frac{(2J+1)\lambda^6\hat{v}^6}{80\pi^2m^2\hat{v}^4} \\ & + \frac{J^2(2J+1)m_h^2m_W^6}{140\pi^2m^4\hat{v}^4} + \frac{(2J+1)\lambda^2\hat{v}^2(224J^2m_h^2m_W^4 + 112Jm_h^2m_W^4 - 79m_h^2m_W^4 + 3m_h^6)}{6720\pi^2m^4\hat{v}^4} \\ & + \frac{3(2J+1)\lambda^4\hat{v}^4m_h^4}{320\pi^2m^4\hat{v}^4} + \frac{(2J+1)\lambda^6\hat{v}^6m_h^2(206J-1)}{26880\pi^2m^4\hat{v}^4} - \frac{3(2J+1)\lambda^8\hat{v}^8}{2240\pi^2m^4\hat{v}^4} \end{aligned} \quad (\text{B.4})$$

$$\begin{aligned} \delta_{\mu^2} = & -\frac{(2J+1)\lambda^2m^2(3\log(\frac{\mu^2}{m^2}) + \frac{3}{\epsilon} + 1)}{4\pi^2} \\ & -\frac{(2J+1)\lambda^2m_h^4}{160\pi^2m^2} - \frac{(2J+1)\lambda^4\hat{v}^2m_h^2}{32\pi^2m^2} + \frac{(2J+1)\lambda^6\hat{v}^4}{160\pi^2m^2} \\ & -\frac{(2J+1)\lambda^2m_h^6}{2240\pi^2m^4} - \frac{3(2J+1)\lambda^4\hat{v}^2m_h^4}{320\pi^2m^4} - \frac{(2J+1)\lambda^6\hat{v}^4m_h^2}{2240\pi^2m^4} + \frac{(2J+1)\lambda^8\hat{v}^6}{1120\pi^2m^4} \end{aligned} \quad (\text{B.5})$$

## C. VBS Plots for $W^+W^- \rightarrow ZZ$ , $W^+Z \rightarrow W^+Z$ and $ZZ \rightarrow ZZ$

As  $W^+W^- \rightarrow ZZ$ ,  $W^+Z \rightarrow W^+Z$  and  $ZZ \rightarrow ZZ$  do not add significant insight the corresponding plots to the ones shown in 5.5.1 are shown in this section.

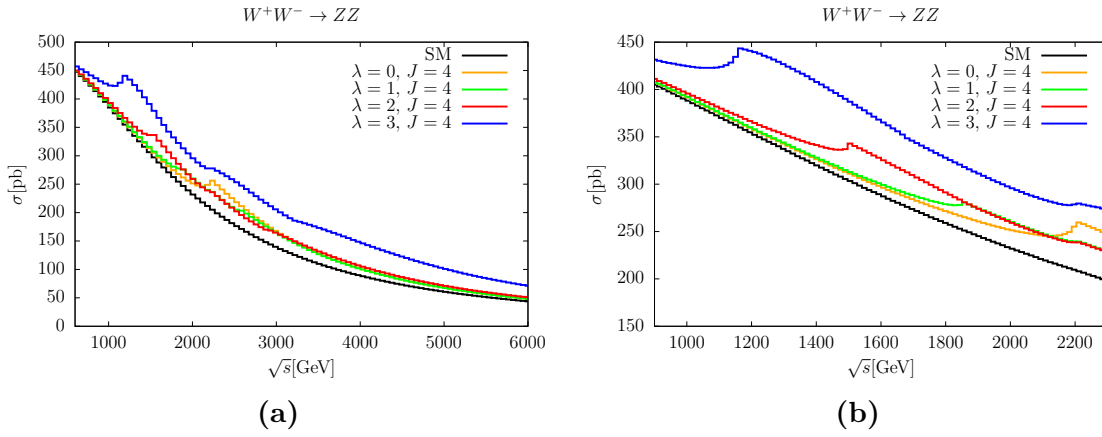


**Figure C.1.:** Cross section of the full model with  $m = 1100$  GeV for  $W^+W^- \rightarrow ZZ$  for different invariant masses of the vector boson pair. C.1b provides a closer look at the threshold region. The SM distribution (black) and the full model distributions for  $J = 4$  and  $\lambda = 0, 1, 2, 3$  (yellow, green, red, blue) are shown.

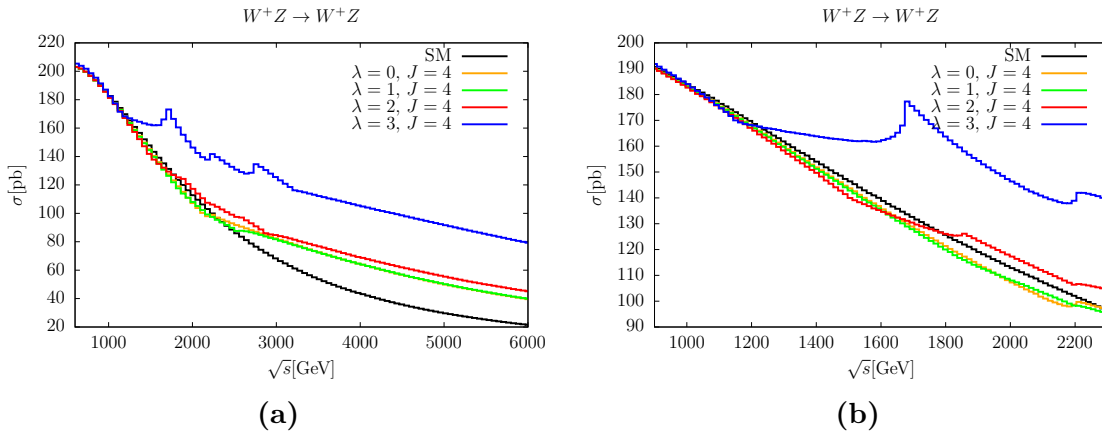


**Figure C.2.:** Cross section of the full model with  $m = 1100$  GeV for  $W^+Z \rightarrow W^+Z$  for different invariant masses of the vector boson pair. C.2b provides a closer look at the threshold region. The SM distribution (black) and the full model distributions for  $J = 4$  and  $\lambda = 0, 1, 2, 3$  (yellow, green, red, blue) are shown.

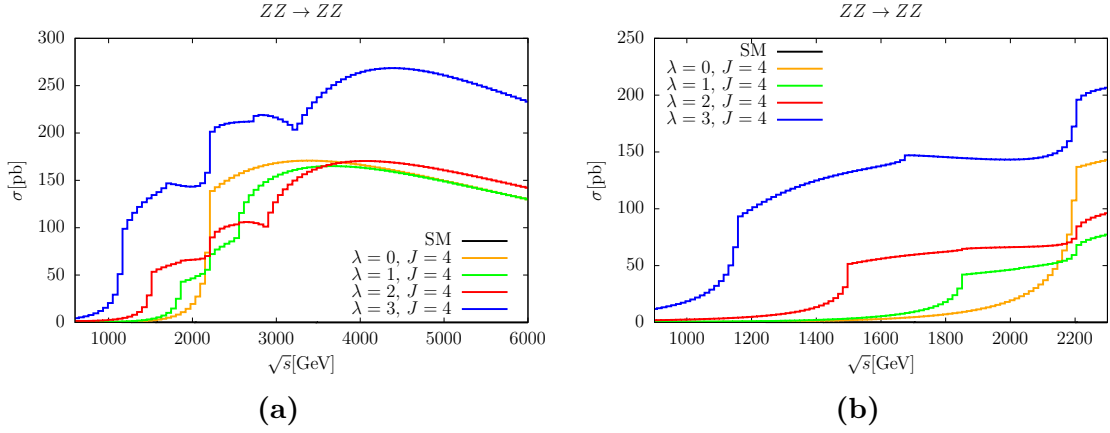


**Figure C.3.:** Cross section of the full model with  $m = 1100$  GeV for  $ZZ \rightarrow ZZ$  for different invariant masses of the vector boson pair. C.3b provides a closer look at the threshold region. The SM distribution (black) and the full model distributions for  $J = 4$  and  $\lambda = 0, 1, 2, 3$  (yellow, green, red, blue) are shown.

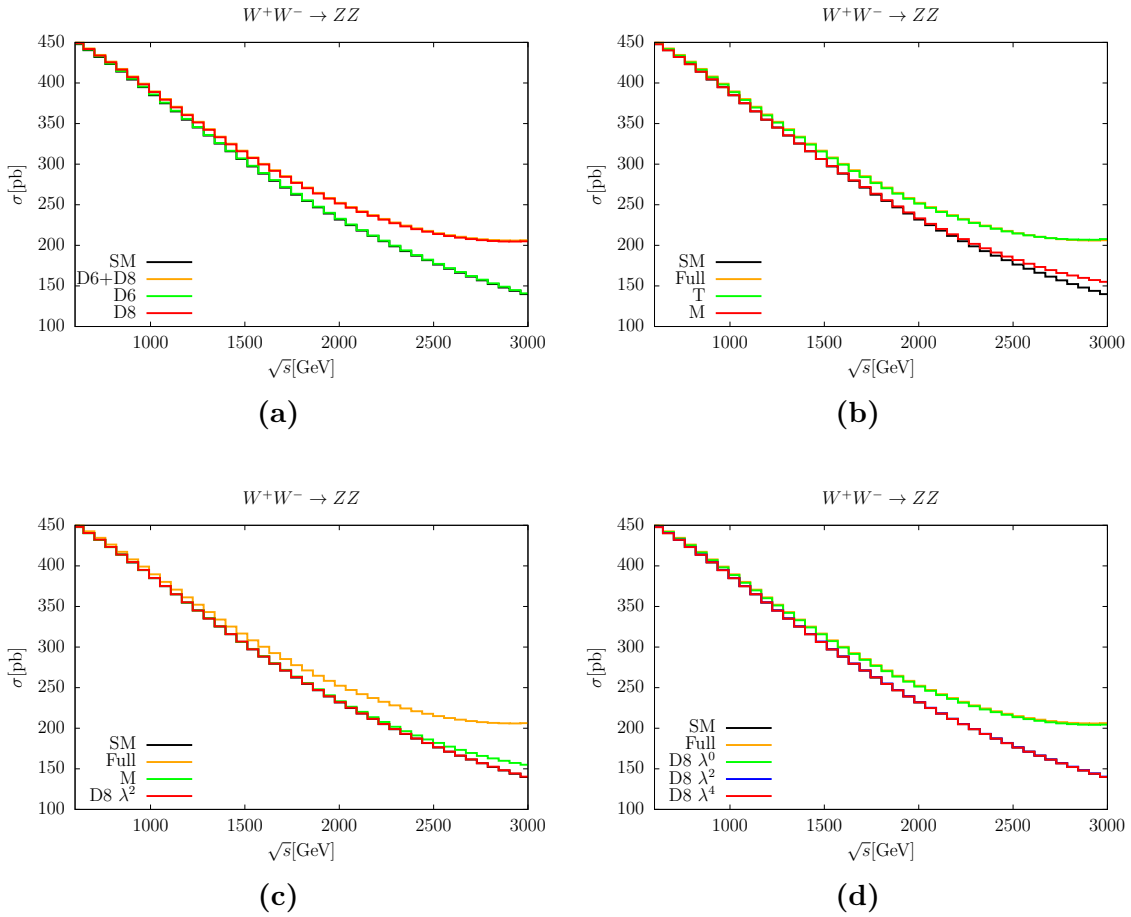


**Figure C.4.:** Cross section of the EFT for  $m = 700$  GeV,  $J = 3$  and  $\lambda = 1$  for  $W^+W^- \rightarrow ZZ$  for different invariant masses of the vector boson pair. C.4a shows the SM (black) the full EFT (yellow) the dimension 6 (green) and the dimension 8 (red) contributions. C.4b shows the SM (black) the full EFT (yellow) the contributions from the T-operators (green) and the M-operators (red). In C.4c the contribution from the M-operators (green) is compared to the one from all connected operators (red). C.4d shows the contribution from the T-like operators (green), M-like operators (blue) and the T-like operators (red).

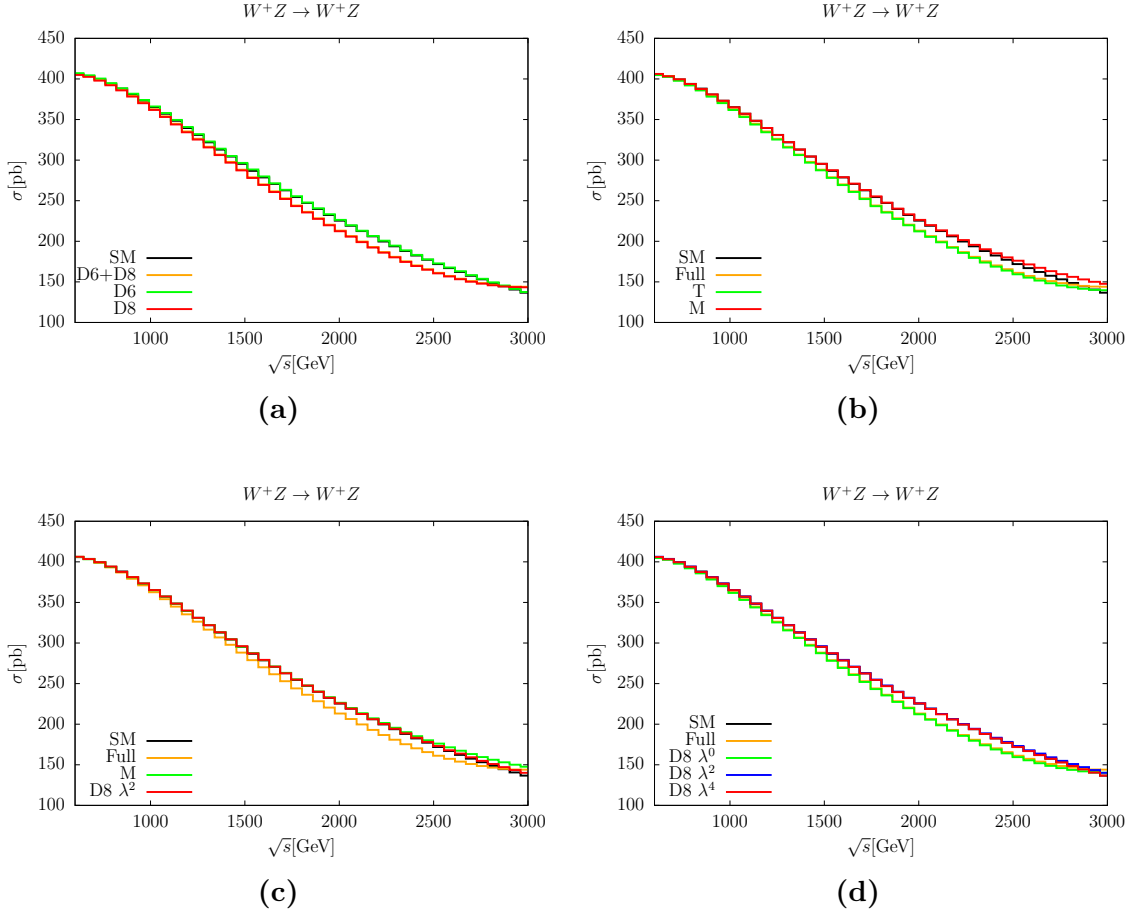


**Figure C.5.:** Cross section of the EFT for  $m = 700$  GeV,  $J = 3$  and  $\lambda = 1$  for  $W^+Z \rightarrow W^+Z$  for different invariant masses of the vector boson pair. C.5a shows the SM (black) the full EFT (yellow) the dimension 6 (green) and the dimension 8 (red) contributions. C.5b shows the SM (black) the full EFT (yellow) the contributions from the T-operators (green) and the M-operators (red). In C.5c the contribution from the M-operators (green) is compared to the one from all connected operators (red). C.5d shows the contribution from the T-like operators (green), M-like operators (blue) and the T-like operators (red).

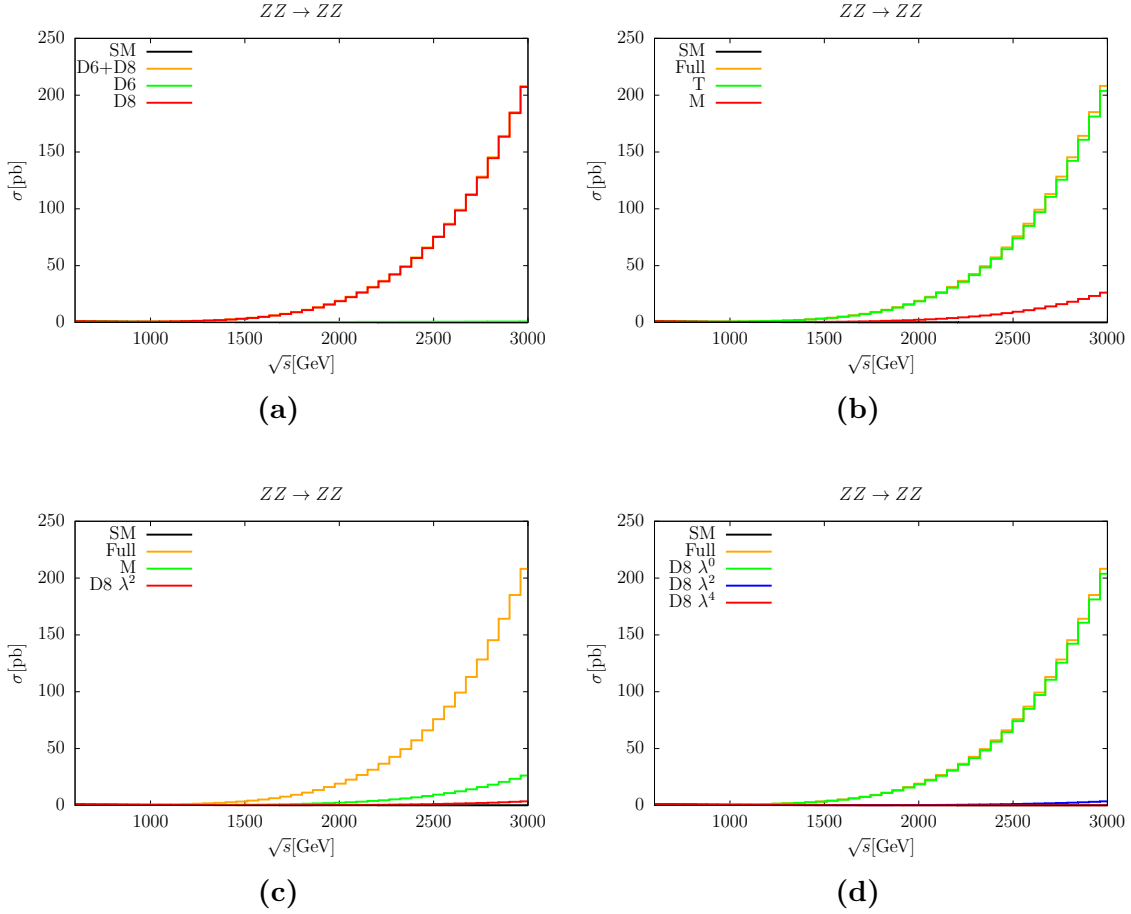


**Figure C.6.:** Cross section of the EFT for  $m = 700$  GeV,  $J = 3$  and  $\lambda = 1$  for  $ZZ \rightarrow ZZ$  for different invariant masses of the vector boson pair. C.6b shows the SM (black) the full EFT (yellow) the dimension 6 (green) and the dimension 8 (red) contributions. C.6a shows the SM (black) the full EFT (yellow) the contributions from the T-operators (green) and the M-operators (red). In C.6c the contribution from the M-operators (green) is compared to the one from all connected operators (red). C.6d shows the contribution from the T-like operators (green), M-like operators (blue) and the T-like operators (red).

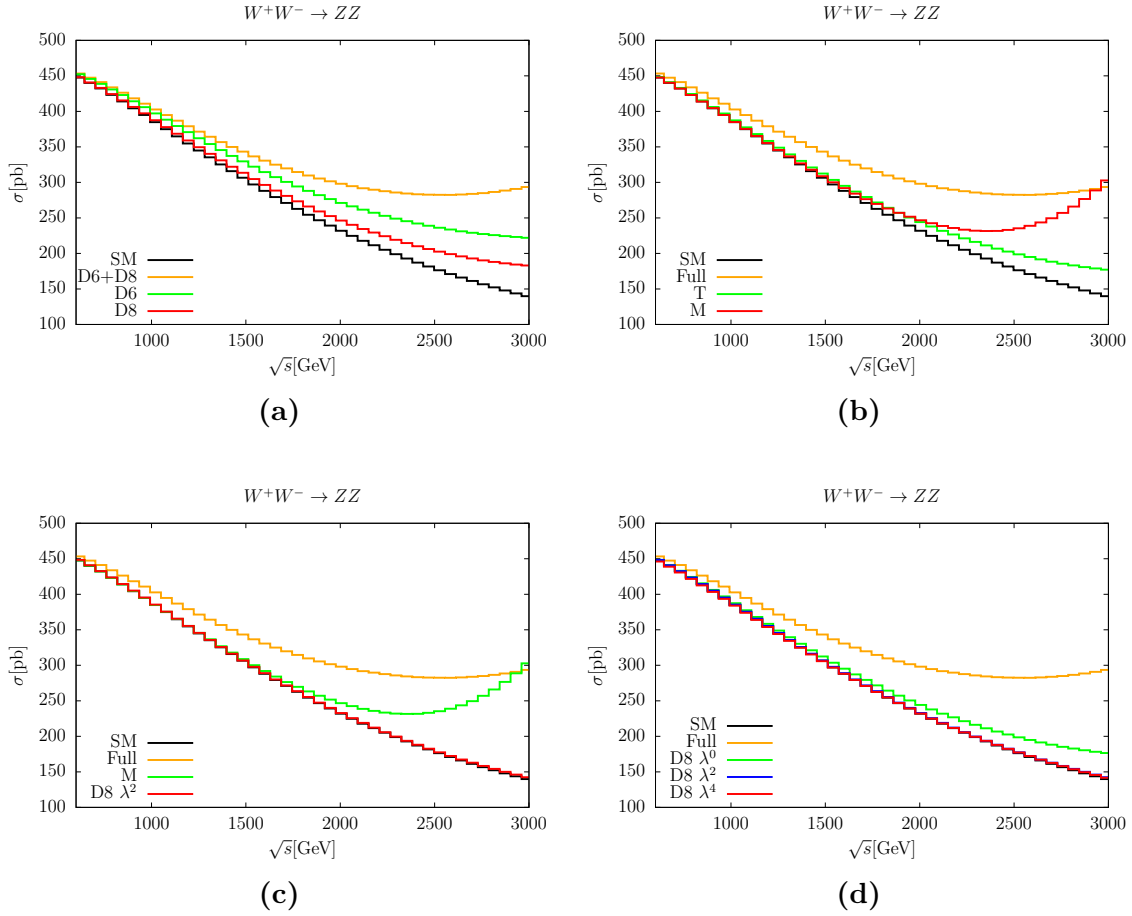


**Figure C.7.:** Cross section of the EFT for  $m = 1100$  GeV,  $J = 4$  and  $\lambda = 3$  for  $W^+W^- \rightarrow ZZ$  for different invariant masses of the vector boson pair. C.7a shows the SM (black) the full EFT (yellow) the dimension 6 (green) and the dimension 8 (red) contributions. C.7b shows the SM (black) the full EFT (yellow) the contributions from the T-operators (green) and the M-operators (red). In C.7c the contribution from the M-operators (green) is compared to the one from all connected operators (red). C.7d shows the contribution from the T-like operators (green), M-like operators (blue) and the T-like operators (red).

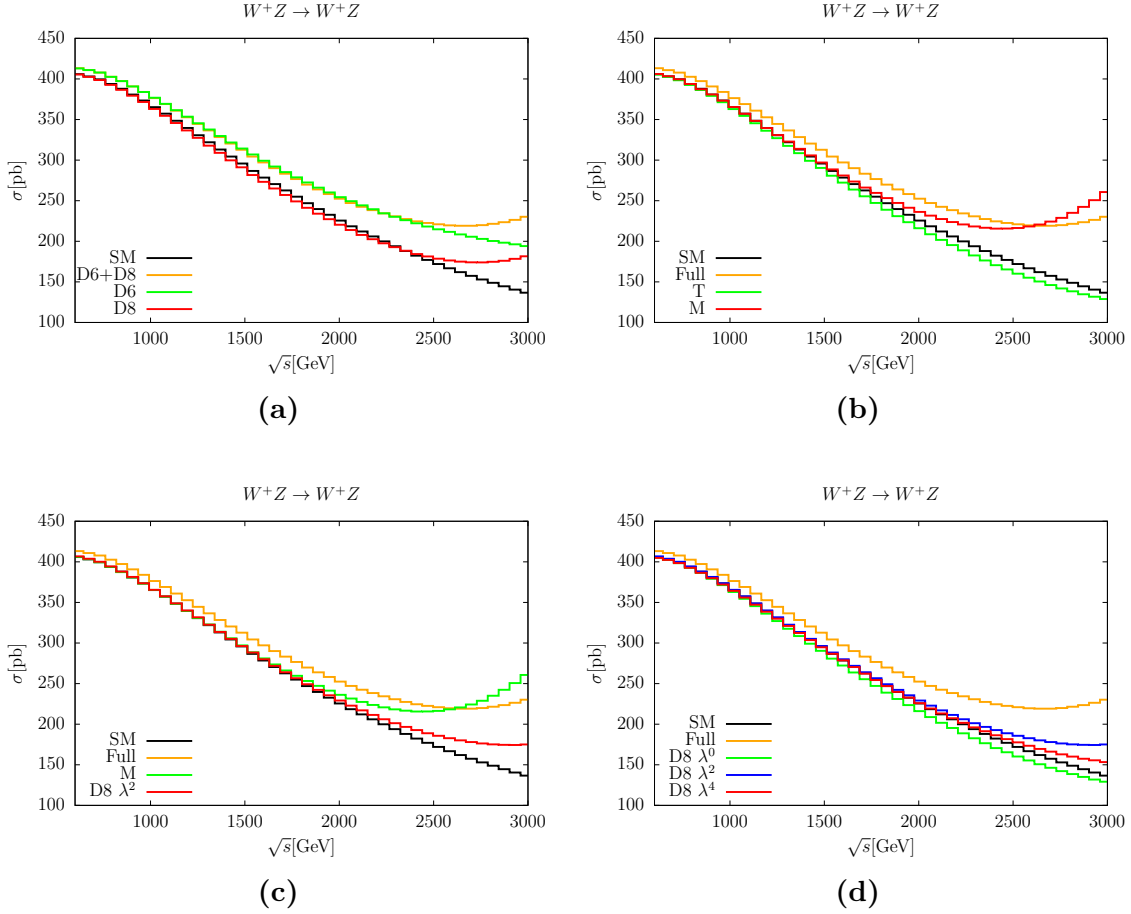


**Figure C.8.:** Cross section of the EFT for  $m = 1100$  GeV,  $J = 4$  and  $\lambda = 3$  for  $W^+Z \rightarrow W^+Z$  for different invariant masses of the vector boson pair. C.8a shows the SM (black) the full EFT (yellow) the dimension 6 (green) and the dimension 8 (red) contributions. C.8b shows the SM (black) the full EFT (yellow) the contributions from the T-operators (green) and the M-operators (red). In C.8c the contribution from the M-operators (green) is compared to the one from all connected operators (red). C.8d shows the contribution from the T-like operators (green), M-like operators (blue) and the T-like operators (red).

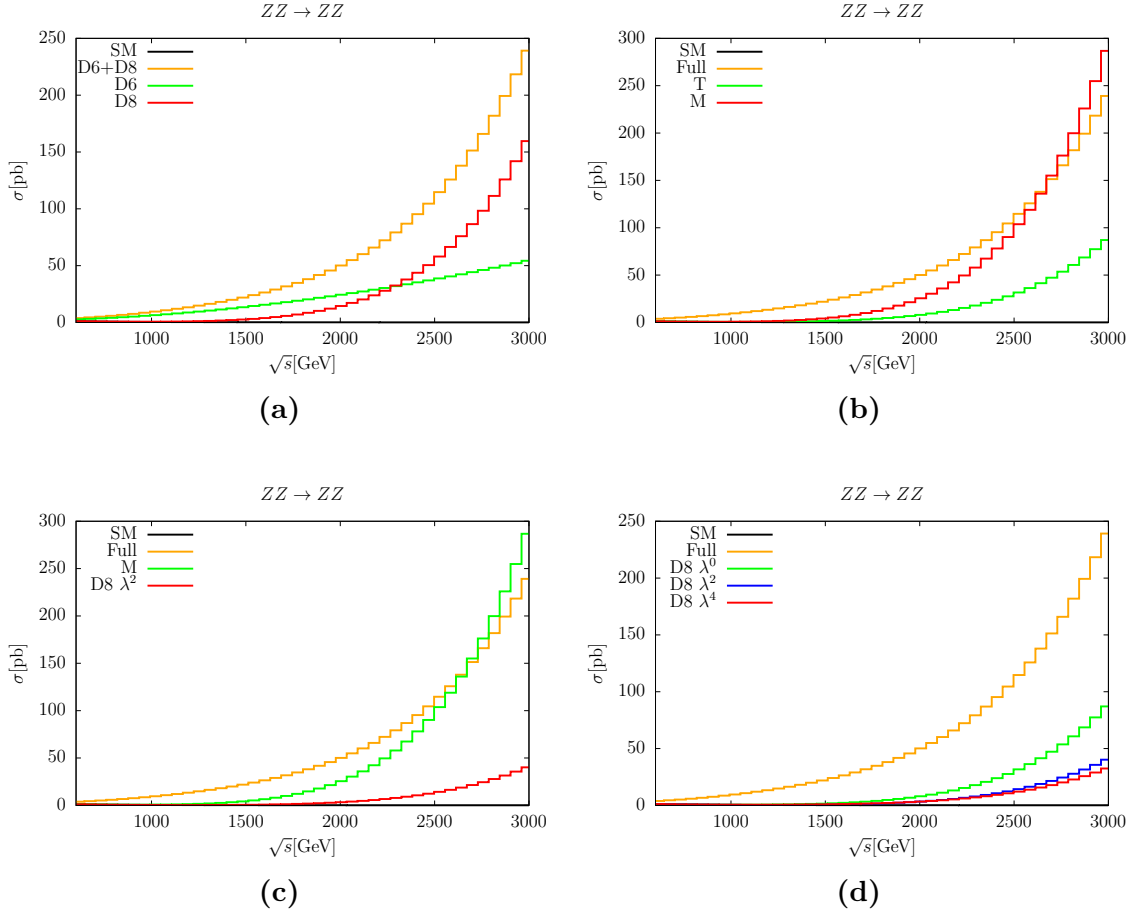


**Figure C.9.:** Cross section of the EFT for  $m = 1100$  GeV,  $J = 4$  and  $\lambda = 3$  for  $ZZ \rightarrow ZZ$  for different invariant masses of the vector boson pair. C.9a shows the SM (black) the full EFT (yellow) the dimension 6 (green) and the dimension 8 (red) contributions. C.9b shows the SM (black) the full EFT (yellow) the contributions from the T-operators (green) and the M-operators (red). In C.9c the contribution from the M-operators (green) is compared to the one from all connected operators (red). C.9d shows the contribution from the T-like operators (green), M-like operators (blue) and the T-like operators (red).

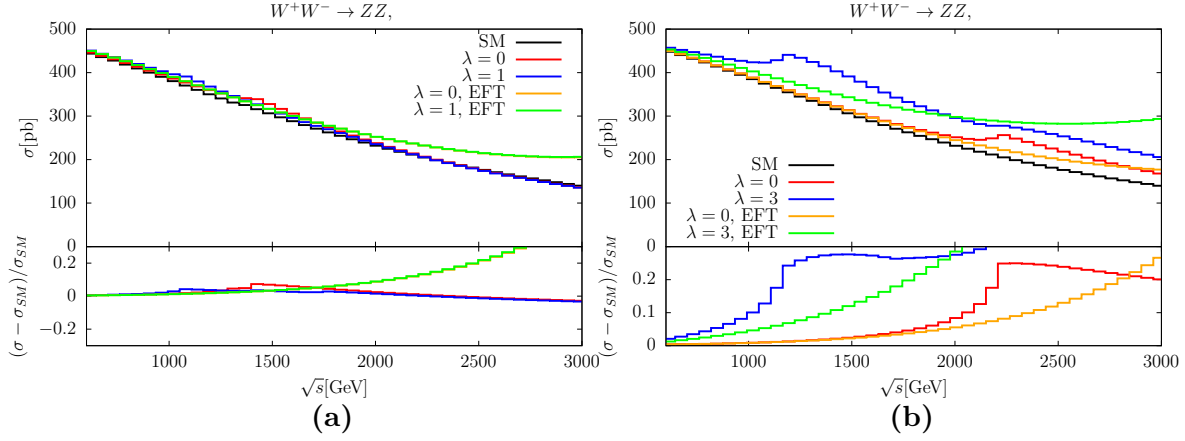


**Figure C.10.:** Cross section of the full model (red, blue) and the EFT (yellow, green) for  $m = 700$  GeV,  $J = 3$  and  $\lambda = 0, 1$  (C.10a) and for  $m = 1100$  GeV,  $J = 4$  and  $\lambda = 0, 3$  (C.10b) for  $W^+W^- \rightarrow ZZ$  for different invariant masses of the vector boson pair. The lower part shows the difference from the SM distribution normalized by the SM.

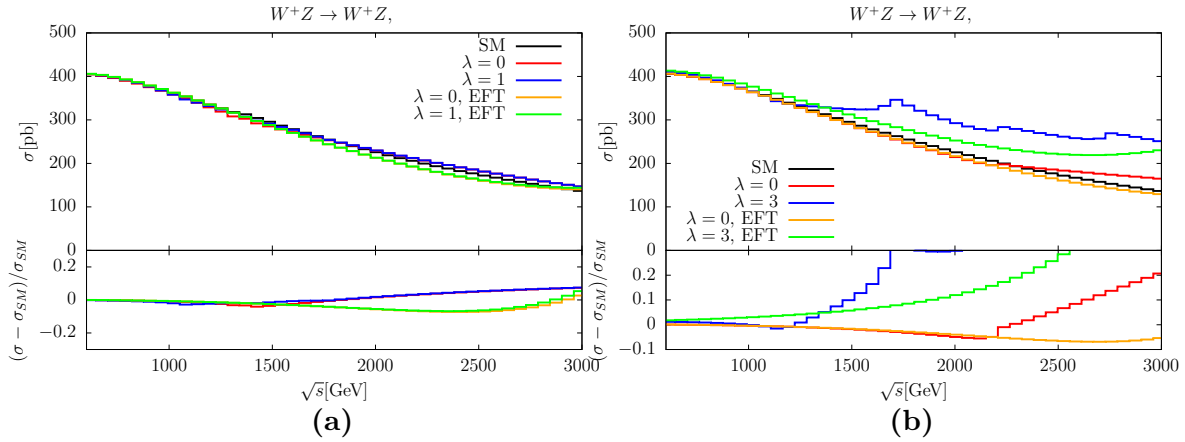


**Figure C.11.:** Cross section of the full model (red, blue) and the EFT (yellow, green) for  $m = 700$  GeV,  $J = 3$  and  $\lambda = 0, 1$  (C.11a) and for  $m = 1100$  GeV,  $J = 4$  and  $\lambda = 0, 3$  (C.11b) for  $W^+Z \rightarrow W^+Z$  for different invariant masses of the vector boson pair. The lower part shows the difference from the SM distribution normalized by the SM.

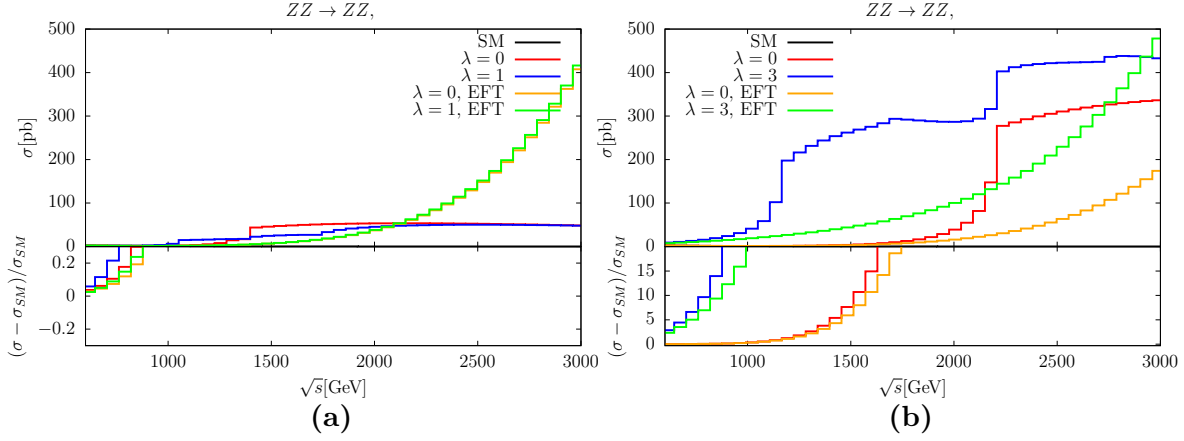


**Figure C.12.:** Cross section of the full model (red, blue) and the EFT (yellow, green) for  $m = 700$  GeV,  $J = 3$  and  $\lambda = 0, 1$  (C.12a) and for  $m = 1100$  GeV,  $J = 4$  and  $\lambda = 0, 3$  (C.12b) for  $ZZ \rightarrow ZZ$  for different invariant masses of the vector boson pair. The lower part shows the difference from the SM distribution normalized by the SM.

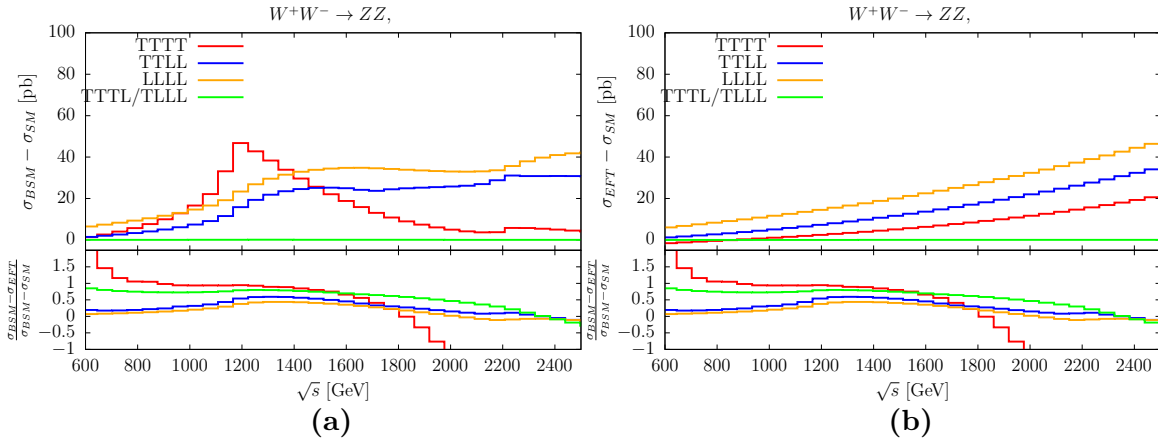


**Figure C.13.:** Polarized cross section of the full model (C.13a) and the EFT (C.13b) for  $m = 1100$  GeV,  $J = 4$  and  $\lambda = 3$  for  $W^+W^- \rightarrow ZZ$  for different invariant masses of the vector boson pair. The purely transverse (red), the mixed (TTLL, blue), purely longitudinal (yellow) and the remaining (green) contributions are shown. The lower part shows the difference between the full model and the EFT normalized by the difference of the full model from SM.

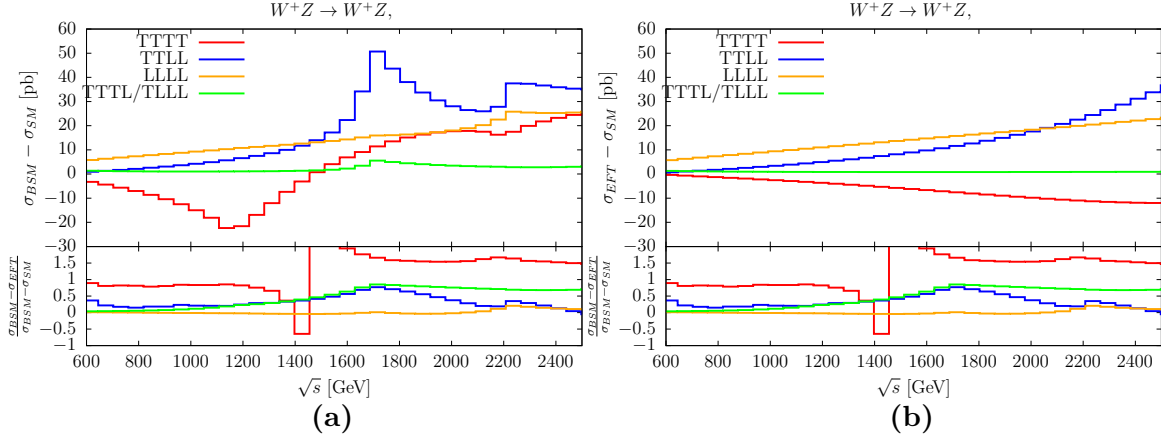


**Figure C.14.:** Polarized cross section of the full model (C.14a) and the EFT (C.14b) for  $m = 1100$  GeV,  $J = 4$  and  $\lambda = 3$  for  $W^+Z \rightarrow W^+Z$  for different invariant masses of the vector boson pair. The purely transverse (red), the mixed (TTLL, blue), purely longitudinal (yellow) and the remaining (green) contributions are shown. The lower part shows the difference between the full model and the EFT normalized by the difference of the full model from SM.

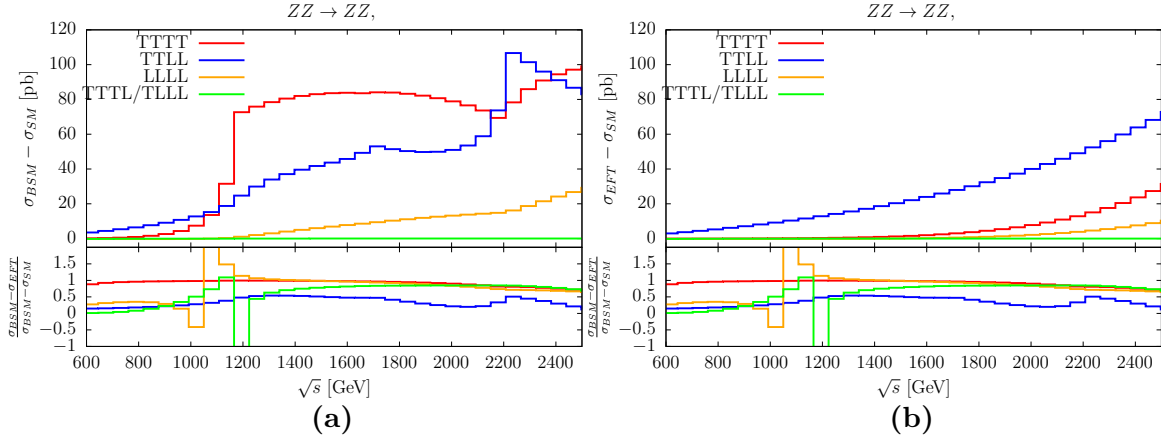


**Figure C.15.:** Polarized cross section of the full model (C.15a) and the EFT (C.15b) for  $m = 1100$  GeV,  $J = 4$  and  $\lambda = 3$  for  $ZZ \rightarrow ZZ$  for different invariant masses of the vector boson pair. The purely transverse (red), the mixed (TTLL, blue), purely longitudinal (yellow) and the remaining (green) contributions are shown. The lower part shows the difference between the full model and the EFT normalized by the difference of the full model from SM.

# Bibliography

- [1] Ellis, Joshua: *TikZ-Feynman: Feynman diagrams with TikZ*. Comput. Phys. Commun., 210:103–123, 2017.
- [2] Sirunyan, Albert M *et al.*: *Constraints on anomalous Higgs boson couplings to vector bosons and fermions in its production and decay using the four-lepton final state*. Phys. Rev. D, 104(5):052004, 2021.
- [3] Sirunyan, Albert M *et al.*: *Search for anomalous triple gauge couplings in  $WW$  and  $WZ$  production in lepton + jet events in proton-proton collisions at  $\sqrt{s} = 13$  TeV*. JHEP, 12:062, 2019.
- [4] Sirunyan, A.M. *et al.*: *Search for anomalous electroweak production of vector boson pairs in association with two jets in proton-proton collisions at 13 TeV*. Physics Letters B, 798:134985, nov 2019. <https://doi.org/10.1016%2Fj.physletb.2019.134985>.
- [5] Aad, Georges *et al.*: *Observation of a new particle in the search for the Standard Model Higgs boson with the ATLAS detector at the LHC*. Phys. Lett. B, 716:1–29, 2012.
- [6] Chatrchyan, Serguei *et al.*: *Observation of a New Boson at a Mass of 125 GeV with the CMS Experiment at the LHC*. Phys. Lett. B, 716:30–61, 2012.
- [7] Fartoukh, Stephane *et al.*: *LHC Configuration and Operational Scenario for Run 3*. Technischer Bericht, CERN, Geneva, Nov 2021. <http://cds.cern.ch/record/2790409>.
- [8] Apollinari, G., O. Brüning, T. Nakamoto und Lucio Rossi: *High Luminosity Large Hadron Collider HL-LHC*. CERN Yellow Report, (5):1–19, 2015.
- [9] Khachatryan, V. *et al.*: *Study of Vector Boson Scattering and Search for New Physics in Events with Two Same-Sign Leptons and Two Jets*. Phys. Rev. Lett., 114:051801, Feb 2015. <https://link.aps.org/doi/10.1103/PhysRevLett.114.051801>.
- [10] Aaboud, M. und othres: *Measurement of  $W^\pm W^\pm$  vector-boson scattering and limits on anomalous quartic gauge couplings with the ATLAS detector*. Phys. Rev. D, 96:012007, Jul 2017. <https://link.aps.org/doi/10.1103/PhysRevD.96.012007>.
- [11] Schael, S. *et al.*: *Electroweak Measurements in Electron-Positron Collisions at  $W$ -Boson-Pair Energies at LEP*. Phys. Rept., 532:119–244, 2013.
- [12] Fayolle, D: *Anomalous couplings at LEP2*. Technischer Bericht, CERN, Geneva, Jan 2002. <https://cds.cern.ch/record/535312>.

- 
- [13] Falkowski, Adam und Francesco Riva: *Model-independent precision constraints on dimension-6 operators*. JHEP, 02:039, 2015.
- [14] Efrati, Aielet, Adam Falkowski und Yotam Soreq: *Electroweak constraints on flavorful effective theories*. JHEP, 07:018, 2015.
- [15] Buchmüller, W. und D. Wyler: *Effective lagrangian analysis of new interactions and flavour conservation*. Nuclear Physics B, 268(3):621–653, 1986, ISSN 0550-3213. <https://www.sciencedirect.com/science/article/pii/0550321386902622>.
- [16] Hagiwara, K., S. Ishihara, R. Szalapski und D. Zeppenfeld: *Low energy effects of new interactions in the electroweak boson sector*. Phys. Rev. D, 48:2182–2203, Sep 1993. <https://link.aps.org/doi/10.1103/PhysRevD.48.2182>.
- [17] Grzadkowski, B., M. Iskrzynski, M. Misiak und J. Rosiek: *Dimension-Six Terms in the Standard Model Lagrangian*. JHEP, 10:085, 2010.
- [18] Éboli, O. J. P., M. C. Gonzalez-Garcia und J. K. Mizukoshi:  *$pp \rightarrow jje^\pm\mu^\pm\nu\nu$  and  $jje^\pm\mu^\mp\nu\nu$  at  $\mathcal{O}(\alpha_{\text{em}}^6)$  and  $\mathcal{O}(\alpha_{\text{em}}^4\alpha_s^2)$  for the study of the quartic electroweak gauge boson vertex at CERN LHC*. Phys. Rev. D, 74:073005, Oct 2006. <https://link.aps.org/doi/10.1103/PhysRevD.74.073005>.
- [19] Lang, Jannis, Stefan Liebler, Heiko Schäfer-Siebert und Dieter Zeppenfeld: *Effective field theory versus UV-complete model: vector boson scattering as a case study*. The European Physical Journal C, 81, Juli 2021.
- [20] Higgs, Peter W.: *Broken Symmetries and the Masses of Gauge Bosons*. Phys. Rev. Lett., 13:508–509, 1964. [160(1964)].
- [21] Englert, F. und R. Brout: *Broken Symmetry and the Mass of Gauge Vector Mesons*. Phys. Rev. Lett., 13:321–323, 1964. [157(1964)].
- [22] Appelquist, Thomas und Claude Bernard: *Strongly interacting Higgs bosons*. Phys. Rev. D, 22:200–213, Jul 1980. <https://link.aps.org/doi/10.1103/PhysRevD.22.200>.
- [23] Longhitano, Anthony C.: *Heavy Higgs Bosons in the Weinberg-Salam Model*. Phys. Rev., D22:1166, 1980.
- [24] Fermi, E.: *An attempt of a theory of beta radiation. 1*. Z. Phys., 88:161–177, 1934.
- [25] Degrande, Celine, Nicolas Greiner, Wolfgang Kilian, Olivier Mattelaer, Harrison Mebane, Tim Stelzer, Scott Willenbrock und Cen Zhang: *Effective Field Theory: A Modern Approach to Anomalous Couplings*. Annals Phys., 335:21–32, 2013.
- [26] Murphy, Christopher W.: *Dimension-8 operators in the Standard Model Effective Field Theory*. JHEP, 10:174, 2020.
- [27] Li, Hao Lin, Zhe Ren, Jing Shu, Ming Lei Xiao, Jiang Hao Yu und Yu Hui Zheng: *Complete set of dimension-eight operators in the standard model effective field theory*. Phys. Rev. D, 104(1):015026, 2021.
- [28] Éboli, O. J. P. und M. C. Gonzalez-Garcia: *Classifying the bosonic quartic couplings*. Phys. Rev. D, 93(9):093013, 2016.

- [29] Degrande, Celine, Oscar Eboli, Bastian Feigl, Barbara Jäger, Wolfgang Kilian, Olivier Mattelaer, Michael Rauch, Jürgen Reuter, Marco Sekulla und Doreen Wackerroth: *Monte Carlo tools for studies of non-standard electroweak gauge boson interactions in multi-boson processes: A Snowmass White Paper*. In: *Community Summer Study 2013: Snowmass on the Mississippi*, September 2013.
- [30] Sekulla, Marco: *Anomalous couplings, resonances and unitarity in vector boson scattering*. Dissertation, Universität Siegen, 2015. <https://dspace.uni-siegen.de/handle/ubsi/979>.
- [31] Perez, Genessis, Marco Sekulla und Dieter Zeppenfeld: *Anomalous quartic gauge couplings and unitarization for the vector boson scattering process  $pp \rightarrow W^+W^+jjX \rightarrow \ell^+\nu_\ell\ell^+\nu_\ell jjX$* . Eur. Phys. J. C, 78(9):759, 2018.
- [32] Passarino, G. und M. Veltman: *One-loop corrections for  $e+e-$  annihilation into  $\mu+\mu-$  in the Weinberg model*. Nuclear Physics B, 160(1):151–207, 1979, ISSN 0550-3213. <https://www.sciencedirect.com/science/article/pii/0550321379902347>.
- [33] 't Hooft, G. und M. Veltman: *Scalar one-loop integrals*. Nuclear Physics B, 153:365–401, 1979, ISSN 0550-3213. <https://www.sciencedirect.com/science/article/pii/0550321379906059>.
- [34] Patel, Hiren H.: *Package-X 2.0: A Mathematica package for the analytic calculation of one-loop integrals*. Comput. Phys. Commun., 218:66–70, 2017.
- [35] Hahn, Thomas: *Loop calculations with FeynArts, FormCalc, and LoopTools*. Acta Phys. Polon. B, 30:3469–3475, 1999.
- [36] Schwartz, Matthew D.: *Quantum Field Theory and the Standard Model*. Cambridge University Press, März 2014, ISBN 978-1-107-03473-0, 978-1-107-03473-0.
- [37] Zyla, P.A. *et al.*: *Review of Particle Physics*. PTEP, 2020(8):083C01, 2020. and 2021 update.
- [38] Heisenberg, W und H Euler: *Consequences of dirac theory of the positron*. arXiv preprint physics/0605038, 2006.
- [39] Cirelli, Marco, Nicolao Fornengo und Alessandro Strumia: *Minimal dark matter*. Nucl. Phys. B, 753:178–194, 2006.
- [40] 't Hooft, G.: *Dimensional regularization and the renormalization group*. Nuclear Physics B, 61:455–468, 1973, ISSN 0550-3213. <https://www.sciencedirect.com/science/article/pii/0550321373903763>.
- [41] Weinberg, Steven: *New Approach to the Renormalization Group*. Phys. Rev. D, 8:3497–3509, Nov 1973. <https://link.aps.org/doi/10.1103/PhysRevD.8.3497>.
- [42] Bardeen, William A., A. J. Buras, D. W. Duke und T. Muta: *Deep-inelastic scattering beyond the leading order in asymptotically free gauge theories*. Phys. Rev. D, 18:3998–4017, Dec 1978. <https://link.aps.org/doi/10.1103/PhysRevD.18.3998>.

- 
- [43] Bohm, M., H. Spiesberger und W. Hollik: *On the One Loop Renormalization of the Electroweak Standard Model and Its Application to Leptonic Processes*. Fortsch. Phys., 34:687–751, 1986.
- [44] Sperling, Marcus, Dominik Stöckinger und Alexander Voigt: *Renormalization of vacuum expectation values in spontaneously broken gauge theories*. JHEP, 07:132, 2013.
- [45] Bakshi, Supratim Das, Joydeep Chakraborty, Christoph Englert, Michael Spannowsky und Panagiotis Stylianou: *Landscaping CP-violating BSM scenarios*. Nucl. Phys. B, 975:115676, 2022.
- [46] D’Ambrosio, G., G. F. Giudice, G. Isidori und A. Strumia: *Minimal flavor violation: An Effective field theory approach*. Nucl. Phys. B, 645:155–187, 2002.
- [47] Cirigliano, Vincenzo, Benjamin Grinstein, Gino Isidori und Mark B. Wise: *Minimal flavor violation in the lepton sector*. Nucl. Phys. B, 728:121–134, 2005.
- [48] Kagan, Alexander L., Gilad Perez, Tomer Volansky und Jure Zupan: *General Minimal Flavor Violation*. Phys. Rev. D, 80:076002, 2009.
- [49] Brivio, Ilaria, Yun Jiang und Michael Trott: *The SMEFTsim package, theory and tools*. JHEP, 12:070, 2017.
- [50] Alloul, Adam, Neil D. Christensen, Céline Degrande, Claude Duhr und Benjamin Fuks: *FeynRules 2.0 - A complete toolbox for tree-level phenomenology*. Comput. Phys. Commun., 185:2250–2300, 2014.
- [51] Angelescu, Andrei und Peisi Huang: *Integrating Out New Fermions at One Loop*. JHEP, 01:049, 2021.
- [52] Sirunyan, Albert M *et al.*: *Search for resonant and nonresonant new phenomena in high-mass dilepton final states at  $\sqrt{s} = 13$  TeV*. JHEP, 07:208, 2021.
- [53] Ajjath, A. H., Goutam Das, M. C. Kumar, Pooja Mukherjee, V. Ravindran und Kajal Samanta: *Resummed Drell-Yan cross-section at  $N^3LL$* . JHEP, 10:153, 2020.
- [54] Sirunyan, Albert M *et al.*: *Measurement of the differential Drell-Yan cross section in proton-proton collisions at  $\sqrt{s} = 13$  TeV*. JHEP, 12:059, 2019.
- [55] Kummer, Christian: *Search for supersymmetry events with two same-sign leptons*, March 2010. <http://nbn-resolving.de/urn:nbn:de:bvb:19-112726>.
- [56] Hagiwara, K., R.D. Peccei, D. Zeppenfeld und K. Hikasa: *Probing the weak boson sector in  $e+e-W+W-$* . Nuclear Physics B, 282:253–307, 1987, ISSN 0550-3213. <https://www.sciencedirect.com/science/article/pii/0550321387906857>.
- [57] Dittmaier, S. *et al.*: *Handbook of LHC Higgs Cross Sections: 2. Differential Distributions*. CERN Yellow Reports: Monographs. CERN, Geneva, 2012. <http://cds.cern.ch/record/1416519>, The authors dedicate this Report to the memory of Robert Brout and Simon van der Meer.
- [58] Hahn, T.: *CUBA: A Library for multidimensional numerical integration*. Comput. Phys. Commun., 168:78–95, 2005.

- 
- [59] Aad, Georges *et al.*: *Search for the  $HH \rightarrow b\bar{b}b\bar{b}$  process via vector-boson fusion production using proton-proton collisions at  $\sqrt{s} = 13$  TeV with the ATLAS detector*. JHEP, 07:108, 2020. [Erratum: JHEP 01, 145 (2021), Erratum: JHEP 05, 207 (2021)].



# Acknowledgments

I would like to thank Prof. Dr. Dieter Zeppenfeld for giving me the opportunity to work with him for the last couple of years, and for sharing his insights in theoretical particle physics and especially vector boson scattering with me. I also want to express my gratitude to Prof. Dr. Milada M. Mühlleitner for accepting the position of second reviewer.

I also want to thank M.Sc J. Lang, Dr. M. Löschner and Dr. T. Ježo for many fruitful discussions and meetings. Moreover I want to thank the ITP for many great years and especially Renate Weiß who helped with every kind of administrative issues.

I also want to acknowledge the support by the DFG-funded Doctoral School "Karlsruhe School of Elementary and Astroparticle Physics: Science and Technology" and by the DFG-funded Collaborative Research Center "Particle Physics Phenomenology after the Higgs Discovery" who funded my work.

I am deeply grateful to my wife Viktoria Dietrich. I can't imagine the past years without you by my side, without your support, without your love.

Finally I want to thank my parents Dagmar and Dr. Dietrich Schäfer-Siebert. You stoked my interest in science and especially physics. You supported me throughout all these years, you enabled me to study physics and were always there for me.